ASSESSING THE POTENTIAL OF USING MICRO-COMPUTERIZED TOMOGRAPHY TO DETERMINE THE PHYSICAL PROPERTIES OF DIFFERENT TEXTURED SOILS

By

Emke Kim Hartnick

Thesis presented in partial fulfilment of the requirements for the degree of
Master of Agricultural Science (Soil Science)

at
Stellenbosch University
Department of Soil Science, Faculty of AgriSciences

Supervisor: Prof A du Plessis
Co-supervisor: Mr EL Lategan

December 2020

Declaration

By submitting this thesis electronically, I declare that the entirety of the work contained therein is my own, original work, that I am the sole author thereof (save to the extent explicitly otherwise stated), that reproduction and publication thereof by Stellenbosch University will not infringe any third party rights and that I have not previously in its entirety or in part submitted it for obtaining any qualification.

Date: 19/11/2020

Summary

The physical properties of soil, particularly the structure, texture, and pore geometry affect hydraulic conductivity in soils. The hydraulic conductivity is an important parameter for understanding the flow of water through different soil types for determining irrigation rates, monitoring of groundwater, and runoff. The hydraulic conductivity is a highly variable soil property and there are several methods for determining the hydraulic conductivity in soils. Each has its advantages and limitations.

Traditional methods are time-consuming and the application of X-ray micro-computer tomography (microCT) offers fast and effective analysis and results. The additional use of microCT for this purpose might improve the accuracy of laboratory constant hydraulic head tests if these methods are used in combination. The application of microCT technology can visualize the internal pore geometry of a soil sample without destroying the soil sample. Thus, the microCT technology can examine the porosity and the pore connectivity in soils, which influence the hydraulic conductivity. The purpose of this study was to apply microCT technology to examine the range within it can be used to determine the saturated hydraulic conductivity (K_{sat}) and porosity of homogeneous and heterogeneous soils. This was done in the context of considering if the advantages of this application (fast and efficient analysis) exceed the disadvantages (cost). The investigation of an effective sampling method for soil samples for X-ray microCT scans and associated image-based analysis were examined.

The saturated hydraulic conductivity (K_{sat}) and porosity of five different soil types (homogeneous and heterogeneous soil) will be obtained through standard laboratory methods (constant hydraulic head test and calculating the porosity from the bulk and particle density) and microCT image-based simulations and analysis. Additional calculation of the K_{sat} based on grain size theoretical equations such as Hazen and Kozenzy & Carman equation will be used.

The results showed that the K_{sat} of the homogeneous soil very coarse, coarse, and medium sand were underestimated by the microCT simulations. The K_{sat} of the fine and very fine sand determined through microCT simulations and constant hydraulic head tests compared well. MicroCT simulations underestimated the K_{sat} of the heterogeneous soil. The porosity values for the homogeneous soil were overestimated by microCT image-based analysis. The porosity values of the heterogeneous soil obtained from microCT image-based analysis for the coarse and pure fine sand were higher than the sandy clay loam, sandy loam and sandy clay soils. The sandy clay loam, sandy loam and sandy clay soils porosity were measured inaccurately by microCT due to resolution limitations. The K_{sat} of the homogeneous soil analysed by microCT simulation, however, fell within the same order of magnitude as the K_{sat} obtained from the constant hydraulic head test.

Fundamentally, the microCT technology demonstrated great capabilities for analysing both the K_{sat} and porosity of homogeneous soils. The microCT application is best used for soils with larger particle sizes due to image resolution limits. The 2D visualization of the microCT scans can be useful for investigating structural changes within a soil sample caused by laboratory analysis. Such analysis may include constant hydraulic head tests or the examination of soil samples after sample preparations.

Opsomming

Die fisiese eienskappe van grond, spesifiek die struktuur, tekstuur en poriegeometrie het 'n invloed op die hidrouliese geleidingsvermoë in gronde. Die hidrouliese geleidingsvermoë is 'n belangrike parameter om die vloei van water deur verskillende grondsoorte te verstaan vir die bepaling van besproeiingstempo, monitering van grondwater en dreinering van afloop water. Die hidrouliese geleidingsvermoë is 'n baie veranderlike grondeienskap en daar is baie verskillende metodes om die hidrouliese geleidingsvermoë in gronde te bepaal, elk met sy eie voordele en beperkings.

Tradisionele metodes is tydrowend en die toepassing van X-straal-mikro-rekenaartomografie (mikroCT) bied vinnige, effektiewe analise en resultate. Die bykomende gebruik van mikroCT vir hierdie doel kan die akkuraatheid van konstante hidrouliese toetse in laboratorium verbeter, indien hierdie metodes in kombinasie gebruik word. MikroCT-tegnologie kan die interne poriegeometrie van 'n grondmonster visualiseer sonder om die grondmonster te vernietig. Die mikroCT-tegnologie kan dus die porositeit en porieverbinding in gronde ondersoek wat die hidrouliese geleidingsvermoë beïnvloed. Die doel van hierdie studie was om die toepassing van mikroCT-tegnologie te gebruik om die reikwydte te ondersoek, wat gebruik kan word om die versadigde hidrouliese geleidingsvermoë (K_{sat}) en porositeit van homogene en heterogene gronde te bepaal. Dit word gedoen in die konteks van die oorweging of die voordele van hierdie toepassing (vinnige en doeltreffende ontleding) die nadele (koste) oorskry. Die assessering na n effektiewe steekproefmetode vir grond monsters vir X-straal mikroCT-skanderings en gepaardgaande beeldgebaseerde analise was ondersoek.

Die versadigde hidrouliese geleidingsvermoë (K_{sat}) en porositeit van vyf verskillende grondtipes (homogene en heterogene grond) sal gemeet word deur standaard laboratoriummetodes (konstante hidrouliese drukhoogte en digtheidsmetode) en op mikroCT beeldgebaseerde simulasies en analise. Bykomende berekening van die K_{sat} gebaseer op teoretiese vergelykings met korrelgrootte, soos Hazen en Kozenzy & Carman, sal gebruik word.

Vir die homogene grond is die K_{sat} van baie growwe, growwe en medium sand deur die mikroCT-simulasies onderskat. Die K_{sat} van die fyn en baie fyn sand bepaal deur mikroCT-simulasies en konstante hidrouliese drukhoogte vergelyk goed. MikroCT-simulasies het die K_{sat} van die heterogene grond onderskat. Die porositeit waardes van die homogene grond, gemeet deur mikro-gebaseerde beeldanalise, was oorskat. Die porositeit van die growwe en suiwer fyn sand heterogene grond was hoër gewees as die sandkleileem, sandleem en sandklei wat geanaliseer was deur mikroCT. Die porositeit van die sandkleileem, sandleem en sandklei, wat geanaliseer was deur mikroCT, was foutief as gevolg van die resolusie limitasie. Die K_{sat} van die homogene grond wat deur mikroCT-simulasie geanaliseer was, het egter binne dieselfde groottevlak as die K_{sat} wat verkry is uit die konstante hidrouliese drukhoogte geval.

Fundamenteel het die mikroCT-tegnologie groot moontlikhede getoon om sowel die K_{sat} as die porositeit van homogene grond te ontleed. Die mikroCT-toepassing word die beste gebruik vir gronde met groter deeltjiegroottes soos growwe sand as gevolg van die beperking van die beeld resolusie. Die 2D-visualisering van die mikroCT-skanderings kan nuttig wees om strukturele veranderinge binne 'n grondmonster te ondersoek. Dit sluit in veranderinge wat veroorsaak word deur die analise wat in die laboratorium uitgevoer is, soos die konstante hidrouliese drukhoogte of die ondersoek van grondmonsters na monstervoorbereidings.

This thesis is dedicated to my Heavenly Father.

Biographical sketch

Emke Hartnick is from Macassar in the Western Cape, born on the 22 May 1990. She matriculated in 2008 from Gordon Secondary School in Somerset West. In 2015 she graduated from the University of the Western Cape with a BSc (Hons) in Environmental and Water Science.

Acknowledgements

I wish to express my sincere gratitude and appreciation to the following persons and institutions:

- Prof Anton du Plessis from the CT Scanner Facility at the University of Stellenbosch, who has given me the opportunity to pursue my MScAgric-degree. He believed in my ability to complete my MSc and motivated me. He offered up his time to help me in every situation and helped me to believe in myself. Thank you.

- Mr Vink Lategan of the Department of Soil Sciences at the University of Stellenbosch, who assisted me with my thesis, laboratory work and offered up his time to help me. Thank you for teaching me how to work independently and take my own initiative.

- Dr Eduard Hoffman from the Department of Soil Sciences at the University of Stellenbosch, who always gave me good advice and motivated me.

- Everyone at Welgevallen experimental farm and the Houmoed farm who allowed me to sample my soil samples on their premises.

- My family (mom, dad and sister) and friends who supported me throughout my thesis, both financially and emotionally.

- My fellow student and friend Ncumisa Madubela who was always there at the Department of Soil Science listening to my burdens and giving me great advice on life and work.

- Kenwinn Wiener, my friend and mentor, who helped me, and believed in my ability to complete my MSc.

- Everyone at the Department of Soil Science at the University of Stellenbosch, including the lecturers, students and staff who advised and assisted me.

- To everyone at the CT scanner facility in Stellenbosch who assistance and hospitality.

- To my heavenly father for giving me all the strength to complete this thesis.

TABLE OF CONTENTS

LIST OF FIGURES

LIST OF TABLES

CHAPTER 1 : GENERAL INTRODUCTION AND OBJECTIVES

1.1 GENERAL INTRODUCTION

The physical properties of soil, specifically the structure and texture, affect the hydraulic conductivity in the soil (Hillel 2004). Hydraulic conductivity is the discharge, or effective velocity of fluid flow through a medium and is equal to the fluid flux or volume of fluid passing through a cross-section during a time interval, divided by the cross-sectional area (Nolen-Hoeksema 2014). In many materials, the porosity is usually proportional to the hydraulic conductivity, however, this is not a rule because this property is also influenced by the properties of the fluid (Nolen-Hoeksema 2014).

Hydraulic conductivity is an important parameter for understanding the movement of water through different soil types for determining irrigation rates, monitoring surface runoff, estimating seepage from dams, and hydrological modelling (Elhakim 2016). Hydraulic conductivity is a highly variable soil property and it can vary within a soil profile due to textural and structural variations. There are many different methods for determining the hydraulic conductivity of soils, including *in situ* methods and laboratory methods. These traditional methods are time consuming, laborious and require large volumes of water. Nagy *et al.* (2013) stated that there are diverse methods for determining the hydraulic conductivity of soils, and the methods have benefits and limitations. Investigating the potential of other application such as X-ray micro-computed tomography (microCT) can add value to the study of soil sciences.

The application of X-ray microCT is an alternative that offers fast, effective analysis and results. The use of microCT might improve the understanding of a soil's hydraulic behaviour due to its imaging capability and hence related changes in hydraulic behaviour and specific features such as large pore spaces or connectivity of pore spaces. The use of X-ray microCT technology is growing. It is a non-destructive technique that has been successfully used for three-dimensional (3D) examinations of soil for more than two decades (Pires *et al.* 2010), excluding simulations. X-ray microCT allows for the visualization of a soil's interconnected pores, pore sizes and particle size distribution. Using the non-destructive 3D image-based analysis and simulation capabilities of this technique, the porosity and pore connectivity in soils, which influence the hydraulic conductivity, can be examined. MicroCT simulation can provide useful outputs such as the variation of flow velocities through a single scanned soil sample due to the pore geometry and heterogeneity, as well as soil porosity and the variation thereof.

Several methodologies exist within the application of microCT and therefore the comparison of results from previous studies are challenging (Taina *et al.* 2007). The disadvantages of this

application are the imaging energy levels and spatial resolution. These issues can influence the accuracy of analysed results. For more detail within an object, it is best to scan objects at a higher or finer resolution, but this will require a smaller sample size.

Given the above-mentioned challenges, this study will investigate an effective and simplified methodology which can be used for microCT simulation and analysis. The application of X-ray microCT technology will be used to examine to what extent it can practically be used on soils and if the advantages of this application (non-destructive imaging of pore structure, fast and efficient analysis) exceed the disadvantages (cost, limited field of view due to resolution and imaging energy levels).

1.2 OBJECTIVES AND AIMS

The objectives of the study were:

- To identify an effective sampling method of soil samples for X-ray microCT scans and associated image-based analysis;
- To determine to what extent X-ray microCT imaging and simulations can be used for the analysis of soil samples for their saturated hydraulic conductivity;
- To examine the use of microCT simulation on homogeneous and heterogeneous soil;
- To investigate whether X-ray microCT could improve current soil laboratory methods and detect problems in sampling methods when the unexpected laboratory results occur; and
- To determine if the advantages of X-ray microCT analysis exceeds the disadvantages of established laboratory methods.

CHAPTER 2 : LITERATURE REVIEW

2.1 PHYSICAL SOIL PROPERTIES

2.1.1 Background

The physical properties of soil such as the texture and structure, influence the porosity and pore connectivity within the soil (Hillel 2004). The pore connectivity and the porosity of soil influence the ease by which water or any fluid moves through a soil medium (Scheidegger 1957). The water movement in soil is controlled by the rate of water flow, also known as the hydraulic conductivity (Hillel 2004). The porosity is a soil property that is usually expressed in percentage (%) or volume fraction (cm^3/cm^3) (Scheidegger 1957). The porosity of the soil is defined by Hillel (2004) as the relationship between the volume of pores in the soil and the total volume of soil.

The porosity of soil is influenced by the bulk density of a soil, which influences the soil structure. Soil structure can be categorized as loosely structured to well or massive structured soils (Hillel 2004). Soils that are loosely structured will have a low bulk density and well-structured soil will have a high bulk density (Jaynes & Tyler 1984).

However, high porosity is not always equivalent to high hydraulic conductivity. The hydraulic conductivity of soils is highly influenced by the pore connectivity and larger pore areas within a soil that creates the preferential flow paths through which the fluid will move (Elhakim 2016).

2.1.2 Soil Texture

Soil texture represents the relative proportion of soil particles with different sizes, which is a fundamental physical property of soils (Nemes & Rawls 2004). In most parts of the world, the textural classification of soils is based on particle-size analyses (Nemes & Rawls 2004). The texture of a soil is classified according to the mass ratio of the three different soil particle types that are present within the soil, namely sand, silt and clay (Fernandez-Illescas *et al.* 2001; Hillel 2004).

Based on the classification of the U.S Department of Agriculture (USDA) the sand particles are between 2 mm – 0.05 mm diameter, the silt particles are between 0.05 mm – 0.002 mm and the clay particles are < 0.002 mm (Hillel, 2004). The different sand fractions are further categorized into very coarse sand (2 mm – 1 mm), coarse sand (1 mm – 0.5 mm), medium sand (0.5 mm – 0.25 mm), fine sand (0.25 mm – 0.1 mm) and very fine sand (0.1 mm – 0.05 mm) (Hillel 2004).

Soil texture is also used as a descriptor of soil physical properties such as porosity, saturated hydraulic conductivity (K_{sat}), and pore size distribution within soils (Fernadez-Illescas *et al.* 2001). Soil texture alone has been reported to be a good predictor of K_{sat} (Nemes & Rawls 2004). Soil

structure may be a very important input, along with soil texture, for the estimation of soil properties like K_{sat} (Nemes & Rawls 2004).

2.1.3 Soil Structure

The arrangement of soil particles to form a single soil unit is known as the soil structure (Hillel 2004). The soil structure of a soil is dependent on the texture of the soil. Soil structure is an important soil property of the hydraulic behaviour within the soil. Soil structure is divided into different categories, including single grained, massive, and aggregated (Hillel 2004). Sandy soils are categorized as a single grained soil structure because the soil particles are loose and not attached (non-cohesive) (Hillel 2004). Higher silt and clay content soils tend to be naturally more compacted in nature than sandy soils, and the structure of these soils will be categorized into massive and aggregated soils (Hillel 2004). Soils that are less compacted with loose particles are expected to have high hydraulic conductivity and compacted soil with cohesive particles will have low saturated hydraulic conductivity (Jaynes & Tyler 1984; Fernandez-Illescas *et al.* 2001).

2.2 HYDRAULIC CONDUCTIVITY: BACKGROUND

The concepts of permeability and hydraulic conductivity were invented by the French engineer Henry Darcy in 1856 when he experimented on sandy soils to determine the hydraulic conductivity. He introduced an equation (Eq. 2.1) to calculate the hydraulic conductivity, which became known as Darcy's law. Darcy's law is only valid for laminar flow and not turbulent flow (Hillel 2004).

$$Q = -KiA \qquad (2.1)$$

where:

Q	=	Flux of water (cm/s);
K	=	Hydraulic conductivity (m/h or cm/s);
i	=	Change in head (cm); and
A	=	Cross-sectional area (cm^2)

The term *hydraulic conductivity* is often confused with the term *permeability*. Permeability and hydraulic conductivity are two separate parameters, each with its own system of units (SI) (Nolen-Hoeksema 2014). These two parameters are influenced by different properties (Nolen-Hoeksema 2014). Permeability is influenced by soil medium properties only, such as the pore connectivity, grain size, and shape of grains (roundness/roughness) and not the fluid (Nolen-Hoeksema 2014). Hydraulic conductivity, also known as the coefficient of permeability, is influenced by the soil medium properties and the properties of the fluid, such as the viscosity (McKenzie & Jacquier 1997). The units of the hydraulic conductivity are expressed as length over time (cm/s or m/h) (Hillel 2004) and permeability as the square area (m^2) or millidarcy (mD) (Nolen-Hoeksema 2014).

The hydraulic conductivity is an important parameter within the engineering and water sector (Elhakim 2016). The hydraulic conductivity is a highly variable soil parameter (Judge 2013; Nagy *et al.* 2013; Fatehnia *et al.* 2014; Onur 2014; Elhakim 2016). There are various methods used universally for determining the hydraulic conductivity, and each method has its own particular range of accuracy (Fig. 2.1) (Nagy *et al.* 2013).

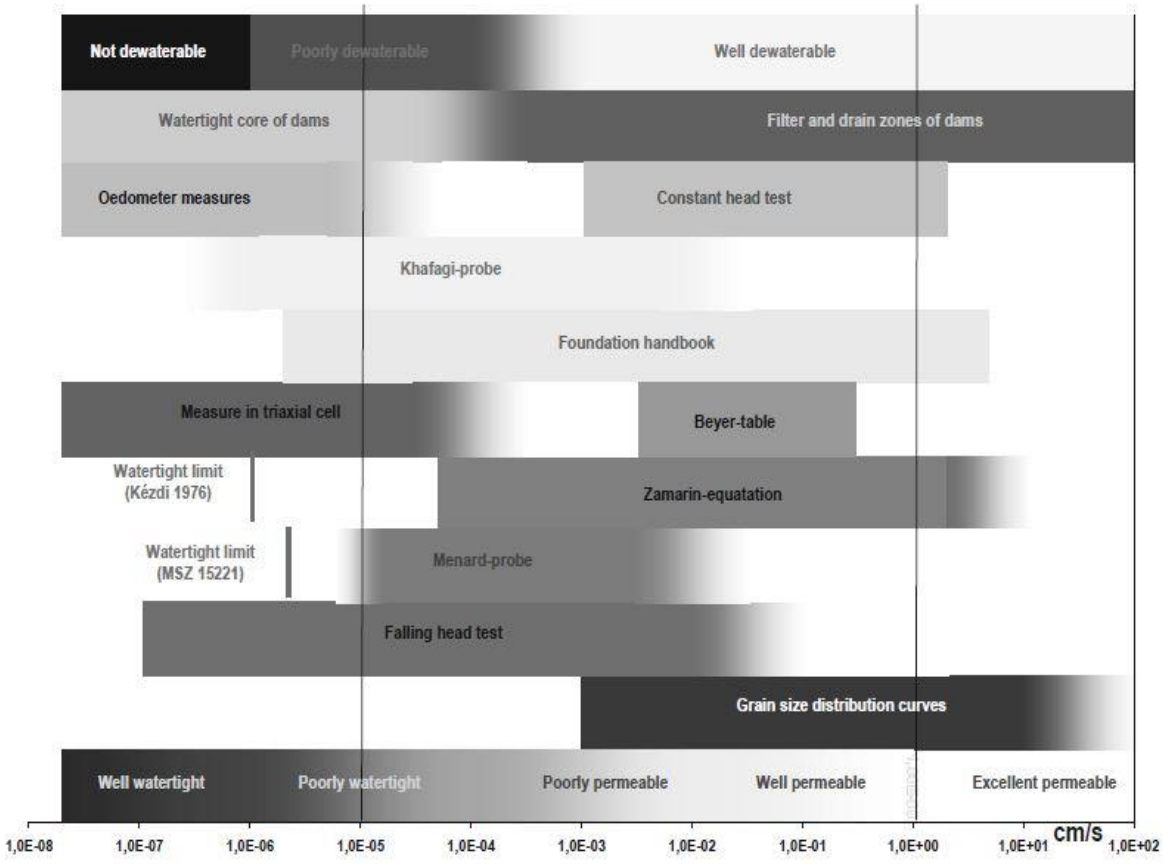

Figure 2.1. The predicted hydraulic conductivity of different methods by Nagy et al. (2013) that range from excellent permeable (coarse-textured or loose structured soils) to poorly permeable porous mediums (finer textured soils).

This makes the comparison of the hydraulic conductivity results between different methods challenging, however. Hydraulic conductivity can be determined by *in situ* methods, laboratory methods, and theoretical equations based on grain size distribution (Elhakim 2016). Recently it became possible to obtain the hydraulic conductivity of soil from microCT simulations as shown in Tracey *et al.* (2015) and Parvin *et al.* (2017).

The measurement of the hydraulic conductivity is essential for different industries, including the agricultural, engineering, petroleum, and water management industries (Elhakim 2016). In the agricultural industry, it is an important parameter for determining soil infiltration for crop production (Tracey *et al.* 2015).

The management of water is important for hydrological modelling to monitor runoff and groundwater flow for accurate measurements of the flow of water through soil (Tracey *et al.* 2015). Other concerns would be the leaching of fertilizers and other hazardous pollutants into

groundwater systems (Elhakim 2016). With accurate hydraulic conductivity results, modelling of groundwater flow can estimate or predict whether groundwater resources may be polluted (Elhakim 2016). In the engineering industry, for the development of landfill areas to cover efficiency, the soil needs to have a low hydraulic conductivity and avoid the drainage of contaminated water into valuable groundwater resources (Elhakim *et al.* 2016).

2.3 STANDARD METHODS FOR MEASURING THE HYDRAULIC CONDUCTIVITY

The hydraulic conductivity is a highly variable soil property (Nagy *et al.* 2013). Hydraulic conductivity can be measured in saturated (K_{sat}) and unsaturated conditions. During saturated hydraulic conductivity (K_{sat}) the movement of water is driven by the gravitational potential and with unsaturated hydraulic conductivity (K_{Ψ}) the movement of water is driven by the matric potential (Hillel 2004). The focus of this study is on the movement of water in saturated conditions. The reason for this is that the study of interest is focused on the wetting of soil to determine irrigation rates, the leaching of nutrients or pollutants into groundwater resources, and runoff for hydrological modelling.

The most commonly used *in-situ* method for determining the hydraulic conductivity is the pumping test method (Sandhoval *et al.* 2017) The most commonly used laboratory methods for determining the hydraulic conductivity are the constant hydraulic head test and the falling head test (Sandhoval *et al.* 2017). The *in-situ* and laboratory methods used to measure the hydraulic conductivity are time-consuming and laborious (Nagy *et al.* 2013; Elhakim 2016 and Sandhoval *et al.* 2017). These limitations have urged researchers to find alternative estimates. Researchers such as Hazan (1892); Kozeny (1927) and Carman (1956) cited in Chapius (2004); Terzagi & Peck (1964); Kenney *et al.* (1984); Alyamani & Sen (1993) cited in Onur (2014) developed theoretical equations to determine the hydraulic conductivity based on grain size. According to Nagy *et al.* (2013), however, the K_{sat} results of the same soil type differ for each method.

Nagy *et al.* (2013) and Elhakim (2016) stated that there is no relevant worldwide method for determining the hydraulic conductivity, because each method has its own range of validity and limitations. Rosza (1977 cited in Nagy *et al.* 2013) rejected the measurement of hydraulic conductivity in the laboratory, stating that laboratory results are inaccurate and recommending *in situ* methods such as the pumping test. The porosity of the soil that changes due to seasonal variations could make it difficult to measure the hydraulic conductivity *in situ* (McKenzie & Jacquier 1997). Kovacs (1972) recommended the use of theoretical equations based on grain size to determine the hydraulic conductivity due to its reliability and stated that both laboratory and *in situ* methods are laborious and time-consuming. The grain size distribution however, differs within heterogeneous soils. The theoretical equations do not make provision for this and the calculated K_{sat} value may be inaccurate (Chapius 2004). Therefore, only homogeneous soils with the same grain or particle size can provide reliable results from theoretical equations.

Other researchers such as Rethati & Kezdi (1972) preferred using laboratory methods for determining hydraulic conductivity. The advantages of laboratory methods include that they are less laborious than *in situ* methods. The K_{sat} can be determined for separate layers and the calculations can be done fairly easily by eliminating the corrections for three-dimensional flow (Elhakim 2016). The limitations with laboratory methods include that soils that swell are confined, creating unrealistic boundary conditions and the surface area is small (Nagy *et al.* 2013). Other limitations with the laboratory methods include that it is difficult to get undisturbed soil samples and the soil samples used for the experiment are always disturbed in some way (Elhakim 2016). Advancements in technology and associated software for high resolution microCT have introduced new possibilities for simulating fluid flow processes on a micro-scale based on pore-scale imaging, using computational fluid dynamics (CFD) models such as the Lattice and Boltzmann methods (Wildenschild *et al.* 2002).

2.4 X-RAY MICROCT APPLICATION

Computerized tomography (CT) involves the acquisition of projection images at various angles in a full 360° rotation around an object. The images are reconstructed into a three-dimensional (3D) volume (Du Plessis *et al.* 2016). The industrial CT scanner makes use of a microfocus X-ray source and a detector to obtain 2D images of a sample that, in turn, can be combined to create a 3D reconstruction of an object (Du Plessis *et al.* 2017). X-ray CT was first used in the medical field by Cormack (1973, cited in Taina *et al.* 2007) and, because it offers an internal non-destructive examination of objects, it provoked interest in the fields of geology and soil science in the early 1980s by Petrovic *et al.* (1982, cited Taina *et al.* 2007). The use of X-ray microCT is growing while there is also growth in computing power in terms of hardware and software, which opens up new application capabilities (Du Plessis *et al.* 2016).

MicroCT image-based data are constructed on the different densities of the material, based on the atomic numbers and physical density of the material (Cantatore & Muller 2011). The CT image-based data are presented based on grey values where dense material is lighter and less dense material is darker (Cantatore & Muller 2011). The benefits of X-ray microCT is that it can analyse an object in 3D and show the internal structures of objects non-destructively, therefore creating a better understanding of the object (Taina *et al.* 2007). In addition, the 3D images allow for realistic simulations, including the real irregular structures, to better understand the materials, as compared to idealized models. For example, the packing of irregularly shaped particles might be different in a real sample compared to an ideal model, and this might vary across the sample creating preferential flow paths.

2.4.1 X-ray microCT application in soil

The first CT results in soil science were presented by Petrovic *et al.* (1982), where the experiment showed a relationship between the bulk density and X-ray attenuation (Taina *et al.* 2007). Since

then X-ray microCT has been used widely in geological materials and its use is still growing in the fields of soil sciences and geological sciences (Cnudde & Boone 2013). The application of X-ray microCT is less time-consuming than laboratory methods and offers an analysis of several soil proxies such as 3D pore characterization, 3D grain analysis, fraction analysis, the monitoring of structural dynamics processes, fluid dynamics and many more (Cnudde & Boone 2013). The application is also very efficient and can analyse different parameters from one scanned soil sample, which will be time-consuming with laboratory methods. The use of X-ray microCT in soil science offers a good understanding of the nature and spatial configuration of soil components, and how it is related to the hydraulic behaviour of soil (Taina *et al.* 2007). X-ray microCT's ability to examine an object internally makes it favourable for use in the study of soil sciences (Taina *et al.* 2007). A microCT scanned soil sample can be visually examined by observing the internal structure of the soil, including particle size, pore connectivity, and pore sizes (Taina *et al.* 2007).

The use of X-ray microCT in soil has been applied in different areas of soil sciences, including soil solid constituents, physical properties, hydro-physical characteristics, and soil micro-biology as reviewed in Taina *et al.* (2007). This technique has been widely accepted in agricultural research, mainly because it is non-invasive and allows for repeated measurements on the same sample without causing changes to the object and without the need for any pre-treatment of the sample under study (Pires *et al.* 2010). The development of more modern scanners has also allowed for analyses with better and better resolutions (Pires *et al.* 2010). In the past, Crestana *et al.* (1986) highlighted the potential of CT to investigate soil water content. Rogasik *et al.* (2003), and Peth *et al.* (2010) used microCT to examine soil compaction and observe how hydraulic behaviour within soil influences the structure of the soil.

2.4.2 Limitations of X-ray microCT application in soil

The lack of a standardised sampling methodology makes the comparison of previous studies challenging (Taina *et al.* 2007). The resolution in X-ray microCT plays an important role in the acquisition of the CT images. The resolution is one of the factors that determine the image quality of a scanned object (Du Plessis *et al.* 2017). Higher resolution can produce good image quality but limit the field of view, much like in the case of an optical microscope (Du Plessis *et al.* 2017). A higher resolution is best used when analysing smaller objects, such as small soil particles, for more detail (Taina *et al.* 2007). In the case of soils with smaller particle sizes, for example soils with higher clay content, particles will not be visible since they are the same size or smaller than the scanned voxel size and features cannot be identified if they comprise of a single voxel (Mees *et al.* 2003). Therefore, the identification of the soil material/particles and air/void spaces is a challenging procedure. The resolution is one of the main limitations within the application of X-ray microCT. A higher resolution will require a smaller sample size (Mees *et al.* 2003). This can be challenging in the study of soil science. How representative is a soil sample size in relation to experiments happening *in situ*?

The energy (voltage) of the X-rays also affects the image quality of the X-ray CT scans (Wildenschild *et al.* 2002). Voltage (kV) is a key scan parameter and influences the intensity as well as the penetration depth of the X-ray beam (Cantatore & Muller 2011). If a soil sample is scanned at a lower voltage, it can affect the image quality of the soil sample, resulting in artefacts in the CT scan images (Du Plessis *et al.* 2020). Soil or geological formations are often made up of dense particles and therefore it is best to scan geological formations including soil at a higher voltage (Wildenschild *et al.* 2002). Soil materials consist of high-density material because of the high atomic number of the elements present in the soil material or particles (Taina *et al.* 2007). Both the resolution and voltage influence the image quality. The subsequent processing and analysis for an ideal CT scan image of a soil sample will be discussed. For more information on ideal scan parameters, the general guidelines in Du Plessis *et al.* (2017) can be consulted. The guidelines include aspects on artefacts.

2.5 X-RAY MICROCT FLUID FLOW SIMULATIONS

The growth in technology and software for fluid flow simulations based on pore-scale imaging are now performed on geological material (Bultreys *et al.* 2015). In a recent study, Bultreys *et al.* (2015) reviewed microCT flow simulations based on geological materials such as fractured coal (Cai *et al.* 2013) and sandstone (Raeini *et al.* 2014). Raeini *et al.* (2014) presented direct two-phase flow simulations on micro-CT images of sandstone and a sand pack for primary oil flooding followed by water injection. They used this upscaling approach to obtain the relative permeability curves from their simulations and compared their results with experimental measurements from other literature (Raeini *et al.* 2014). Fractured coal core samples were investigated for fracture analysis and to determine the influence of fracture network evolution on permeability through imaging X-ray microCT (Cai *et al.* 2013).

Fourie *et al.* (2007) showed that pore-scale fluid flow modelled by the Navier-Stokes equation can be used to derive the macro parameters, such as the hydraulic conductivity, of Darcy's Law. In their study, a real world geometry of coarse sand was obtained through X-Ray CT and then imported into Comsol to show that the microscopic modelling of flow mirrors the macroscopic results that can be obtained through regular laboratory analyses and calculation of flow through Darcy's Law (Fourie *et al.* 2007). Tracey *et al.* (2015) focused on the wet end of the water release characteristic (WRC) to investigate changes in soil water distribution in contrasting soil textures (sand and clay) and structures (disturbed and undisturbed samples) as well as to determine the impact of soil structure on hydraulic behaviour. Stokes equations for flow were used computationally for each measured structure to estimate the hydraulic conductivity, rather than Lattice Boltzmann simulation (Tracey *et al.* 2015). In their study, Tracey *et al.* (2015) presented hydraulic conductivity results based on microCT simulations, where the K_{sat} of sandy soils and clay soils were compared to a standard laboratory method (constant head device). The microCT simulated K_{sat} values compared very well with the standard laboratory method in their study

(Tracey *et al.* 2015). The sandy soil K_{sat} for the laboratory was 0.0013 cm/s, microCT simulated was 0.0014 cm/s and for the clay soils, the K_{sat} for the laboratory was 0.0004 cm/s, and microCT simulated was 0.0010 cm/s (Tracey *et al.* 2015).

2.5.1 Computational Fluid Dynamics

As previously mentioned, X-ray microCT offers insight into the internal structure of soil such as its pore network. The pore network or pore connectivity of the soil comprises of the areas within the soil where all the fluid transport occurs, such as the movement of water or air. Thus, the pore connectivity is an important aspect of the soil that needs to be investigated when it comes to the flow of fluid in a porous medium (Clausnitzer & Hopmans 1999).

The use of computational fluid dynamics (CFD) is a method that can model the flow of fluids on a micro-, meso- and macro-scale (Van Leer & Powell 2010). Since water and air movement occurs within the soil, the application of CFD is an ideal method to use for fluid flow simulations through the pore network of soil (Bultreys *et al.* 2016). Computational fluid dynamics is a computational tool that predicts fluid flow using mathematical modelling (governed by partial differential equations (PDE), discretization (modelling equations are discretized on computational grids) and iterations (Van Leer & Powell 2010). The PDE represents the conservation laws for the mass, momentum, and energy (Van Leer & Powell 2010). The Navier Stokes equation is part of a PDE. Computational fluid dynamics is the art of replacing such PDE systems with a set of algebraic equations, which can be solved using digital computers (Van Leer & Powell 2010).

2.5.2 Lattice and Boltzmann method

The Lattice and Boltzmann method (LBM) is a simplified CFD method, which closes the gap between macroscale and microscale fluid flow. The LBM is a modern approach to CFD and is considered a class of kinetic theory (Bultreys *et al.* 2016). The method considers the behaviour of a collection of particles as a unit (Bultreys *et al.* 2016). The property of the collection of particles is represented by a distribution function from the Lattice and Boltzmann equation (Eq. 2.2) presented by (Wagner 2008):

$$f(x + v_i, v_i, t + 1) - f(x, v_i, t) + F(v_i) = \frac{1}{\tau}\left[f^0(n, u, \Theta) - f(x, v_i, t)\right] \quad (2.2)$$

where:

v_i	=	Vector velocity;
$x + v_i$	=	Lattice position;
t	=	Time;
u	=	Velocity;
n	=	Density equilibrium;
f^0	=	Equilibrium distribution function; and
f	=	Distribution function;

In LBM, velocity and pressure are compacted as a momentum of the distribution functions (Bultreys *et al.* 2016). Lattice and Boltzmann rely on two simplified algorithms, namely streaming and collision (Bultreys *et al.* 2016). As a pore-scale flow simulation method, LBM considers a collection of fluid particles at each grid point (Tu *et al.* 2018). Each fluid particle moves on a lattice unit at its own velocity along one of the eight links of a grid (Tu *et al.* 2018).

The advantage of LBM is due to its relatively simple implementation, and its suitability for parallelization such as boundary conditions (Bultreys *et al.* 2016), making it computationally efficient. Furthermore, it has natural extensibility to represent multi-phase flow by tracking multiple types of interacting particles, each type representing a fluid phase, thereby removing the need to track interfaces explicitly (Bultrey *et al.* 2016). The run time scales approximately inversely with the real flow rate, making it difficult to accurately capture capillary-controlled flow on representative images (Bultreys *et al.* 2016). Other important limitations are that the numerical stability of the method is problematic in the situation of multiphase flows with large density and low viscosity (Bultreys *et al.* 2016).

CHAPTER 3 : MATERIALS AND METHODS

3.1 SAMPLING OF SOIL

The homogeneous soils were collected on a farm called Houmoed that is located between Stellenbosch and Somerset West (-34.009°, 18.786°) in the Western Cape region. The soil was collected in the field with a spade. The sample of 5 cm deep soil was sieved in the field by a 2 mm sieve to remove all the rocks and organic material from the soil. Thereafter the soil was further sieved in the laboratory which divided the soil into five different sand grades, namely very coarse sand (2 mm - 1 mm), coarse sand (1 mm - 0.5 mm), medium sand (0.5 mm - 0.25 mm), fine sand (0.25 mm - 0.1 mm) and very fine sand (0.1 - 0.05 mm). The sieve machine in the laboratory that divides the soil into different sand grades is also used as a method for textural class analysis for sandy soils. Textural analysis was performed in the laboratory on the soil collected at Houmoed and was classified as a coarse sand.

The heterogeneous soils were collected at different locations on the Welgevallen Experimental farm (-33.941°, 18.866° and -33.949°, 18.871°, respectively) of the Stellenbosch University in the Western Cape region. The soil was collected by means of a spade. This farm was chosen because there were a variety of sandy textured soils. The soil that was collected here included sandy clay, sandy loam and sandy clay loam. A pure fine Aeolic sand was collected near Lutzville (-31.559°, 18.351°) in the lower Olifants River region of the Western Cape. The coarse sand textured soil that was collected at the Houmoed farm was also used for this experiment on heterogeneous soil. In total, there were five different soil types of sandy soil for the heterogeneous soil.

The texture analysis was based on the U.S Department of Agriculture (USDA) classification for soil survey laboratory methods and procedures for collecting soil samples in their soil survey report (1972). The particle sizes were analysed by means of the pipette method (Gee & Bauder 1986). The pipette method uses Stokes Law to determine the silt and clay percentages in a soil sample (Gee & Bauder 1986).

3.2 SOIL SAMPLE PREPARATION FOR THE CONSTANT HYDRAULIC HEAD TEST

The above-mentioned soil with the five sand textural classes (sand fractions) was used for the constant hydraulic head test. The test was conducted in the laboratory on two sample sizes, namely the small column which was 3.5 cm in diameter and 11 cm in length, and the large column which was 19 cm in diameter and 16.3 cm in length.

The soil for both of these samples was packed at a standard bulk density of 1.5 g/cm^3 for the constant hydraulic head tests. The bulk density was calculated based on the core method as found in Blake and Hartge (1986) Equation 3.1. The dry soil was then packed into the columns.

In the small column, the length of the soil was 7 cm and for the large column, the length of the soil was 8.7 cm. The soil sample for the small column was 67.348 cm^3 in volume, which is 3.5 cm in diameter and 7 cm in length. The soil sample of the large column was 2466.700 cm^3 in volume, which is 19 cm in diameter and 8.7 cm in length.

$$\rho_b = \frac{\text{Mass of dry soil}}{\text{Volume of cylinder}} \quad (3.1)$$

At the bottom of the large column, there were four holes, each 5 mm in diameter, which were the outlet points for the water (Fig 3.1A). Half the column of the large sample was packed with gravel and the other half with soil (Fig 3.1B). The gravel was packed at the bottom of the column to allow water to flow gradually, and to prevent clogging or soil particles from falling out of the column through the four holes. A light nylon sieve material was placed between the soil and the gravel (Fig 3.1C). This was also done to prevent the finer particles of the soil from moving into the larger pore areas of the gravel (4 - 10 mm ø). Figure 3.1 shows the order in which the soil was packed in the large column.

At the bottom of the small column, a 3.5 mm diameter cap with five holes was inserted, and gravel (2 - 5 mm ø) was packed in the "cap" (Fig 3.2A & B). The cotton wool glass was placed above the gravel to separate the soil from the gravel within the small column (Fig 3.2C). The soil was then packed on the cotton wool glass up to 7 cm in length.

The standard pycnometer method presented by Blake and Hartge (1986) was used to measure the particle density of the homogeneous and heterogeneous soil. Three replicates of each of the total ten soils (homogeneous and heterogeneous soils) were used for the particle density analysis (3 x 10 = 30 samples). The values of the bulk density and the particle density of the soils were used to calculate the porosity based on equation 3.2 (Danielson & Sutherland 1986).

$$f = 1 - \left(\frac{\rho_b}{\rho_s}\right) \quad (3.2)$$

where:

f = Porosity or pore fraction soil (cm^3/cm^3);

ρ_b = Bulk density (g/cm^3 or kg/m^3); and

ρ_s = Particle density (g/cm^3 or kg/m^3).

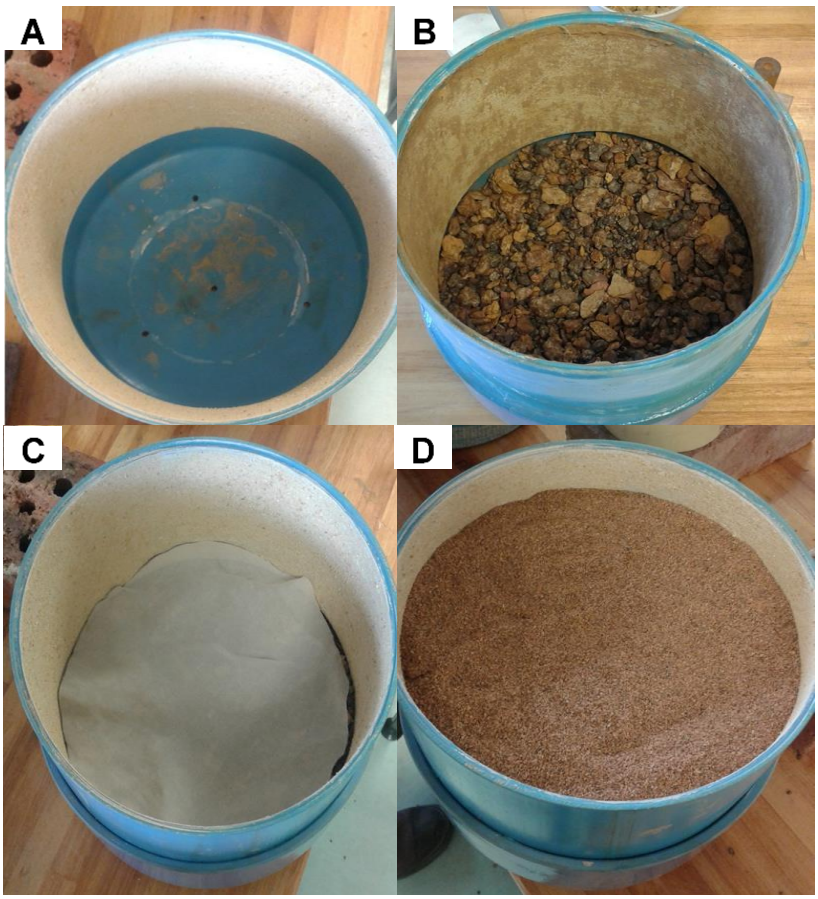

Figure 3.1. Illustration of soil packing for the determination of saturated hydraulic conductivity of homogeneous soils under laboratory conditions, where (A) represents the PVC pot with drainage holes used, (B) indicate is 7 cm thick gravel layer, (C) nylon sieve placed between gravel and selected soil, and (D) selected soil packed at a bulk density of 1.5 g/cm^3.

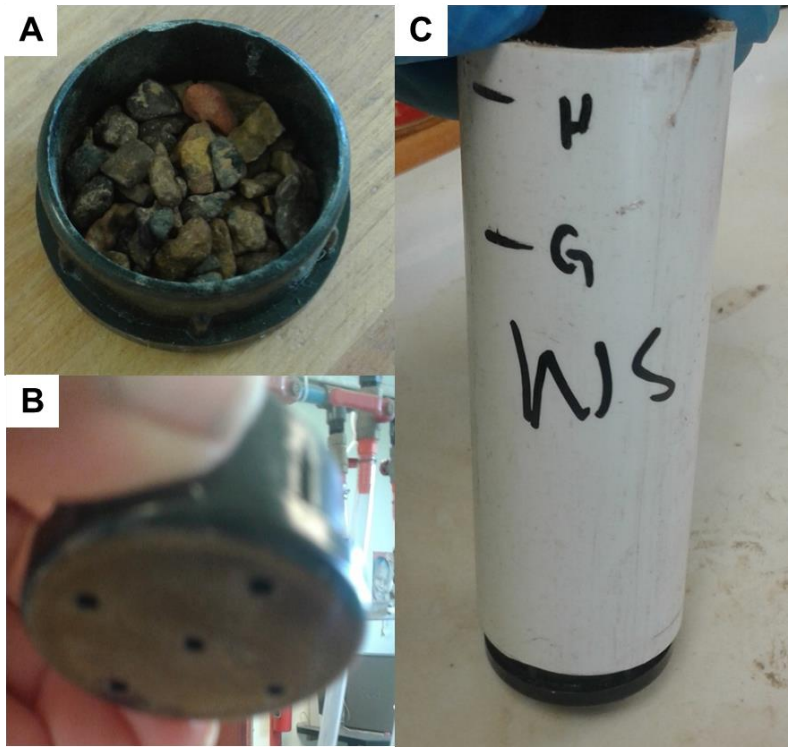

Figure 3.2. Presented in the figure above are (A) the gravel that was packed in the cap and (B) the five holes in the cap. An image of the (C) small column where the soil was packed in at a length of 7 cm for the constant hydraulic head test.

3.3 CONSTANT HYDRAULIC HEAD TEST OF THE LARGE COLUMN

The constant hydraulic head test was performed on the five different sand fractions of homogeneous soil (very coarse, coarse, medium, fine, and very fine sand). Only one soil column was sampled for each of the five sand fractions for the constant hydraulic head test. The constant hydraulic head test was repeated four times on the same sample. The setup of this constant hydraulic head test was not according to the laboratory method described in Klute and Dirksen (1986). The difference with this method was a ring column (8.5 cm in diameter & 10 cm in length) that was placed in the middle of the large column on top of the soil (Fig 3.3). The ring column was used to control the constant head (free-standing water level) above the soil.

Figure 3.4 shows an image of the constant hydraulic head test and Figure 3.3 shows a schematic presentation of the test. There were three inlet points (pipes) that were 2 cm in diameter where the water flowed into the soil column. A valve was used to control the inlet flow of water into the soil. The soil was fully saturated before the constant hydraulic head test was performed to ensure that the soil was completely saturated for measuring the saturated hydraulic conductivity (K_{sat}).

After the soil was fully saturated, only one pipe was used as an inlet point for water and it was placed in the middle of the smaller ring column (8.5 cm in diameter). The reason for not utilising the whole surface area was to prohibit potential preferential flow along the walls of the soil column due to the constant head of water being maintained at the surface. In the middle ring column, there was free-standing water at a level above the soil surface, while the constant hydraulic head test was conducted. The free-standing water level was maintained at a constant hydraulic head of 2 cm above the soil surface by opening and closing the valve only when the water level dropped. The water level had to be at a constant head to ensure that the flow rate of water into the soil column was constant. A funnel was placed under the larger column to capture the volume of water into beakers.

The outflow of water through the soil sample between time intervals was captured by different beakers. The time intervals differed depending on the texture of the soil. For very coarse and coarse sand, the time intervals were 10 sec, for medium sand there were 1-minute time intervals, for fine sand it was 5 minutes and for the very fine sand 10 minute time intervals were used. Eleven beakers were used for the duration of the measurements. The saturated hydraulic conductivity was calculated as follows using the Darcy's Law equation (Eq. 3.3) for the constant hydraulic head test based on Hillel (2004) and Klute and Dirksen (1986):

$$K = \frac{VL}{At\Delta\Psi_h} \tag{3.3}$$

where:

V = Volume water that flows through soil column (cm^3);

L = Length of the soil column (cm);

A = Soil surface area within the soil column (cm^2);

t = Time (seconds); and

$\Delta\Psi_h$ = Change in the hydraulic head potential (cm).

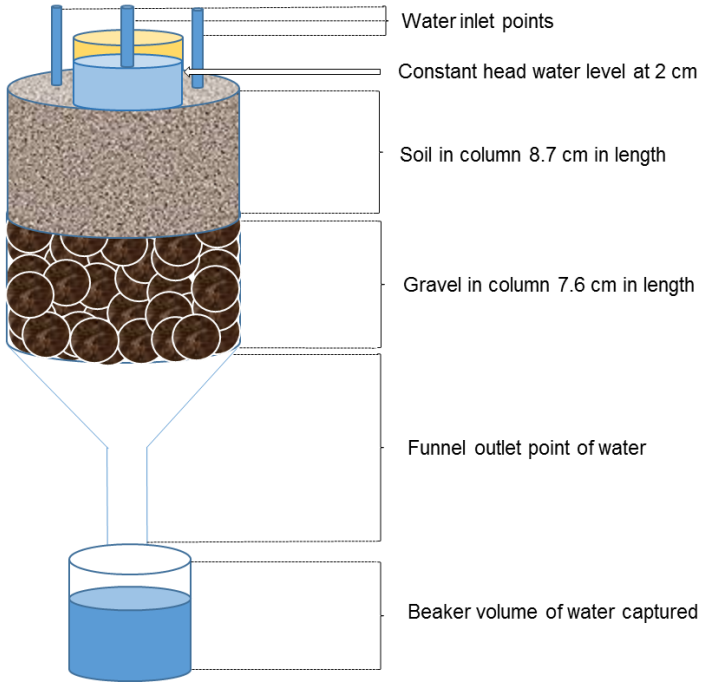

Figure 3.3. A schematic presentation of the constant hydraulic head test setup. There were three inlet points for the water. The small column with a diameter of 8.5 cm was placed in the middle of the larger column, and the soil was packed at 8.7 cm in length of the larger column, separated with the gravel by the nylon sieve. Gravel was packed in the larger column at 7.6 cm in length, and the funnel was the outlet point of the water. The volume of water was then captured in a beaker.

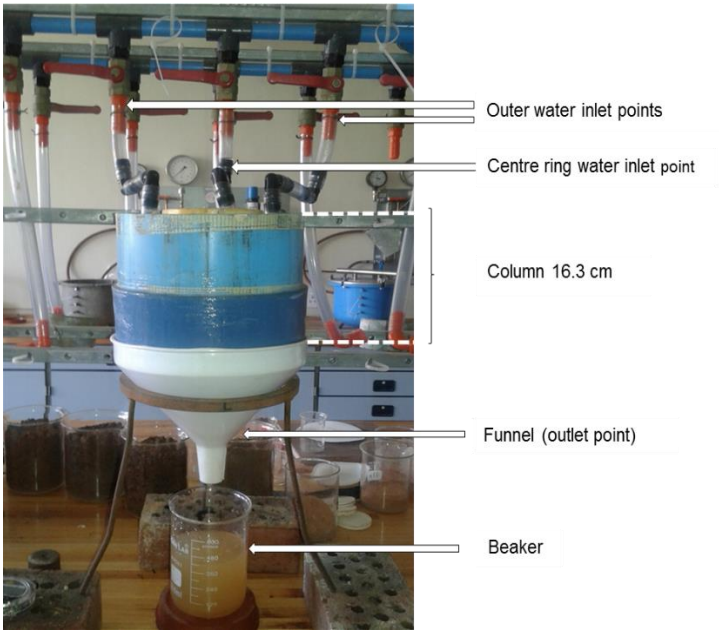

Figure 3.4. An image of the constant hydraulic head test setup showing the three water inlet points, the entire large column of the soil (16.3 cm in length), the funnel which was the outlet point and the beaker in which the volume of water was captured.

The constant hydraulic head of the free-standing water level (2 cm) was used to calculate the change in the hydraulic head potential, based on the principles of the soil water potential (Table 3.1). The soil hydraulic potential (Ψ_h) is driven by the gravitational potential (Ψ_g), matric potential (Ψ_m), and hydrostatic pressure potential (Ψ_{sp}). Water in soil moves from a high hydraulic potential point A to a low hydraulic potential point B (Fig 3.5). The gravitational potential is driven by gravity and is determined relative to the arbitrarily chosen reference level (Fig. 3.5). Above the reference level, the Ψ_g is positive and below the reference level, it is negative (Table 3.1). The Ψ_m originates from the force of adsorption that the soil matrix (pores and particles) exercises on the water molecules. The Ψ_m is always negative and when the soil is saturated it is equal to 0 (Table 3.1). The Ψ_{sp} is only present when there is a water table present. The Ψ_{sp} increases along with the depth below the water table and is always positive (Table 3.1 and Fig. 3.5). The Ψ_h is the sum of the Ψ_g, Ψ_m and Ψ_{sp} and determines the water flow direction (Table 3.1). The change of the hydraulic potential is the difference between points A and B (Fig 3.5) shown in (Table 3.1).

When calculating the K_{sat} it is important to note that the middle ring column (8.5 cm diameter) surface area was used as shown in Figure 3.6. In Figure 3.6 is the schematic presentation example of very coarse sand soil samples to illustrate how the parameters to calculate the K_{sat} was obtained. Equation 3.4 shows an example of how the K_{sat} was calculated for very coarse sand.

Table 3.1. The components for calculating the change in soil hydraulic potential ($\Delta\Psi_h$).

	A	B
Ψ_g (Gravitational potential)	0	-7.25
Ψ_m (Matric potential)	0	0
Ψ_{sp} (Hydrostatic potential)	2	7.25
Ψ_h (Hydraulic potential = Ψg + Ψm + Ψsp)	2	0
$\Delta\Psi_h$ (A – B) = (2 - 0)	2	

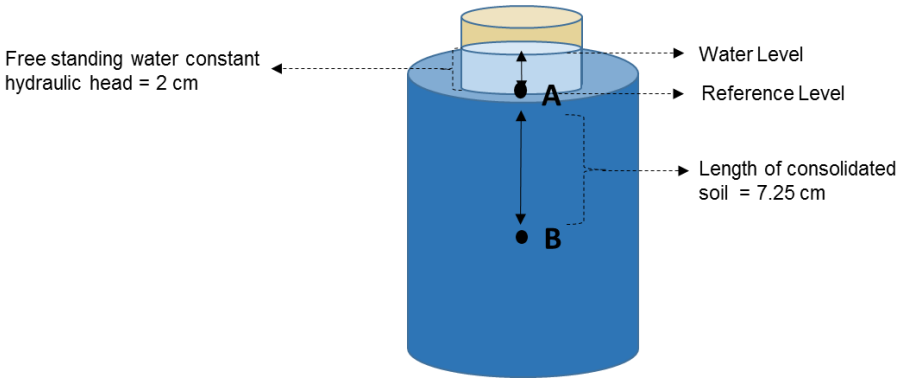

Figure 3.5. A schematic illustration of the change of hydraulic head in the soil based on the principles of the soil water potential, and showing the water level, reference level point (A) and point (B) as the length of the consolidated soil.

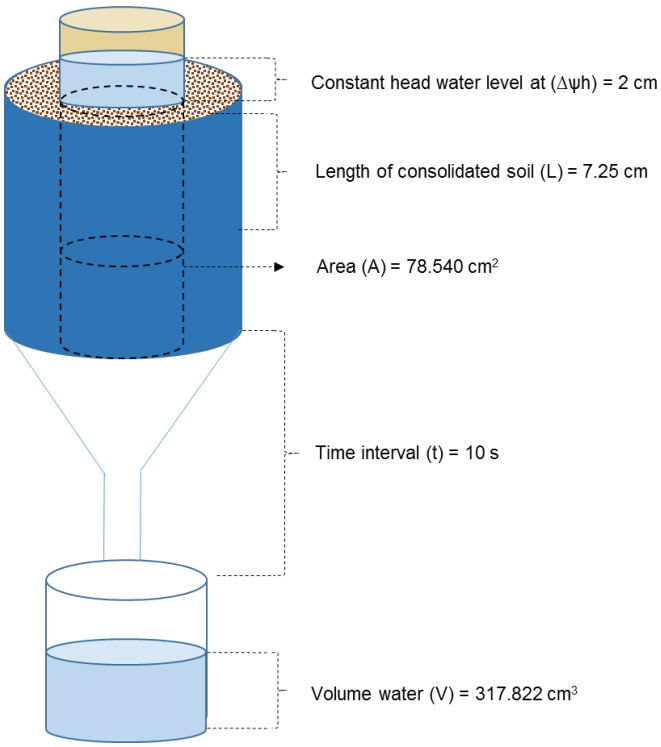

Figure 3.6. A schematic presentation showing the values used to calculate the saturated hydraulic conductivity (K_{sat}) of the very coarse sand.

$$K = \frac{VL}{At\Delta\Psi_h} \tag{3.4}$$

$$K = \frac{(317.822cm)(7{,}25cm)}{(78.540cm^2)(10s)(2cm)}$$

$$K = \frac{2304.201cm^2}{1570.8cm^3/s}$$

$$K = 1.467\ cm/s$$

3.4 CONSTANT HYDRAULIC HEAD TEST OF THE SMALL COLUMN

The constant hydraulic head test was performed on the five different sand fractions of the homogeneous soil and the five different soil types of the heterogeneous soil. A beaker was placed under the sample to capture the outlet flow of water. The inlet point of water was through a burette, and water flow was controlled with a valve. The soil sample was first fully saturated before the test was performed. A free-standing water level of 2 cm was kept above the soil surface to ensure a constant hydraulic head. This was maintained by controlling the flow rate of water through the inlet point. The flow rate through the inlet point of the burette varied depending on the type of soil.

The outlet of water was captured in the beaker at different time intervals with different beakers. The time intervals differed depending on the texture of the soil. For the very coarse sand, the time intervals were 5 sec, for the coarse sand it was 10 sec, for the medium sand it was 1 min, and for the fine and very fine sand it was 5 min. The constant hydraulic head test setup in the laboratory

is presented in Figure 3.7 and a schematic presentation thereof can be seen in Figure 3.8. Provision was made for preferential flow along the sides of the columns. This was done by altering the smooth sides of the column with the help of glue and coarse sand before the soils were packed into the column. The saturated hydraulic conductivity was calculated using Darcy's Law (Equation 3.3) for the constant hydraulic head test.

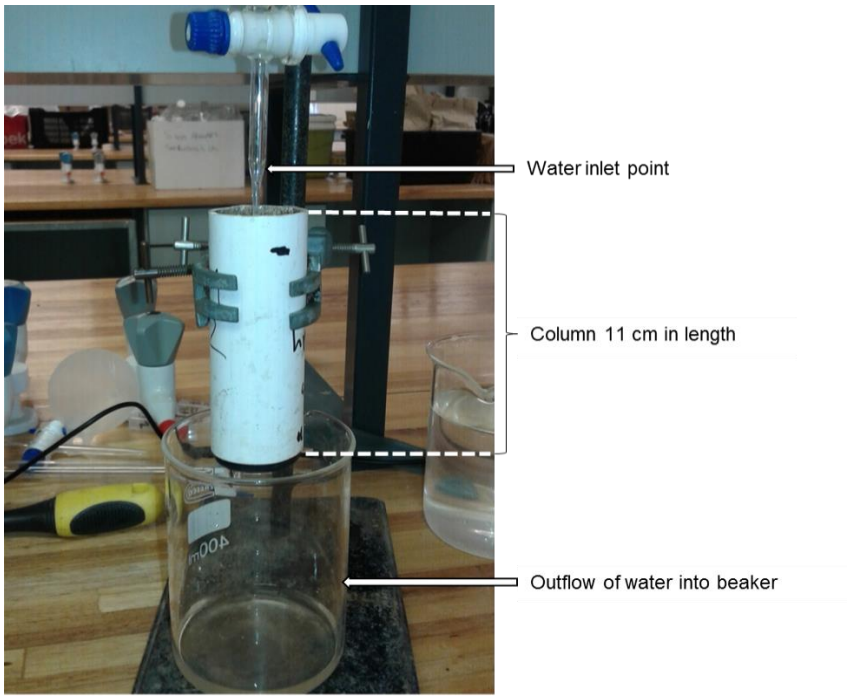

Figure 3.7. This image illustrates the setup of the constant hydraulic head test of the small column. The inlet point of the water was through a burette. The soil column was 11 cm in length and 3.5 cm in diameter. The outflow of the water was captured in a beaker.

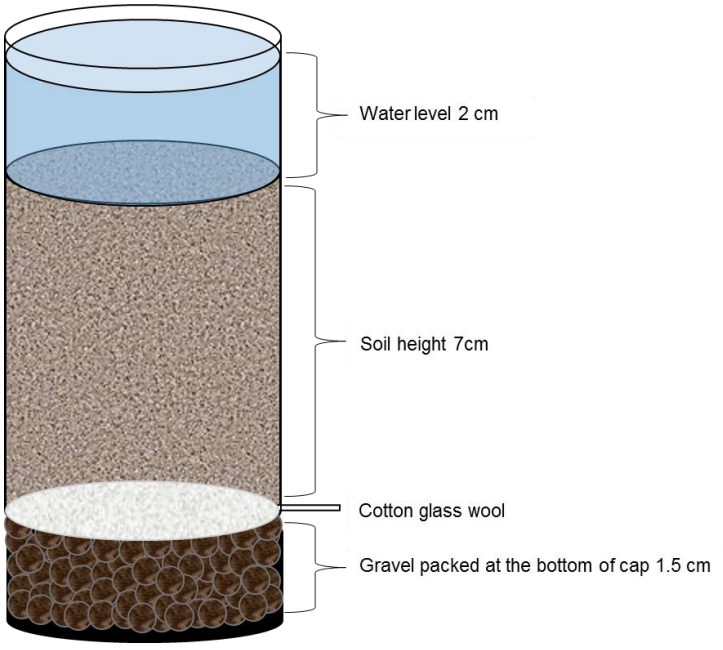

Figure 3.8. A schematic presentation of the inside of the small column, showing the water level at 2 cm, the height of soil at 7 cm, and the cotton glass wool on the top of the gravel that was packed in the cap.

3.5 X-RAY MICROCT SIMULATIONS AND IMAGE ANALYSIS SAMPLE PREPARATION

The homogeneous and heterogeneous soil for the X-ray microCT scans was sampled from both the small and large column that was used for the constant hydraulic head test. Three replicate samples of the homogeneous soil were sampled from the large column with a cuvette, for the microCT scans at 15 µm, and a plastic straw for scans at 5 µm. The heterogeneous soils were sampled from the small column and four replicate samples of the five different textured soil were sampled with a cuvette.

The soil columns of both the homogeneous and heterogeneous soils were first saturated before the soils were sampled for microCT scans. This was to sample the soil in a saturated condition. The sample volume of the cuvette was 3.5 cm^3 (which was a 1 cm × 1 cm square tube, 3.5 cm in length) and the sample volume of the plastic straw was 0.687 cm^3 (which was 0.5 cm in diameter and 3.5 cm in length). The cuvettes and plastic straw were inserted into the small and large soil column that was used for the constant hydraulic head test (Fig 3.9).

After the soils were sampled with the cuvettes and the plastic straws, super glue was applied underneath the sample to prevent the soil from dislodging. The cuvette and plastic straw samples were placed in a refrigerator freezer overnight. The samples were frozen to prevent water from draining out of the soil and ensure that the soil sample remained in its saturated condition.

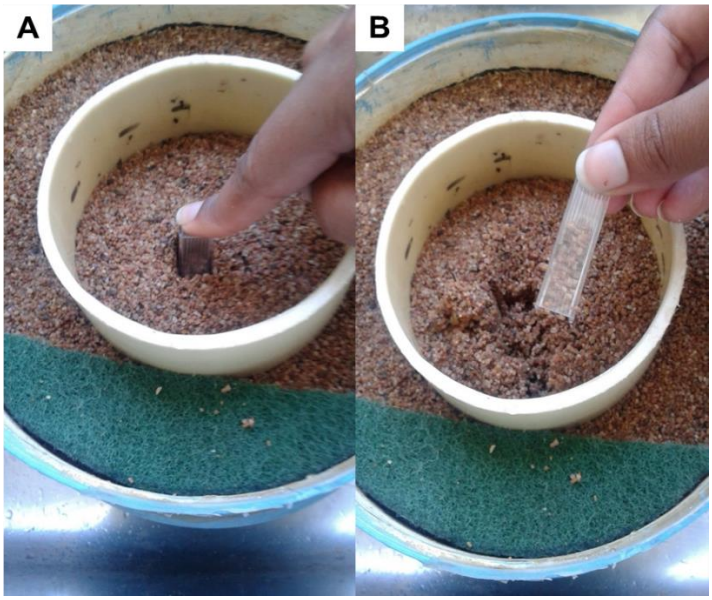

Figure 3.9. An example of the cuvette (3.5 cm^3 volume, 1x1 cm square tube and 3.5 cm in length) that was used to sample the coarse sand soil. The cuvette was (A) inserted into the larger soil column and then removed by scooping up the soil (B).

3.6 X-RAY MICROCT SCANNING OF THE SOIL SAMPLES

The experiment was performed on a high-resolution industrial X-ray microCT system. First, an experimental test scan was performed on a medium sand sample to test the effects of the voltage parameter. The medium sand sample was scanned at a resolution of 10 µm. The X-ray

parameters were set to a voltage of 80 kV and a current of 200 µA. The parameters were set at a lower voltage and higher current to observe the effects it might have on a scanned soil sample.

The time duration for the scan was 45 minutes. The scan time is the acquisition time of single projection images, which can vary from system to system due to detector sensitivity and dynamic range differences, X-ray tube brightness differences, and differences in physical distance from the source to the detector (Du Plessis *et al.* 2017). All systems have variable image acquisition times, and therefore scan times can vary considerably. To obtain the highest possible scan quality, the full dynamic range of the detector should be explored. By doing so, the image contrast is maximized by raising the image acquisition time to near saturation of the detector for a particular x-ray setting. If the image acquisition time is too low, the resulting contrast will be poor and it may even result in grainy images in extreme cases.

For the microCT simulations and porosity analysis, the homogeneous soils were scanned at different resolutions. The homogeneous soil samples were scanned at 15 µm for the 3.5 cm^3 cuvette samples and 5 µm for the 0.687 cm^3 plastic straw samples (Fig. 3.10). The heterogeneous soil samples of the cuvettes were scanned at a resolution of only 15 µm. Other scan parameters were set at 180 kV voltage and 80 µA current.

Scans were also performed on the one sample of the small column 67.348 cm^3 in volume (3.5 cm in diameter, 7 cm in length) used for the constant hydraulic head test of the different sand fractions (homogeneous soil). One sample (small column) of each of the five different soils (heterogeneous soils) were scanned before and after the constant hydraulic head test (small column). These samples were all scanned at 40 µm with scan parameters of 180 kV voltage and 80 µA current. A 0.5 mm copper (Cu) filter was used for beam filtering to reduce the polychromaticity of the beam by preventing streaky artefacts. The estimated scanning time was approximately 30 min for each scan. The scanning and considerations for optimized scan parameters are described in Du Plessis *et al.* (2016); Du Plessis *et al.* (2017).

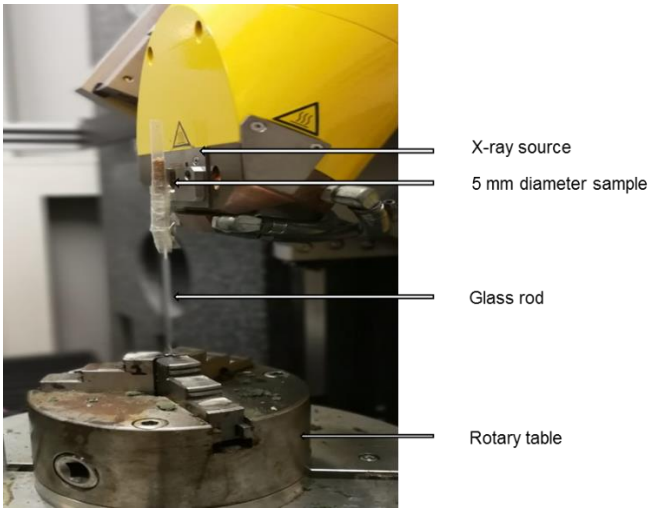

Figure 3.10. The setup of the X-ray micro-computer tomography (microCT) scan of the plastic straw soil sample that is mounted on a glass rod for scanning using micro-computer tomography at a 5 µm resolution.

3.7 RECONSTRUCTION, IMAGE ANALYSIS AND FLOW SIMULATIONS

The software used for the reconstruction was Phoenix Datos© and produced a 3D volumetric data set. The reconstructed 3D microCT volumes were visualized and analysed using VGStudioMax© 3.1 (Volume Graphics) software. The original 3D CT volume of the cuvette soil samples scanned at 15 µm (3.5 cm^3) was further segmented by the region of interest (ROI) tool into a subvolume (0.519 cm^3) with the following dimensions for each soil sample: 0.54 cm in height, 0.59 cm in width and 1.63 cm in depth. This was done to ensure that there were no boundary effects from sampling. The CT volume of the plastic straw soil samples (0.687 cm^3) that were scanned at 5 µm were segmented using the ROI tool, into a subvolume (0.077 cm^3) with the following dimensions: width of 0.31 cm, height of 0.30 cm and depth of 0.83 cm.

The small column (67.348 cm^3) of the different sand fractions used for the constant hydraulic head test was scanned at 40 µm, and segmented using the ROI tool into a subvolume of 37.989 cm^3 with the following dimensions: 2.50 cm in height, 2.52 cm in width and 6.03 cm in depth for each soil sample. Due to resolution limitations, the microCT analysis and simulations were performed only on the very coarse sand. The same dimensions were used on all the samples for the extraction of the subvolumes from the plastic straw (0.687 cm^3), cuvette (3.5 cm^3) and small column (67.348 cm^3).

The microCT analysis and simulations of the samples scanned at 5, 15 and 40 µm were performed on the extracted subvolumes. The segmentation of the soil material was done with the use of the surface determination tool found in the VGStudioMax© 3.1. The surface determination tool is a thresholding technique based on a greyscale value of each voxel. The advanced surface determination tool was used, and the selection of the material threshold was done manually from the isosurface graph. This method is described in more detail in Le Roux *et al.* (2015).

Image segmentation involves the classification of voxels (3D volumetric pixel = voxel) within a 3D CT volume that have the same grey scale values. In this case, the segmentation of the soil material aims to distinguish between the soil particles and pore spaces within a soil sample through the segmentation process. After the segmentation of the soil material, an absolute permeability test (microCT simulation) was performed and the porosity was analysed.

To validate the methodology, a series of simulations were conducted using one 3D volume data set of the medium sand sample scanned at 10 µm. The microCT simulation was performed at different simulation cell sizes, namely 1, 2, 3, 4, 5, 10, 15, 20, 25 and 30, respectively. This is a typical convergence test to show how the absolute permeability results converge to a more accurate result, as the simulation cell size decreases.

The microCT simulations performed on the VGStudioMax© 3.1 software is an absolute permeability test. Simulation is based on Stokes flow (Eq. 3.5) which is a simplification of the Navier-Stokes equation.

$$\mu\Delta v\text{-}grad\ p=0; div\ v=0 \quad (3.5)$$

where:

v = Velocity of fluid;

p = Pressure;

μ = Viscosity;

Δ = Laplace operate;

grad = Gradient operate; and

div = Divergence operate

This implies that when the viscosity is high, flow velocity and Reynolds number is low because the flow is laminar within a saturated porous medium. The simulation is performed based on the Lattice and Boltzmann equation (Du Plessis *et al.* 2018). Inputs in the simulation are the material and pore spaces (use of surface determination tool), only single fluid type, the chosen inlet and outlet planes for the simulation (parallel planes), open or sealed boundaries, the pressure difference between inlet and outlet planes, and the viscosity of the fluid. The embedded boundary conditions are prescribed by Darcy's Law (Eq. 3.6) which postulates a linear pressure drop in the sample. If the average flow velocity is in the same direction as the applied pressure gradient, the permeability (k) is computed from the simulation results as per equation 3.7 from Darcy's Law.

$$\langle v \rangle = \frac{k}{\mu}\frac{dp}{dL} \quad (3.6)$$

$$k = -\langle v \rangle\ \mu dL/dp \quad (3.7)$$

where:

‹v› = Volume average velocity;

k = Permeability;

μ = Viscosity;

dp = Pressure difference between inlet and outlet; and

dL = Length of sample

The simulations were performed by selecting the top plane view for both the inlet and outlet plane coordinates. The embedded boundary condition was used to simulate the flow in the laboratory through a soil column. The settings for the viscosity were set at 0.0089 Pa.s, which is the viscosity of water. The maximum number of iterations was set to 5000, and the rest of the settings were kept on default. After the simulations were performed and the computer simulated permeability (k) was obtained, the K_{sat} was calculated by using the equation 3.8 based on Darcy's Law (Hillel 2004).

$$k = \frac{K\eta}{\rho g} \tag{3.8}$$

where:

k	=	Permeability (m^2);
K	=	Hydraulic conductivity (m/h or cm/s);
μ	=	Viscosity (Pa.s or kg/m/h or g/cm/s);
ρ	=	Density of water (kg/m^3 or g/cm^3); and
g	=	Gravitational acceleration (m/s^2 or cm/s^2)

Additional analysis for the porosity was also carried out with VGStudioMax© 3.1. The porosity analysis of the CT volume data was analysed from the morphometric indices based on the surface determination. The material to total volume is express as a volume fraction, and the porosity is calculated with equation 3.2. The material of the volume was the solid fraction (Bone volume BV/ Total volume TV) (Du Plessis *et al.* 2018). The solid fraction replaces the bulk density over particle density as shown in equation 3.2 and is shown below.

$$f = 1 - \left(\frac{\rho_b}{\rho_s}\right) \tag{3.2}$$

or

f = 1 - Solid Soil Fraction

where:

f	=	Porosity or pore fraction soil (cm^3/cm^3);
ρ_b	=	Bulk density (g/cm^3 or kg/m^3); and
ρ_s	=	Particle density (g/cm^3 or kg/m^3)

3.8 CALCULATING THE SATURATED HYDRAULIC CONDUCTIVITY BASED ON GRAIN SIZE

The K_{sat} was calculated from equations based on their grain size distribution for only the homogeneous soils. The two theoretical equations based on grain size distribution that were used for calculating the hydraulic conductivity were the Kozenzy-Carmen equation given in Equation 3.9 and the Hazen equation given in Equation 3.10 (Chapius 2004).

$$K = \frac{150}{(d)^2} \times \frac{(1-n)^2}{n^3} \tag{3.9}$$

where:

n	=	Porosity (%) or (cm^3/cm^3);
d	=	Diameter of grain size (mm); and
K	=	Hydraulic conductivity (m/h or cm/s)

$$K = CD_{10}^{2} \quad (3.10)$$

where:

C = Constant and is 1;

D_{10} = Diameter of particle corresponding 10% passing weight; and

K = Hydraulic conductivity (m/h or cm/s)

The Kozenzy-Carman equation uses the porosity and diameter of grain size to determine the hydraulic conductivity, whereas the Hazen equation only uses the grain size to determine the hydraulic conductivity (Chapius 2004). The porosity values used to calculate the hydraulic conductivity with these equations were determined in the laboratory at a bulk density of 1.5 g/cm^3. The diameter of the grain size used for the equations was the lower limit of the grain size of the homogeneous soil. These two equations are commonly used equations and suitable for homogeneous soils. The equations are also applicable for laminar flow which is the principle of Darcy's Law (Elhakim 2016).

3. 9 STATISTICAL ANALYSIS

The raw data were captured and sorted in Microsoft® Excel. Correlation and regression analysis were done up to 5% significance level with Microsoft® Excel and Statsgraphics® software (Statsgraphics Technologies Inc., The Plains, Virginia).

CHAPTER 4 : RESULTS AND DISCUSSION

4.1. HOMOGENEOUS SOIL RESULTS AND DISCUSSION

4.1.1 Results of the soil texture analysis

The soil textural analysis results of the different sand fractions (very coarse, coarse, medium, fine, and very fine sand) are given in Table 4.1.

Table 4.1. The soil texture analysis results of the different sand fractions.

Sand Fraction	Clay	Silt	Sand	Very coarse sand (%)	Coarse sand	Medium sand	Fine sand	Very fine sand
Very coarse sand	1.1	2.2	96.7	100.0	0.0	0.0	0.0	0.0
Coarse sand	1.5	2.1	96.4	0.0	100.0	0.0	0.0	0.0
Medium sand	3.3	3.0	93.7	0.0	0.0	100.0	0.0	0.0
Fine sand	7.0	16.6	76.5	0.0	0.0	0.0	100.0	0.0
Very fine sand	16.9	23.1	60.0	0.0	0.0	0.0	0.0	100.0

4.1.2 Saturated hydraulic conductivity (K_{sat}) results of the constant hydraulic head test and microCT simulations.

4.1.2.1 The relationship between the saturated hydraulic conductivity and the lower limit particle size

The relationship between the constant hydraulic head test measured K_{sat} of the large soil column and the lower limit of the particle size is given in Figure 4.1. As the particle size increases so does the K_{sat} (Fig. 4.1). The very coarse sand has the highest K_{sat} results and the very fine sand has the lowest K_{sat} results (Fig 4.1). There were four replicate samples for each of the sand fractions. The variation of the K_{sat} results between the number of replicates increases as the particle size of the sand fractions increases, as shown in Figure 4.1. The K_{sat} of the very coarse sand shows more variation between the number of replicates at a lower limit particle size of 1 mm (Fig 4.1). The very fine sand K_{sat} results showed less variation between the number of replicates at a lower limit particle size of 0.05 mm (Fig 4.1).

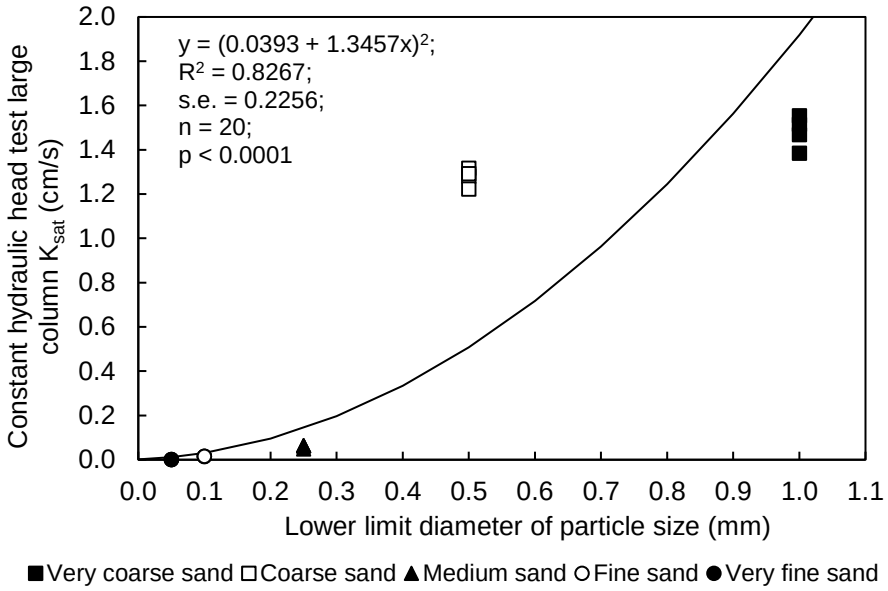

Figure 4.1. The relationship between the saturated hydraulic conductivity (K_{sat}) determined using the constant hydraulic head test within the large soil column and lower limit diameter of the particle sizes of the different sand fractions. The number of sample replicates for each of the sand fractions were four.

The K_{sat} results, measured by the constant hydraulic head test, of the small soil column to the lower limit of the particle size is given in Figure 4.2. There was more variation between the number of replicates of the very coarse sand K_{sat} values (Fig 4.2). Figure 4.2 shows that there was a decrease in the variation between the number of replicates as the K_{sat} and the particle size decreases. The K_{sat} of the very fine sand showed less variation between the number of replicates.

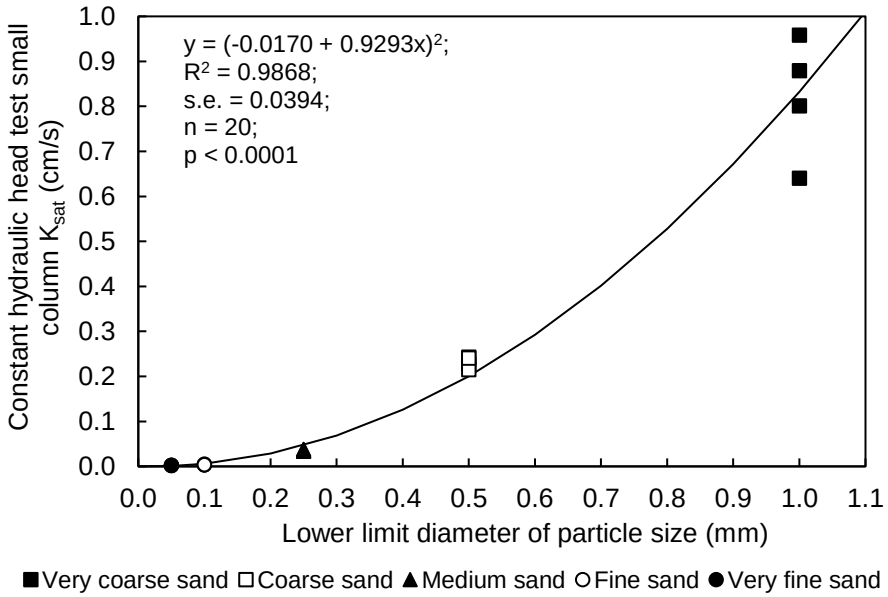

Figure 4.2. The relationship between the saturated hydraulic conductivity (K_{sat}) that was determined by the constant hydraulic head test of the small soil column and the sieve determined lower limit of the particle size of the different sand fractions. The number of replicates for each sand fraction were four.

Figure 4.3 shows the relationship between the microCT simulated K_{sat} (sample scanned at 15 µm) and the lower limit of the particle size for the different sand fractions. The number of sample

replicates was three for each of the different sand fractions of both the 15 µm and 5 µm scanned samples. The larger the particle size, the higher the K_{sat} and the variation between the number of replicate samples (Fig 4.3). Very coarse sand, coarse sand and medium sand showed a high variation in K_{sat} values between the number of replicate samples (Fig 4.3) whereas the fine sand and very fine sand showed no variation in K_{sat} values between the number of replicates.

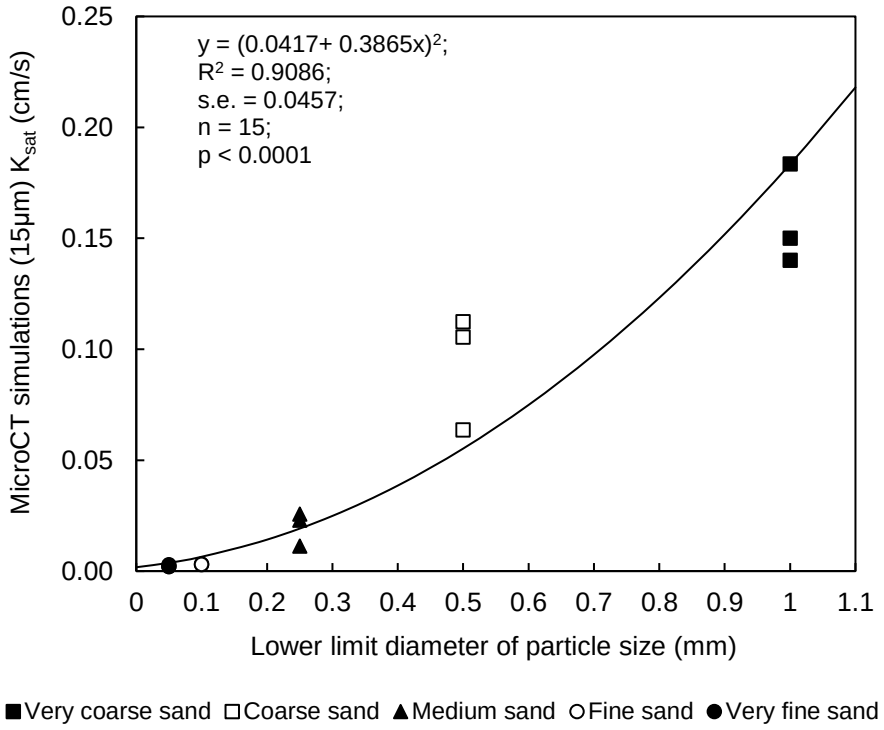

Figure 4.3. The relationship between the saturated hydraulic conductivity (K_{sat}) that was determined by the X-ray micro-computer tomography (microCT) simulation sample scanned at 15 µm resolution (cuvette) and the sieve determined lower limit of the particle size of the different sand fractions. Three sample replicates of each sand fraction were use.

The relationship between the microCT simulated K_{sat} (sample scanned at 5 µm) and the lower limit particle size of the different sand fractions is given in Figure 4.4. The very coarse sand has the highest K_{sat} values and the very fine sand K_{sat} values has the lowest (Fig 4.4). There was a high variation in the K_{sat} values between the number of replicates of the very coarse sand and the coarse sand (Fig 4.4). The variation in the K_{sat} values between the number of replicates of the fine sand and medium sand were low (Fig 4.4). There was no variation between the number of replicates for the K_{sat} of the fine sand (Fig 4.4).

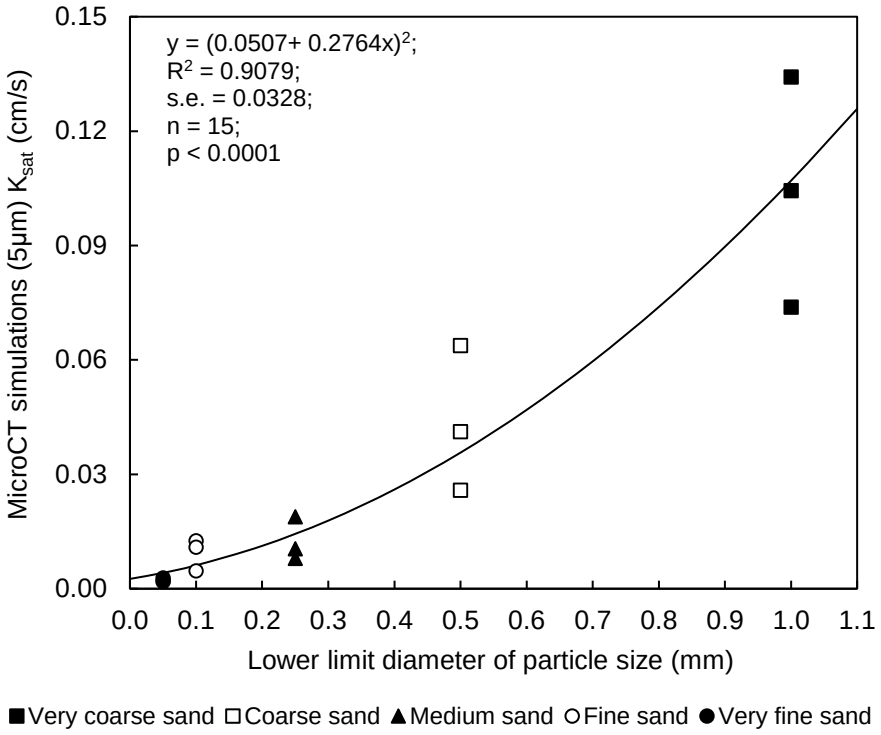

Figure 4.4. The relationship between the saturated hydraulic conductivity (K_{sat}) that was determined by the X-ray micro-computer tomography (microCT) simulations of the sample scanned at 5 µm (plastic straw) and the sieved determined lower limit of the particle size of the different sand fraction. Three sample replicates of the sand fractions were use.

Soil that consists mainly of larger particle sizes have larger pore sizes resulting in more interconnectivity between the pores, therefore water moves faster resulting in a high K_{sat} as shown in Figure 4.1 to 4.4. Soil with mainly smaller particle sizes have smaller pore sizes, resulting in less interconnectivity between the pores, therefore the conduction of water will be slower resulting in a low K_{sat} (Fig 4.1 to 4.4). The order of magnitude of the K_{sat} is determined by the grain size/particle size of soils (Nagy *et al.* 2013, Elhakim 2016). Nolen-Hoeksema (2014) also reported that hydraulic conductivity is proportional to particle size. The texture and structure of soil influence the hydraulic properties of soil, such as the K_{sat} (McKenzie & Jacquier 1997).

The variation between the number of replicates of the very coarse sand was caused by the large pore areas that result in higher flow velocities, making the flow turbulent especially within the constant hydraulic head test. Similar results were found by Sandhoval *et al. (*2017) where they compared the hydraulic conductivity results of the falling head and constant head test of different kinds of permeable cement. The permeable cement that had larger pore areas and larger particles had more variation between the number of replicates of the hydraulic conductivity results (Sandhoval *et al.* 2017). In laminar flow conditions as with the finer particles, the hydraulic conductivity values will be constant which will result in less variation between the hydraulic conductivity (Sandhoval *et al.* 2017).

4.1.2.2 Comparison of saturated hydraulic conductivity determined by different methods

The K_{sat} values of the constant hydraulic head test of the small column (y-axis) and the large column (x-axis) fit against the 1:1 line is given in Figure 4.5 (A) (very coarse and coarse sand) and (B) (medium, fine and very fine sand). The K_{sat} values of the very coarse and coarse sand were underestimated by the constant hydraulic head test of the small column (A) (Fig 4.5). The K_{sat} results of the very coarse and coarse sand determined by both methods showed significant differences between the K_{sat} values of the two methods. The medium and fine sand K_{sat} results were also underestimated by the constant hydraulic head test (B) (Fig 4.5). The K_{sat} of the very fine sand do not deviate from the 1:1 line (B) (Fig 4.5). There was substantial variations between the number of replicates of the very coarse (A) K_{sat} values that were measured by the constant hydraulic head test of the small column (Fig 4.5). The K_{sat} of the medium sand determined by the constant hydraulic head test of the large column showed high variations between the number of replicates (Fig 4.5) (B).

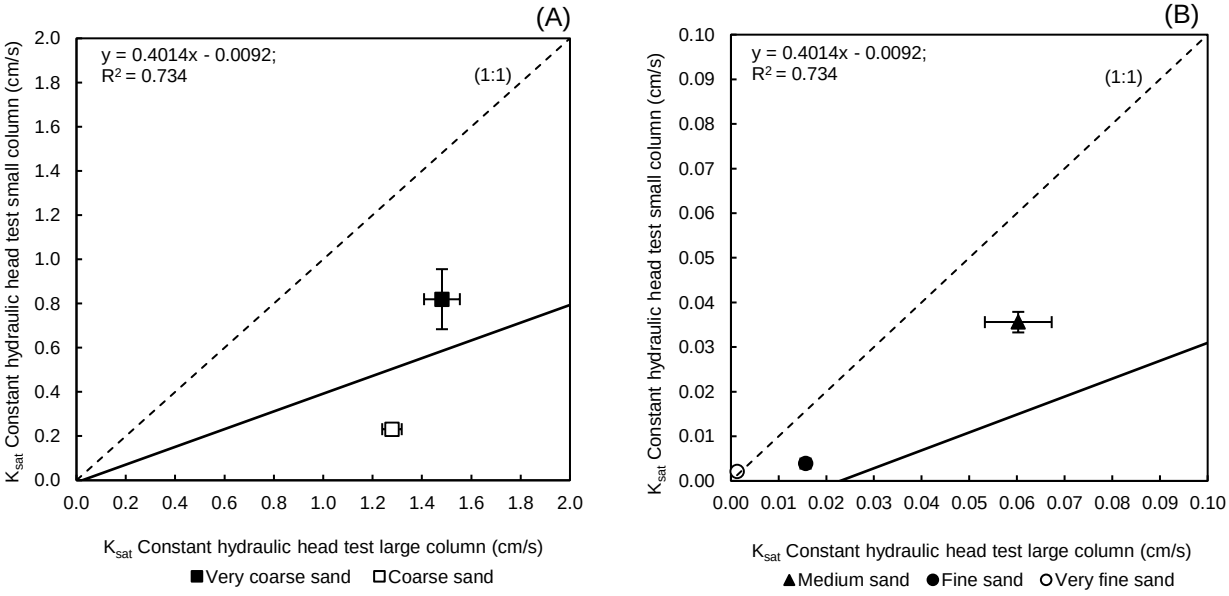

Figure 4.5. The saturated hydraulic conductivity (K_{sat}) results of the constant hydraulic head test of the large and small column fit against a 1:1 line for the different sand fractions (A) very coarse and coarse sand (B) medium sand, fine sand, and very fine sand.

The K_{sat} results determined by the constant hydraulic head test (large column) on the x-axis and the microCT (15 µm scanned) simulated K_{sat} results on the y-axis of the different sand fractions is given in Figure 4.6 (A) very coarse and coarse sand, (B) medium, fine and very fine sand. The K_{sat} values of the very coarse and coarse sand (A), medium and fine sand (B) analysed by the microCT simulation were underestimated when compared to the K_{sat} values determined by the constant hydraulic head test of the large column (Fig 4.6). The K_{sat} values very fine sand analysed by the microCT simulation compared well with the K_{sat} values of the constant hydraulic head test (large column) (Fig 4.6) (B). High variations were found between the four replicates of

the K_{sat} measured by the constant hydraulic head test (large column) of the very coarse and coarse sand (Fig 4.6) (A).

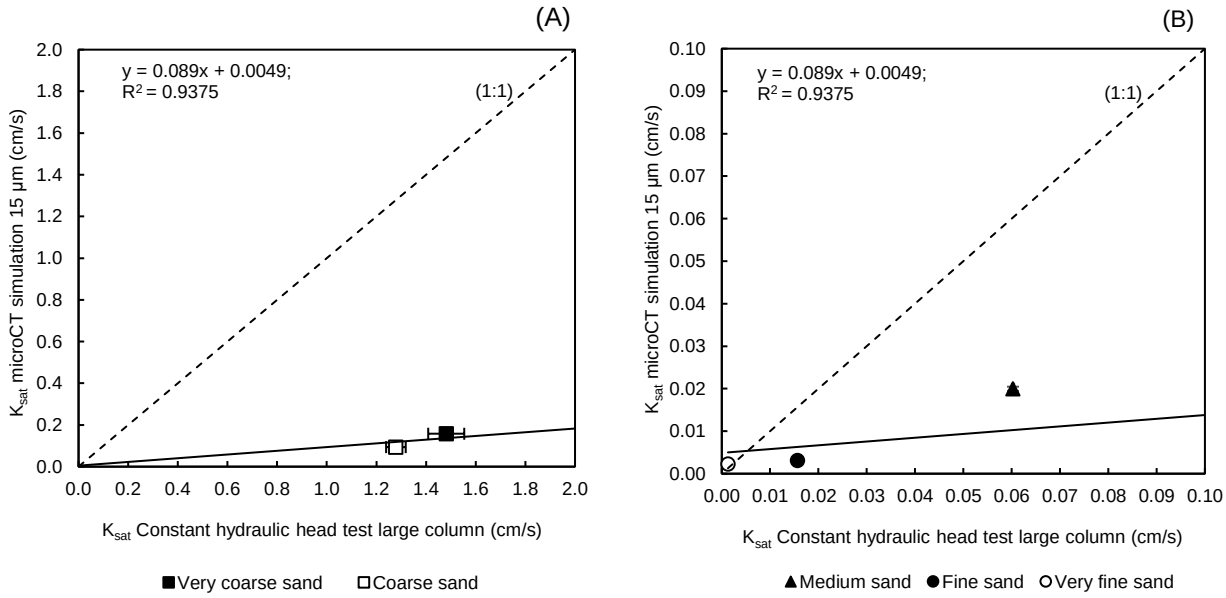

Figure 4.6. The saturated hydraulic conductivity (K_{sat}) values of the microCT simulation (15 µm) and the K_{sat} values of the constant hydraulic head test (large column) of the different sand fractions (A) very coarse, and coarse sand (B) medium, fine and very fine sand fit against the 1:1 line.

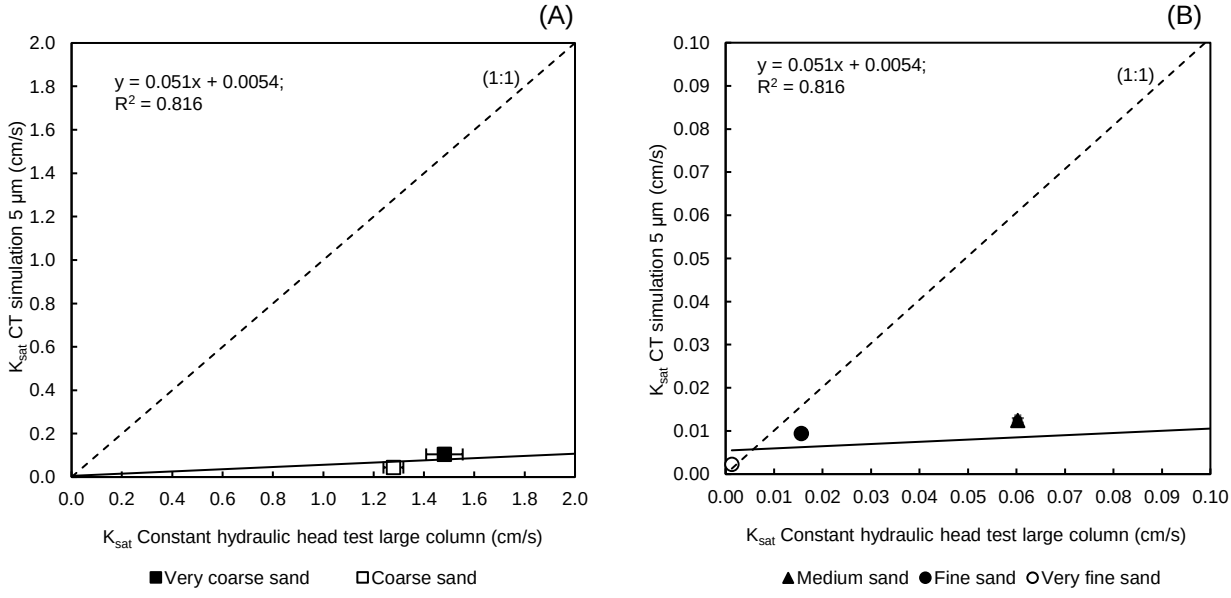

Figure 4.7. The saturated hydraulic conductivity (K_{sat}) values of the microCT simulation (5 µm) and the K_{sat} values of the constant hydraulic head test (large column) of the different sand fractions (A) very coarse and coarse sand (B) medium, fine and very fine sand fit against the 1:1 line.

The same trend was found in Figure 4.7 as in Figure 4.6 and 4.5, where the K_{sat} values of the very coarse and coarse sand (A), medium and fine sand (B) microCT simulation (5 µm) were underestimated when compared to the K_{sat} values determined by the constant hydraulic head test (large column). The K_{sat} values of the microCT simulation and constant hydraulic head test for the very fine sand do not deviate from the 1:1 line, showing no significant differences between the two methods (Fig 4.7) (B). The K_{sat} of the very coarse sand and coarse sand measured by the

constant hydraulic head test showed high variations between the number of replicates (Fig 4.7) (A).

The K_{sat} results of the different sand fraction determined by the microCT simulation (15 µm) (y-axis) and the constant hydraulic head test (small column) (x-axis) were fit against the 1:1 line as shown in Figure 4.8 (A) (very coarse and coarse sand) and (B) (medium, fine and very fine sand). The K_{sat} of the very coarse, coarse sand (A) and medium sand (B) analysed by the microCT simulation were underestimated compared to the constant hydraulic head test (Fig 4.8) (B). The fine, and very fine sand K_{sat} values of both the methods compared very well with each other, showing no significant differences (Fig 4.8) (B). The K_{sat} of the very coarse sand obtained from the constant hydraulic head test showed substantial variation between the four sample replicates as indicated by the large error bars (Fig 4.8) (B).

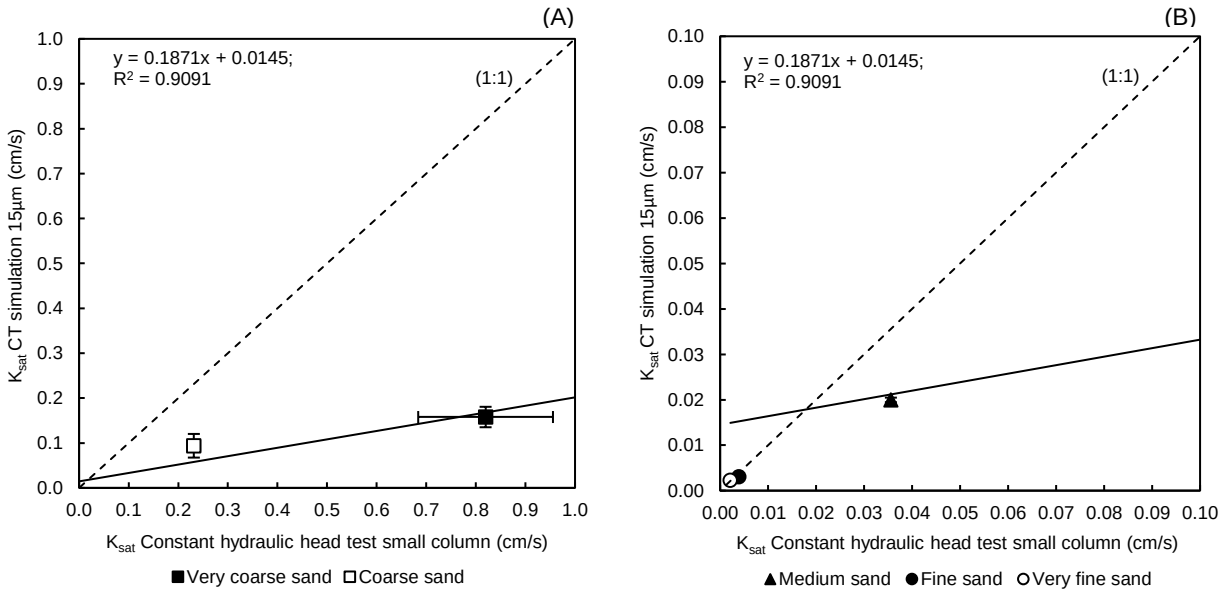

Figure 4.8. The saturated hydraulic conductivity (K_{sat}) values of the microCT simulation (15 µm) and the K_{sat} values of the constant hydraulic head test (small column) of the different sand fractions (A) very coarse, coarse sand (B) medium, fine and very fine sand fit against the 1:1 line.

Figure 4.9 shows that the K_{sat} values of the very coarse, coarse sand (A) and medium sand (B) analysed by the microCT simulation (5 µm) were underestimated compared to the constant hydraulic head test (small column), fit against the 1:1 line. The K_{sat} of the fine sand obtained from microCT simualtions were overestimated, however, the fine sand values did not deviate far from the 1:1 line (Fig 4.9) (B). The very fine sand K_{sat} results that were measured by both methods showed no significant differences (Fig 4.9) (B). This was due to the K_{sat} values of the very fine sand not deviating from the 1:1 line (Fig 4.9) (B). As indicated by the large error bars, high variations of the K_{sat} values occurred between the number of replicates of the very coarse sand that were determined by the constant hydraulic head test (Fig 4.9) (A).

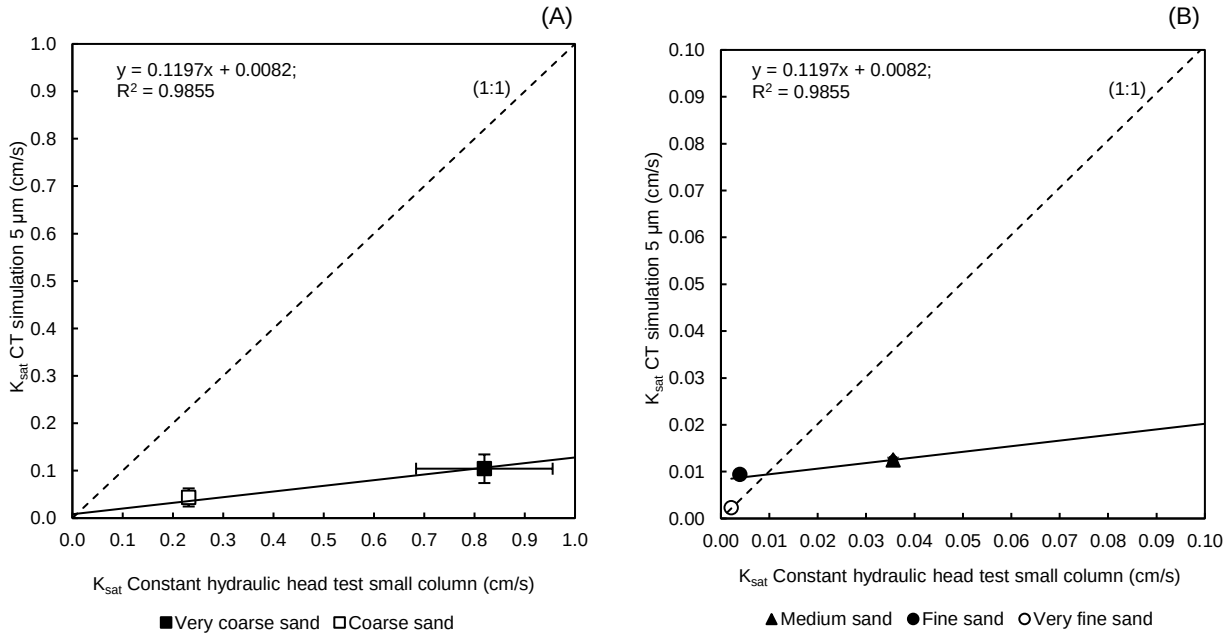

Figure 4.9. The saturated hydraulic conductivity (K_{sat}) values of the microCT simulation (5 µm) and the K_{sat} values of the constant hydraulic head test (small column) of the different sand fractions (A) very coarse, coarse sand (B) medium, fine and very fine sand fit against the 1:1 line.

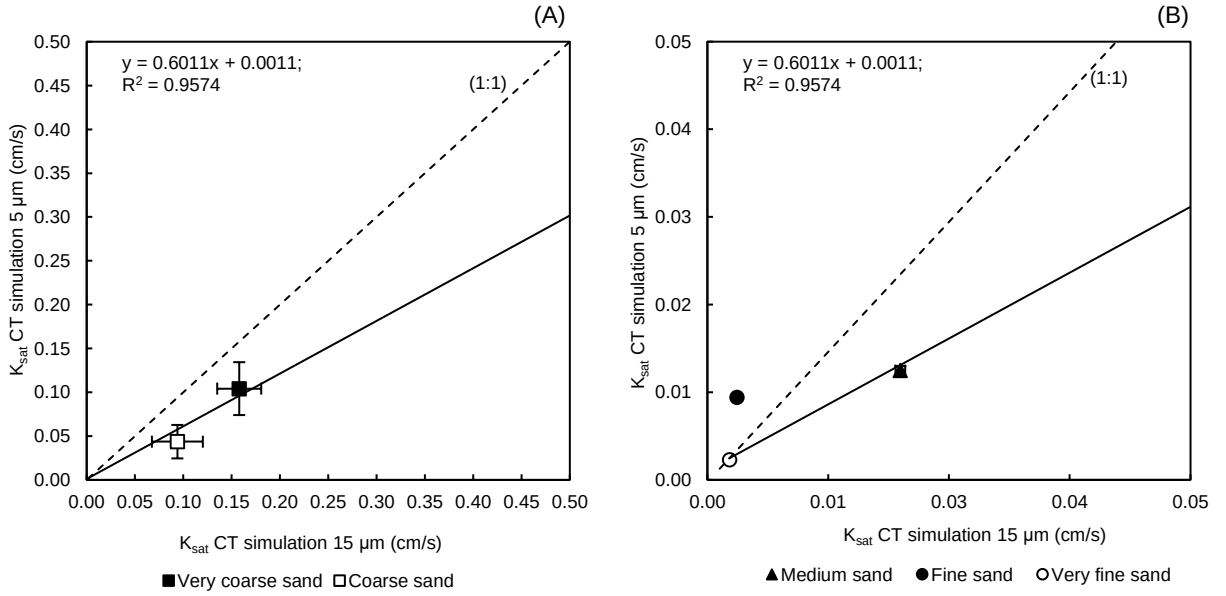

Figure 4.10. The saturated hydraulic conductivity (K_{sat}) values of the microCT simulation (5 µm) and the K_{sat} values of the microCT simulation (15µm) of the different sand grades (A) very coarse and coarse sand (B) medium, fine and very fine sand fit against the 1:1 line.

The results of the K_{sat} for the very coarse, coarse sand (A) and medium sand (B) were underestimated by the microCT simulation (5 µm) compared to the K_{sat} analysed by the micro CT simulation (15 µm) (Fig 4.10). However, the very coarse, coarse and medium sand does not deviate much from the 1:1 line, therefore there is no significant difference between the K_{sat} of the two different methods (Fig 4.10) (A) (B). The K_{sat} of the fine sand obtained from the microCT simulations (5 µm) were overestimated compared to the microCT simulations (15 µm), however

there is not a substantial difference of the K_{sat} between the methods (Fig 4.10) (B). There were good comparisons between the K_{sat} values for very fine sand measured by both methods (Fig 4.10) (B).

The hydraulic conductivity (K) values based on Hillel (2004) in Table 4.2 will be used as the reference K_{sat}. The focus for this study was only on sandy soil types, and comparisons were therefore between the K_{sat} values of the different methods with reference hydraulic conductivity values based on Hillel (2004) sandy soil (Table 4.2). As shown in Table 4.2 the K for sandy soils was between 0.001 – 0.1 cm/s.

Table 4.2. The reference saturated hydraulic conductivity (K_{sat}) for the different soil texture classes proposed by Hillel (2004) with the particle size.

Texture classes	K_{sat} (cm/s)	Particle size (mm)
Clay	0.000001 – 0.00000001	<0.002
Silt	0.00001 – 0.0001	0.05 - 0.002
Sand	0.001- 0.1	2 - 0.05
Gravel	1.00 – 10.00	>2

Table 4.3 shows the mean values of the K_{sat} for the different sand fractions that were measured by the different methods and theoretical equations based on grain size. The K_{sat} of the very coarse sand calculated by Hazen equation and determined by the constant hydraulic head test (large column), were within the same order of magnitude and differed from the K_{sat} of the other methods (Table 4.3). The very coarse sand K_{sat} calculated by the Hazen equation and obtained from the constant hydraulic head test of the large column was also not within the same range of the K_{sat} values for sandy soils based on Hillel (2004) (Table 4.3). The coarse sand obtained from the constant hydraulic head test (large column) K_{sat} mean value were not within the same order of magnitude as the K_{sat} determined by the other methods. The K_{sat} calculated by the Hazen equation and measured by the constant hydraulic head test (small sample) were within the same order of magnitude as well as the K_{sat} determined by the microCT simulation (15 and 5 µm) and calculated by Kozenzy-Carmen equation (Table 3). The medium and very fine sand calculated by Kozenzy and Carman equation were not in the same order of magnitude as the other methods (Table 4.3).

The very fine sand K_{sat} calculated by the Kozenzy-Carman equation did not fall within the same range for the sandy soil based on Hillel (2004) (Table 4.3). The rest of the different sand fractions K_{sat} measured by the different methods were within the same range as the K_{sat} based on Hillel (2004) (Table 4.3). The fine sand K_{sat} of constant hydraulic head test (large column) and Hazen equation were higher as the K_{sat} measured by the other methods and were within the same order of magnitude (Table 4.3). The K_{sat} values obtained from the constant hydraulic head test (small

column), microCT simulations (15 and 5 µm) and Hazen equation of the medium and very fine sand were within the same order of magnitude.

Table 4.3. The mean saturated hydraulic conductivity (K_{sat}) values of the different soil classes determined by the different methods.

Method	Very coarse sand	Coarse sand	Medium sand	Fine sand	Very fine sand
Large (CHHT)[1]	1.4812	1.2785	0.0603	0.0156	0.0013
Small (CHHT)[1]	0.8196	0.2314	0.0356	0.0039	0.0021
microCT 15 µm	0.1578	0.0938	0.0200	0.0031	0.0023
microCT 5 µm	0.1042	0.0436	0.0125	0.0094	0.0023
Kozenzy-Carman eq.	0.1723	0.0414	0.0093	0.0015	0.0003
Hazen-Williams eq.	1.0000	0.2500	0.0625	0.0100	0.0025
Hillel (2004)	0.001- 0.1	0.001- 0.1	0.001- 0.1	0.001- 0.1	0.001- 0.1

[1].Constant hydraulic head test

In Tracey *et al.* (2015) the hydraulic conductivity results for the sandy soils were in the same order of magnitude for the different methods (laboratory test and microCT simulations) and the clay soils hydraulic conductivity were not in the same order of magnitude. In Fourie *et al.* (2007) the hydraulic conductivity of sand soils was determined with laboratory permeability test and X-ray microCT simulations. The results showed that the hydraulic conductivity of the sandy soils fell within the same order of magnitude for the two different methods (Fourie *et al.* 2007).

As mentioned in the methods and materials Section 3.6, scans at 40 µm were performed on the small column to run a microCT simulation, to determine the $K_{sat.}$ However, the microCT simulations could not be performed on the other sand fractions (coarse sand, medium sand, fine sand, and very fine sand) due to resolution limitations, which will be further discussed in Section 4.1.7.1. The small column scanned at 40 µm missed all the smaller pore areas that connected the whole pore structure of these samples. However, the microCT simulation was performed on the very coarse sand small column scanned at 40 µm (Fig 4.11). In Figure 4.11 is a 2D image of the flow simulation where the blue areas indicate low flow velocities and the brighter green areas show the higher flow velocities.

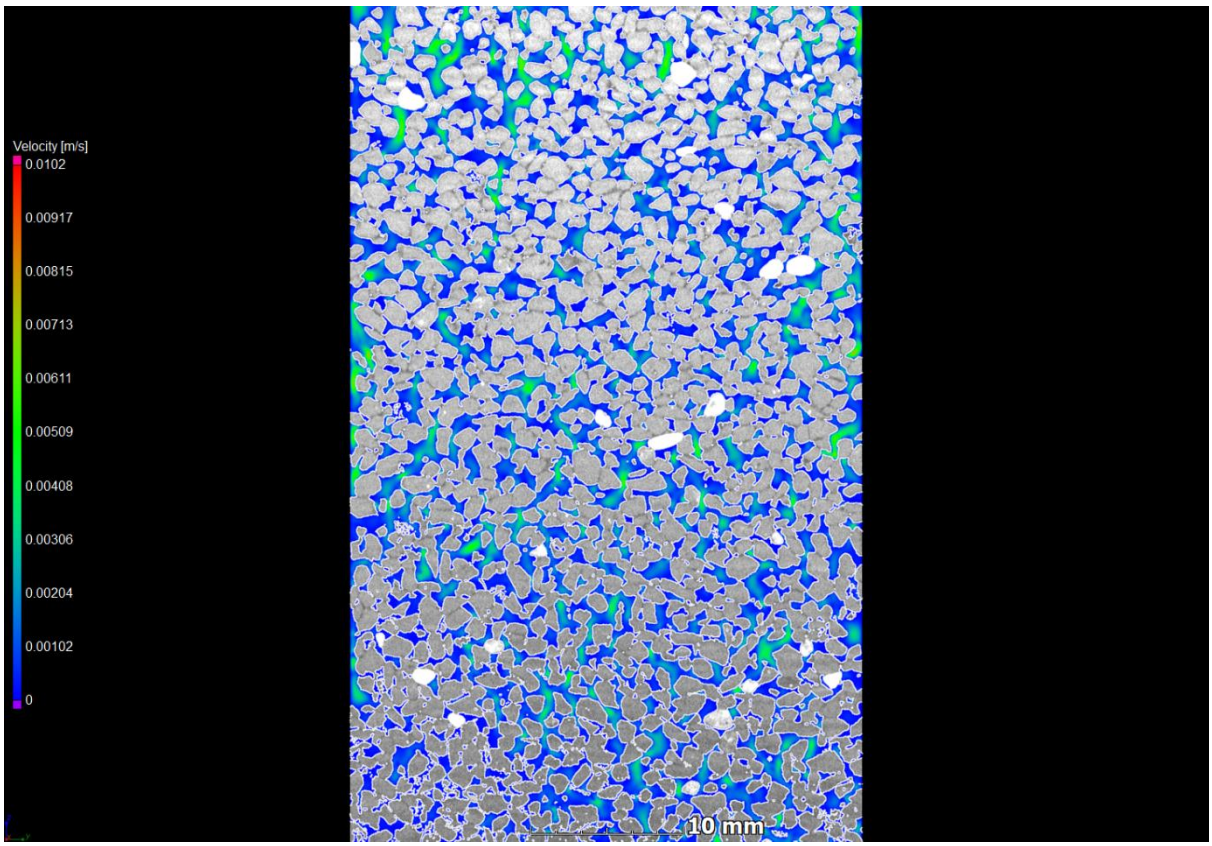

Figure 4.11. An X-ray micro-computer tomography (microCT) 2D slice image of the very coarse sand scanned at 40 µm showing the flow simulation velocities: green indicates higher flow velocities, and blue indicates low flow velocities.

The results showed that the K_{sat} of the constant hydraulic head test and microCT simulations (scanned at 40 µm) were within the same order of magnitude (Table 4.4). The K_{sat} determined by the constant hydraulic head test were higher than the K_{sat} obtained from the microCT simulation (scanned at 40 µm), of the very coarse sand (Table 4.4). This experiment was to highlight the motivation behind the selection of smaller sizes for the study and directly compare the K_{sat} results of the same sample size that were determined by two different methods. This showed that K_{sat} of the same soil type will have differences due to the method used to measure the K_{sat} and not due to the inability of one method to measure the K_{sat}.

Table 4.4. Comparison of the saturated hydraulic conductivity (K_{sat}) of the very coarse sand (sample size of 7 cm in length and 3.5 cm in diameter) scanned at 40 µm micro-computer tomography (microCT) simulation, constant head test K_{sat}.

Method	K_{sat} (cm/s)
microCT simulation scanned at 40 µm	0.214
Constant hydraulic head test small column	0.820

As found in the literature the hydraulic conductivity values were highly variable for the same soil types when the hydraulic conductivity was determined by different methods (Chapuis 2004, Chakraborty *et al.* 2006, Nagy *et al.* 2013, Tracey *et al.* 2014). Therefore, no method for

determining the K_{sat} can be identified as a standard method to measure hydraulic conductivity (Nagy *et al.* 2013).

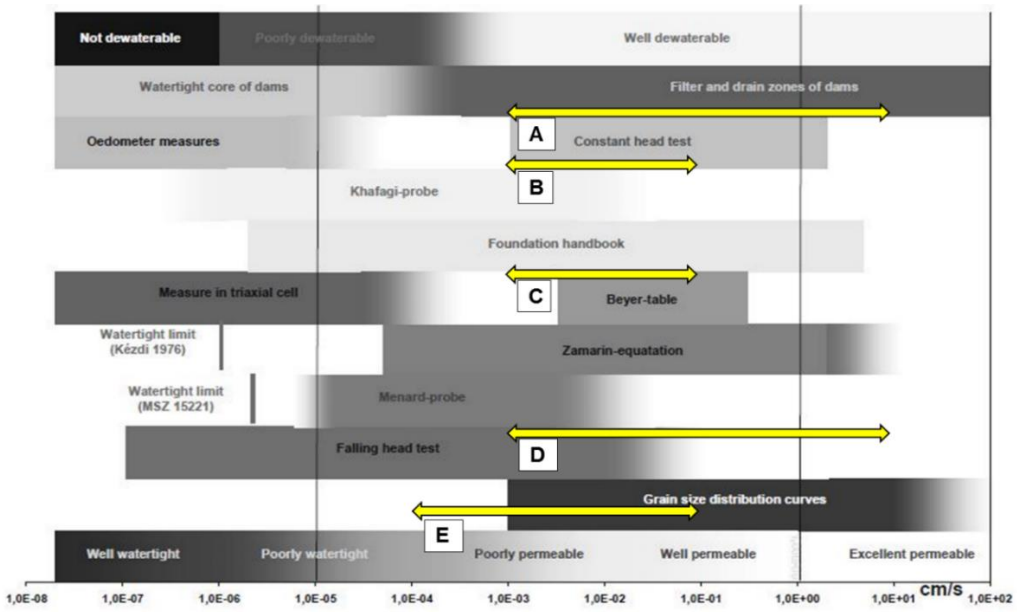

Figure 4.12. The hydraulic conductivity results determined by the different methods where (A) is the constant hydraulic head test of large column, (B) is the constant hydraulic head test of the small column, (C) is the microCT simulation (15 and 5 µm), (D) is the Hazan equation and (E) is the Kozenzy-Carman equation as shown by the yellow arrows compared with the hydraulic conductivity values of different methods estimated by Nagy *et al.* (2013), within a certain range from well watertight material to excellent permeable material.

The results found within this study and the results found by Nagy *et al.* (2013) of the hydraulic conductivity shows that the hydraulic conductivity values are influenced based on the method used to determine the hydraulic conductivity (Fig 4.12). The different methods used within this study hydraulic conductivity values are indicated by the yellow arrows (Fig 4.12). The constant hydraulic head test of the large column (A) hydraulic conductivity values were not within the same range as the hydraulic conductivity values of the constant head test presented by Nagy *et al.* (2013) (Fig 4.12). The K_{sat} value of the constant hydraulic head test (small column) (B) and the microCT simulation (15 and 5 µm) (C) fell within the same range as the constant head test hydraulic conductivity shown by (Fig 4.12). This shows how highly variable the hydraulic conductivity values can be. As Elhakim (2016) stated, there is no generalized method for estimating the hydraulic conductivity in soils because each method comes with its own limitations.

4.1.3 Comparison between the porosity determined in the laboratory with the porosity analyzed by microCT image-based analysis

Additional porosity analysis was measured for this study. It is important to note that the samples of both large and small columns for the constant hydraulic head test were packed at a bulk density of 1.5 g/cm^3. The bulk density of the different sand fractions changed after the constant hydraulic

head test. However, the porosity measurements were only compared between the microCT porosity (15 & 5 µm) and the porosity of the large column after the constant hydraulic head test.

The bulk densities in Table 4.5 of the large column changed after the constant hydraulic head test (CHHT) and will therefore be referred to as laboratory porosity (after CHHT). The bulk density is an important parameter for the porosity analysis because these two parameters are inversely related with each other (Scheidegger 1957). The porosity of the different sand fractions was low for high bulk densities (Table 4.5). High bulk densities indicate high compaction in soil, and low bulk densities can indicate low compaction within the soil (Scheidegger, 1957). The laboratory porosity (after CHHT) values given in Table 4.5 shows that the soil within the large column consolidated after the constant hydraulic head test. Therefore the after porosity values of the very coarse to fine sand are lower than the porosity before the constant head test. Notice that the very fine sand after porosity and bulk density values are incorrect due to soil that were lost during the constant hydraulic head test. The soil of the very fine sand moved through the nylon sieved that was place between the gravel and soil of the large column as mentioned in Section 3.2. The very fine sand have small soil particles and therefore some of the particles were small enough to be transferred through the sieve. Hence, the bulk density of the very fine sand are incorrect.

Table 4.5. The bulk density and porosity of the large soil columns before and after the constant hydraulic head test.

Soil Texture	Before constant hydraulic head test		After constant hydraulic head test	
	Bulk density (g/cm^3)	Porosity (cm^3/cm^3)	Bulk density (g/cm^3)	Porosity (cm^3/cm^3)
Very coarse sand	1.500	0.426	1.800	0.312
Coarse sand	1.500	0.422	1.802	0.306
Medium sand	1.500	0.413	1.908	0.253
Fine sand	1.500	0.413	1.954	0.235
Very fine sand	1.500	0.377	2.609	-0.083

As noted in Table 4.5 that the porosity results of the very fine sand measured after the constant hydraulic head test were incorrect. Therefore the porosity of the very fine sand will not be included when comparing the microCT porosity results with the porosity measured within the laboratory. It is also important to note that only the laboratory porosity results of the different sand fractions measured after the constant hydraulic head test will be compared with the microCT analysed porosity. This is due to the fact that the samples for the microCT scans were sampled after the constant hydraulic head test from the large column.

Figure 4.13 shows the porosity values of the different sand fraction determined by the laboratory method porosity after the constant hydraulic head test and the analysed microCT porosity (15 µm scanned sample) fit against the 1:1 line. The different sand fractions (very coarse, coarse, medium, & fine sand) were overestimated by the microCT image base analysis compared to the porosity measured by the laboratory method (Fig 4.13). This is shown by the deviation of the porosity values of the different sand fractions from the 1:1 line (Fig 4.13).

There were high variations between the very coarse and medium sand of the analysed microCT porosity, as indicated by the large error bars (Fig 4.13). These variations can be because of the sampling procedures such as handling and transportation. High variations of the porosity values analysed by microCT image-based analysis are caused by the sampling procedure which influences the bulk density of the soil (Vogel & Kretzschar 1996).

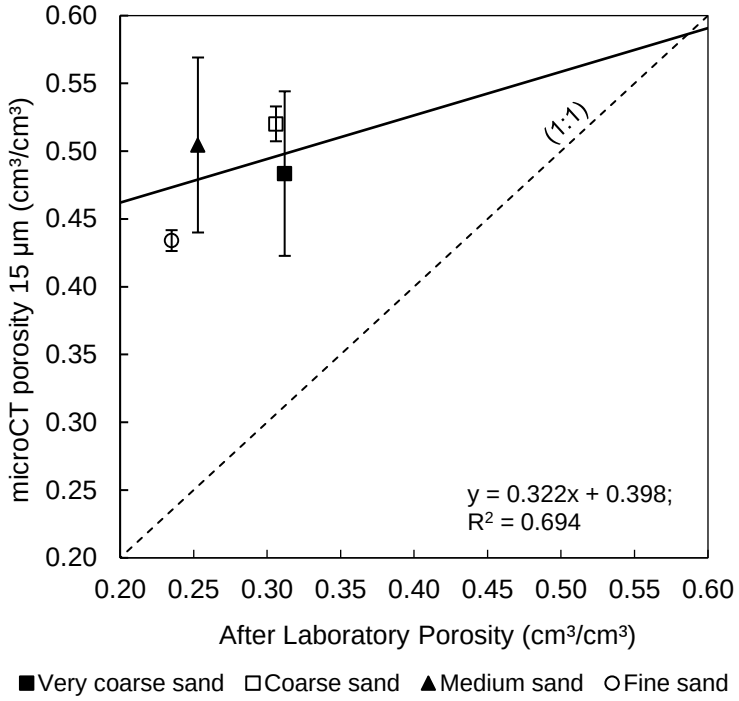

Figure 4.13. The porosity values determined by the laboratory method of the large column (after constant hydraulic head test) and X-ray micro-computer tomography (microCT) image-based analysed porosity scanned at (15 µm) of the different sand fractions (very coarse sand, coarse sand, medium sand, and fine sand) fit against the 1:1 line.

The porosity values of the different sand fractions analysed by the microCT image-based analysis (5 µm scanned sample) and the porosity determined by the laboratory method (after constant hydraulic head test) fit against the 1:1 line are shown in Figure 4.14. The porosity values analysed by the microCT image-based analysis were overestimated compared to the porosity determined by the laboratory method (Fig 4.14). There was substantial variations between the number of replicates porosity values for all the different sand fractions (Fig 4.14). However, the porosity values of the fine sand showed higher variation in comparison with the porosity of the other sand fractions (Fig 4.14).

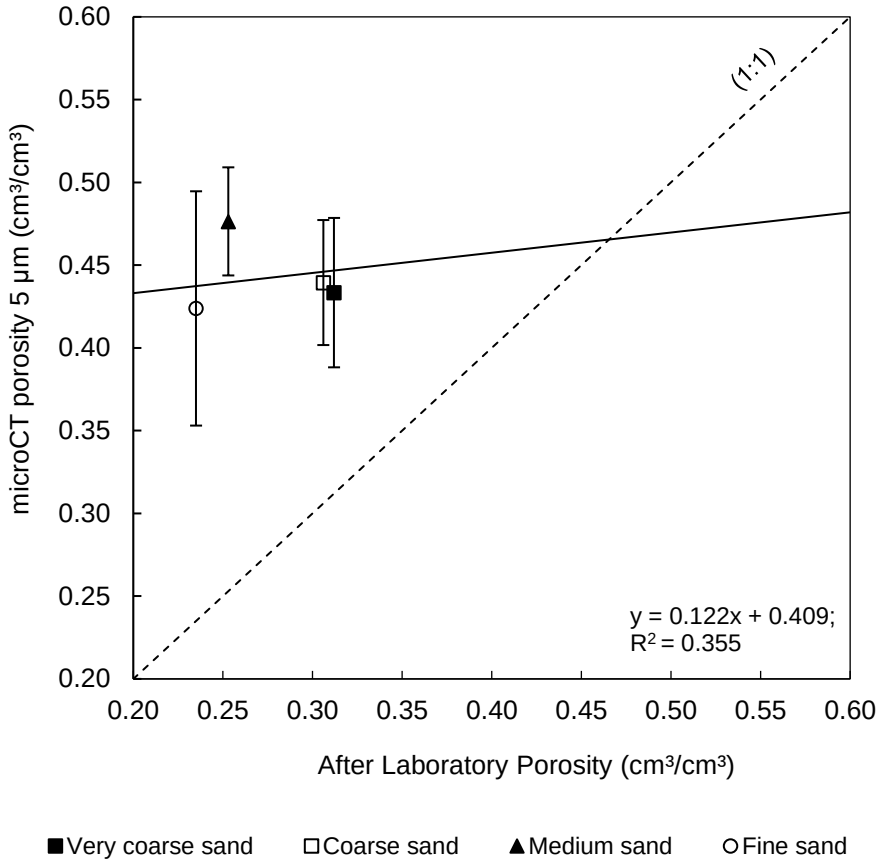

Figure 4.14. The porosity measured by the laboratory method of the large column (after constant hydraulic head test) and X-ray micro-computer tomography (microCT) image-based analysed porosity (mean values) scanned at (5 µm) of the different sand fraction (very coarse sand, coarse sand, medium sand, and fine sand) fitted against a 1:1 line.

Figure 4.15 shows the porosity values of the microCT image-based analysis of the sample scanned at 5 µm compared to the porosity values of the samples scanned at 15 µm. The porosity values of the fine and very fine sand converge to the 1:1 line, showing that the porosity values measured by the two methods compared well (Fig 4.15). The results of the porosity were underestimated by the microCT image-based analysis of the sample scanned at 5 µm (Fig 4.15). There were higher variations between the porosity values of the different sand fractions that were analysed by the microCT image-based analysis scanned at 5 µm, with the porosity of the fine sand showing the highest variation (Fig 4.15). The samples scanned at 15 µm showed high variations between the porosity values of the very coarse and medium sand (Fig 4.15).

The porosity values measured by the microCT image-based analysis (5 & 15 µm) were overestimated compared to the porosity determined in the laboratory (Fig 4.13 & 4.14). High porosity values measured by microCT image-based analysis can be attributed to the application analysing the total porosity whereas with other methods are based on the interconnectivity of pores and therefore excludes isolated pores (Van Geet *et al.* 2003).

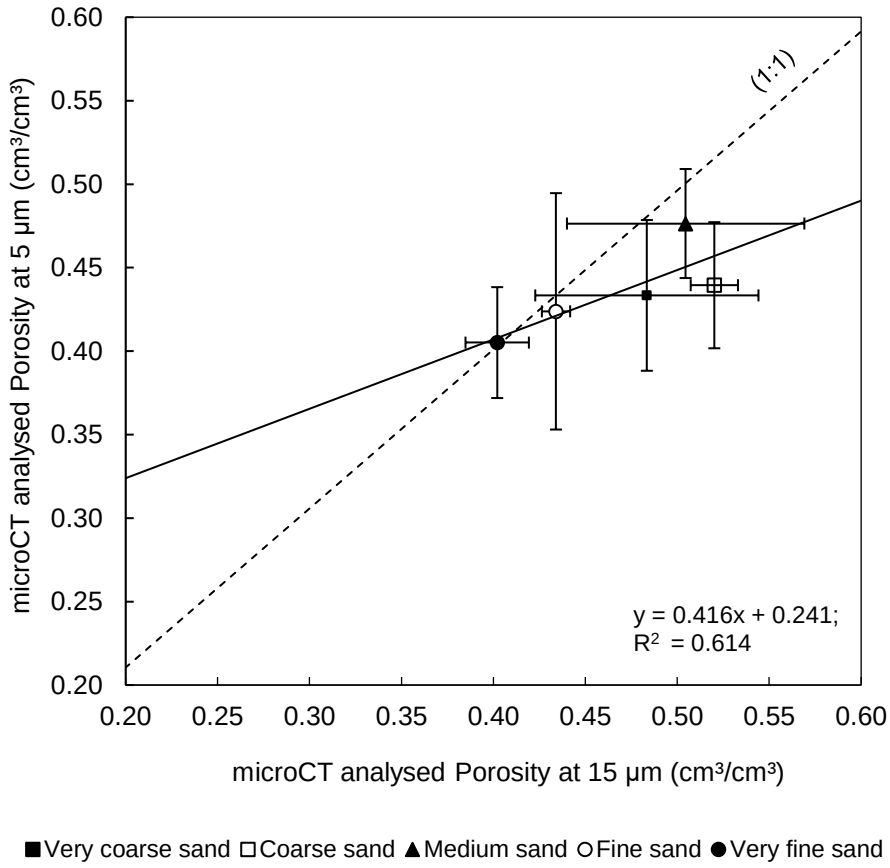

Figure 4.15. The porosity values of the X-ray micro-computer tomography (microCT) image-based analysis scanned at 15 µm porosity and microCT scanned at 5 µm of the different sand grades (very coarse sand, coarse sand, medium sand, fine sand, and very fine sand) fit against the 1:1 line.

The high variations found in Figure 4.15 can be due to the handling of the samples during the mounting process for the microCT scans. The samples scanned at 5 µm were very small and the plastic straw used to sample the soil was very fragile and not as supportive in structure as the cuvette (soil sample holder used for the 15 µm scans) (Fig 4.16). These differences of the sample holder could have changed the bulk density, which would influence the porosity of the soil sample scanned at 5 µm. The changes in bulk density might have occurred during the mounting procedure for the microCT scans that were caused by the handling of a small fragile sample such as the plastic straw, which was challenging (Fig 4.16). These challenges may have been the reason for variation between the porosity values of the sample scanned at 5 µm (plastic straw) (Fig 4.16). Errors with the methodology on a smaller scale can influence the variation between the porosity analysed by microCT (Vogel & Kretzschar 1996).

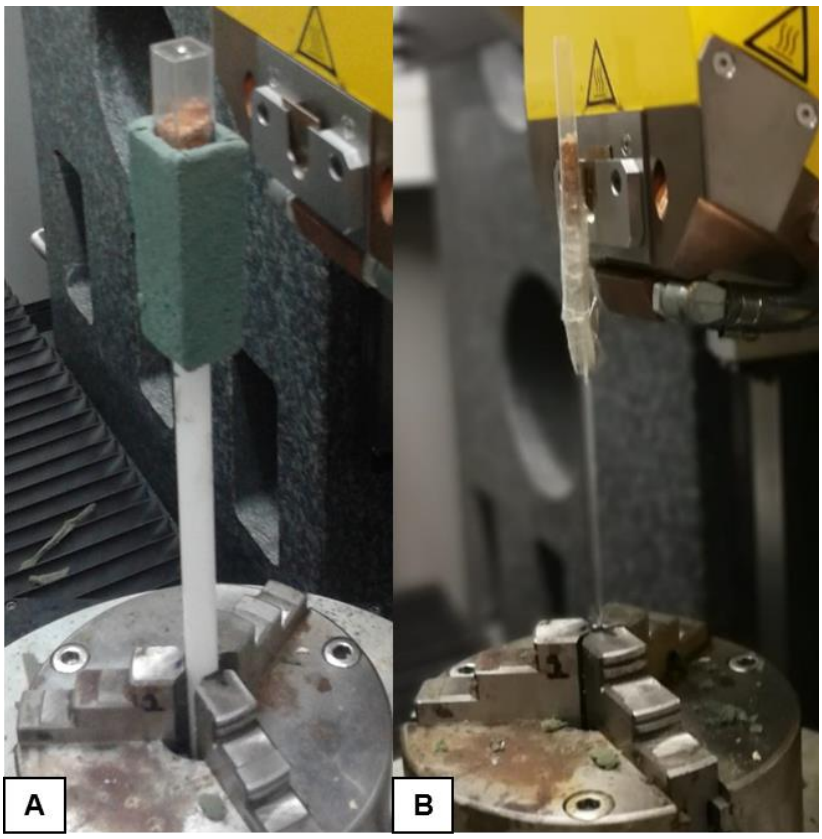

Figure 4.16. The mounting method of the different samples scanned at (A) the 1x1 square tube and 3.5 cm in length diameter sample scanned 15 μm (cuvette) and (B) the 5 mm in diameter and 3.5 cm in length (plastic straw) which is very close to the detector.

The variation and differences in the porosity values with the microCT analysed porosity might be because of the samples that might have moved around during transportation of the samples to the CT scanner laboratory. The sampling method the samples went through also resulted in cracks and larger pores within the soil sample as shown in Figure 4.17. These cracks and larger pores were a result of the freezing procedure of the soil samples as mentioned in Section 3.5 (Fig 4.17). For the microCT scans, the sample was removed from the freezer and due to the sampling method, the soil particles might have moved around and changed the bulk density of the sample which would eventually influence the porosity. Vogel & Kretzschar (1996) reported variations between the number of soil samples on a small scale due to potential methodology errors during sampling. The sampling preparation, handling and procedures can be attributed to errors in the measurement of soil parameters (Arya, 1981). It is important to recall that porosity values for the laboratory method (after porosity) were only measured on one sample, which is why there was no variation between the number of replicates (Fig 4.13 & 4.14).

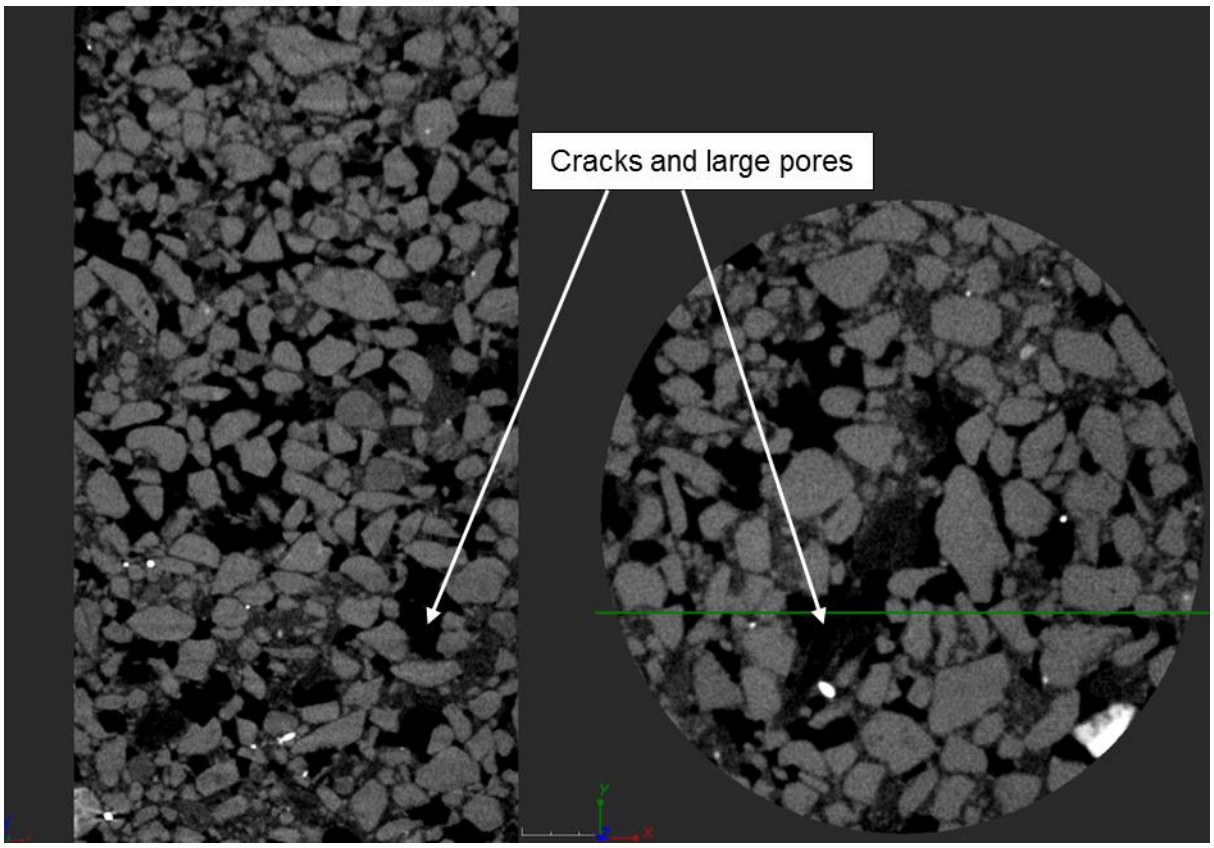

Figure 4.17. A raw X-ray micro-computer tomography (microCT) 2D slice image-based data of the medium sand with fractions and massive pores (black areas) on the left and top slice view, showing the cracks and large pore spaces.

4.1.4 Validation of microCT simulations and image-based analysis

The validation of microCT simulations on a scanned medium sand sample will be discussed in this section. The relationship between the microCT simulation K_{sat} and the simulation cell size (voxel size) is given in Figure 4.18. As can be seen, the experiment was performed by using different simulation cell sizes (Fig 4.18). In order to determine how the simulation cell size influences the K_{sat} results. As shown in Figure 4.18, simulation cell sizes influence the K_{sat} results. If the simulation cell size is made finer, the K_{sat} results will converge strongly to a more accurate and consistent result with not a lot of variance between the K_{sat} values as shown in Figure 4.18. This shows some confidence in the accuracy of the microCT simulations experiment (Fig 4.18). As the simulation cell size becomes finer or smaller, the results become more accurate and satisfactory. If the simulation cell size were higher or coarser the K_{sat} value would increase (Fig 4.18). The simulation flow paths would cross over the material (soil particles) borders, or the white lines in Figure 4.19, thus overestimating the K_{sat} values. Figure 4.19 shows an image-based analysis of the simulation performed at a smaller of finer voxel size. The simulation flow paths do not cross over the borders (white lines) of the material (Figure 4.19).

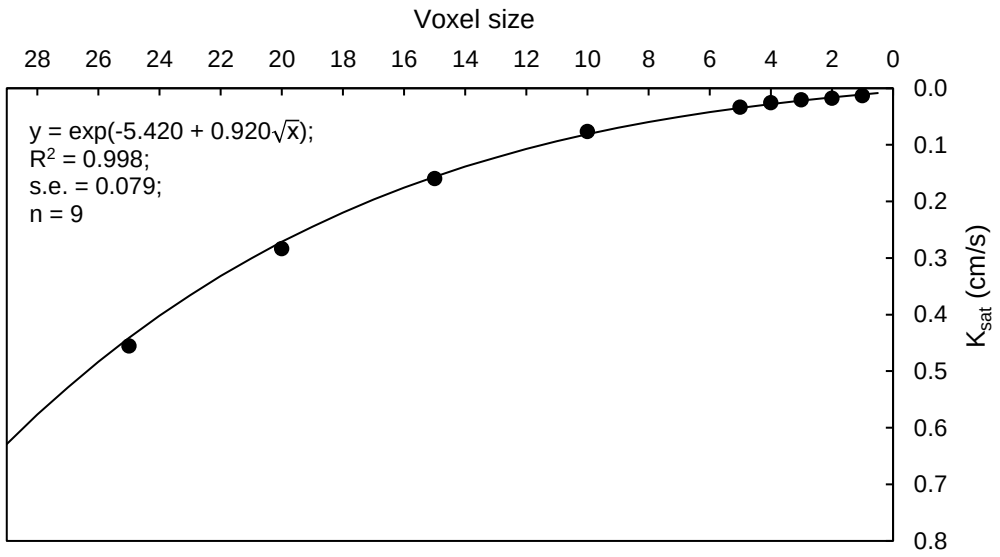

Figure 4.18. The relationship between the X-ray micro-computer tomography (microCT) simulation determined saturated hydraulic conductivity (K_{sat}) of a homogeneous medium sand at different voxel sizes, to show how the K_{sat} values increase with an increase in voxel size. The voxel size illustrates the area where the simulation will occurred.

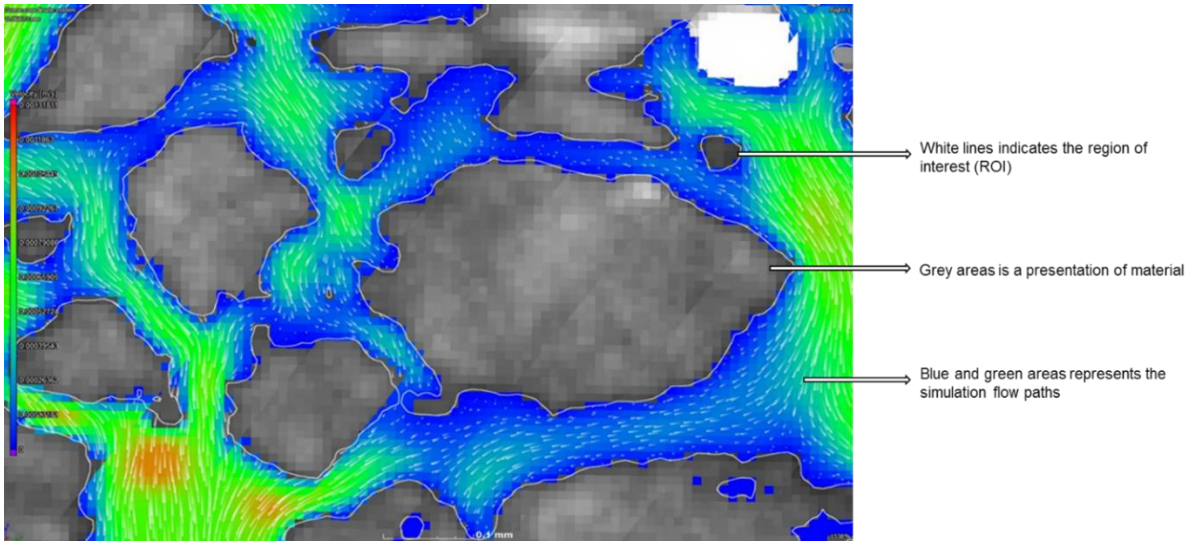

Figure 4.19. A 2D slice image of an X-ray micro-computer tomography (microCT) image-based analysis, illustrating an example of the simulation run at a voxel size of 1, that does not overestimate the hydraulic conductivity results. The blue and green are the simulation flow paths (air & pore spaces), the grey areas are the material (soil) and the white lines indicate region of interest (ROI) which pose as a boundary between the material (soil) and the air spaces (pores).

4.1.5. The internal visualization of the microCT Image-based data of the different sand fractions scanned at a resolution of 15 and 5 µm

In this experiment, the different sand fractions were sampled at two different sample sizes (cuvette 3.5 cm^3 (1 x 1 cm square tube, 3.5 cm length) and the plastic straw 0.687 cm^3 (5 cm diameter and 3.5 cm length) and scanned at different resolutions (15 and 5 µm) as mentioned in section 3.6. In microCT image-based data, the material of an object with higher densities is the light grey (bright) areas and the air spaces or low-density materials are the grey-darker areas. In this study, the material was referred to as the soil and the air spaces are referred to as the pores within the soil.

Figure 4.20 shows the raw 2D slice images of the plastic straw sample of the different sand fractions that were scanned at 5 µm. The raw 2D slice images of the cuvette sample of the different sand fractions scanned at 15 µm is given in Figure 4.21. In both Figure 4.20 and Figure 4.21, it is evident that an increase in particle size of the different sand fractions (very coarse sand (A), coarse sand (B), medium sand (C), fine sand (D) & very fine sand (E)) resulted in an increase in the pore size.

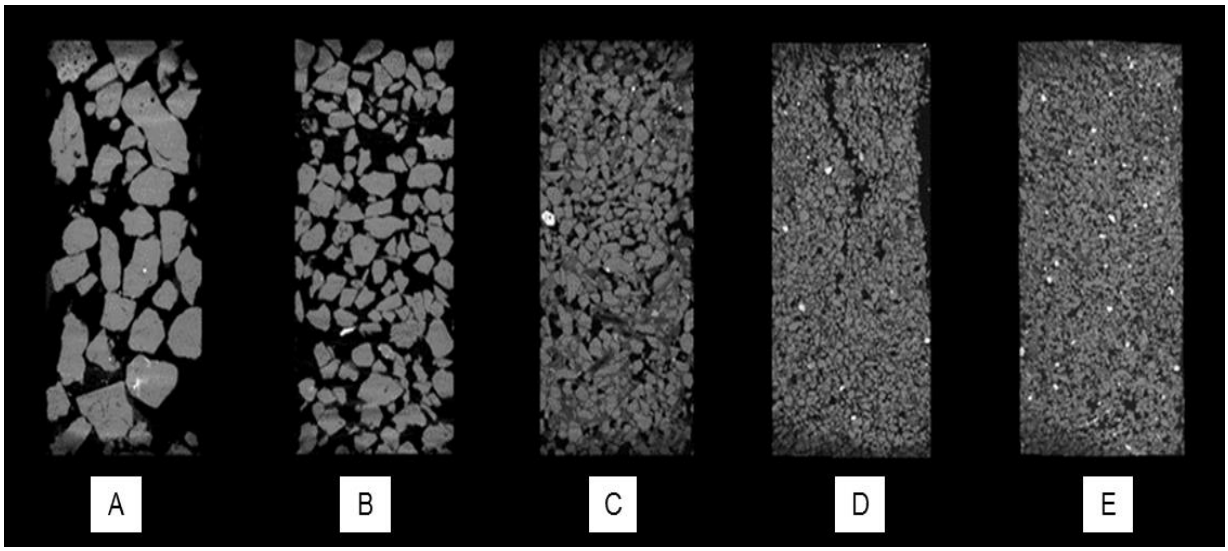

Figure 4.20. A raw X-ray micro-computer tomography (microCT) scan of a 2D slice image at a 5 µm resolution of (A) very coarse sand, (B) coarse sand, (C) medium sand, (D) fine sand and (E) very fine sand. The light-grey areas (dense material) indicate the material (soil particles) and the dark-black areas (less dense or no material) indicate the pore spaces. This shows how the soil particles differ in size from coarser textured to finer textured A-E.

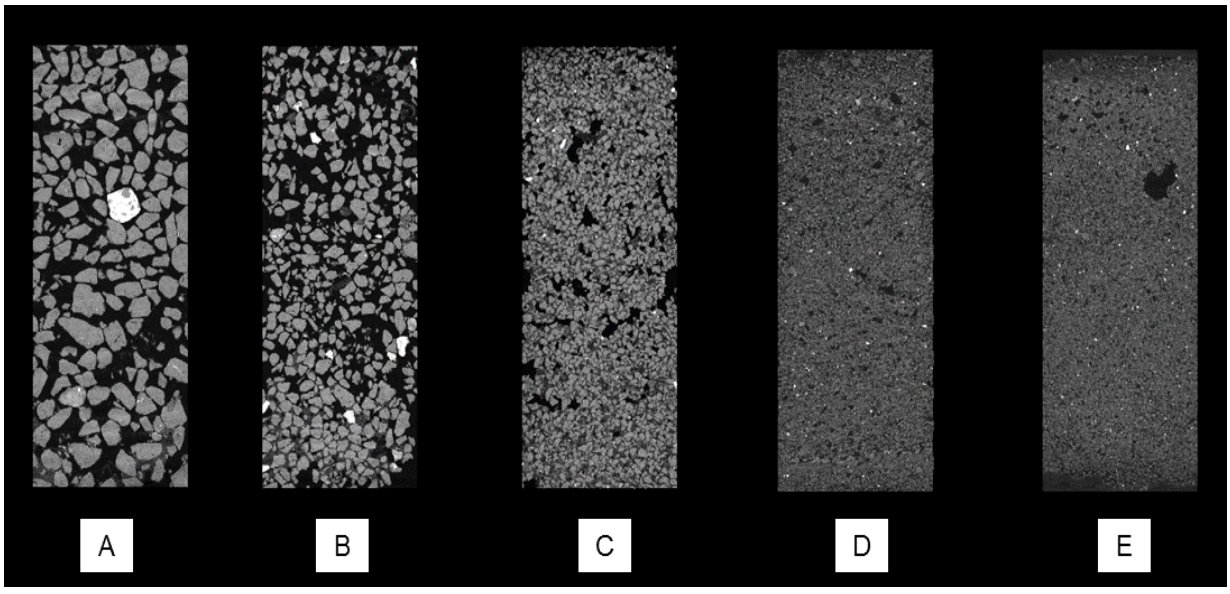

Figure 4.21. An X-ray micro-computer tomography (microCT) scan of a raw 2D slice image scanned at 15 µm of the different sand fractions from left is the (A) very coarse sand, (B) coarse sand, (C) medium sand, (D) fine sand and (E) very fine sand. The light-grey areas (dense material) indicate the material (soil particles) and the dark-black areas (less dense or no material) indicate the pore spaces. This shows how the soil particles differ in size from coarser textured to finer textured A-E.

In Figure 4.20, the particles for all the different sand fractions appear to be larger than the particle sizes in Figure 4.21 due to the samples that were scanned at a higher or finer resolution

of 5 µm (smaller field of view). In Figure 4.20, the soil and pore areas of the fine sand (D) and very fine sand (E) could be easily distinguished and therefore, improving the visualization for quality image-based analysis. The fine sand (D) and very fine sand (E) pore and soil areas were difficult to differentiate in Figure 4.21. Hence, resulting in poor visualization of microCT image data and causing difficulties with image-based analysis. The very coarse (A), coarse (B) and medium sand (C) shows well-connected pores in both Figure 4.20 and 4.21. The fine and very fine sand shows poorly connected pores as shown in Figure 4.20 and Figure 4.21. This was found in Mooney (2000) where the sandy loam soils showed better pore connectivity than the sandy clay soils.

MicroCT image-based analysis can visualize the pore size and pore structure of a soil. In Figure 4.20 the fine sand (D) has two cracks visible within the soil sample. As a result, the cracks are seen as a bigger pore area. Therefore when analysing the porosity of the sample, the porosity will be higher. The cracks also create preferential flow paths that can influence the K_{sat}, analysed by microCT simulation.

4.1.6 Visualization of microCT image data of the simulation analysis flow velocities

MicroCT image data of the simulation flow velocity of the very fine sand are shown in Figure 4.22. The high flow velocities are presented by pink-red and low flow velocity are presented by the purple and blue areas (Fig 4.22). The flow velocity of the very fine sand is low indicated by the predominant blue areas because there were smaller pore areas in the very fine sand (Fig 4.22). Soils with low flow velocities conduct water or fluid slower and therefore the K_{sat} was low whereas, in soil with high flow velocities, water or fluid is conducted faster, and therefore the K_{sat} was higher as with the medium sand in Figure 4.23.

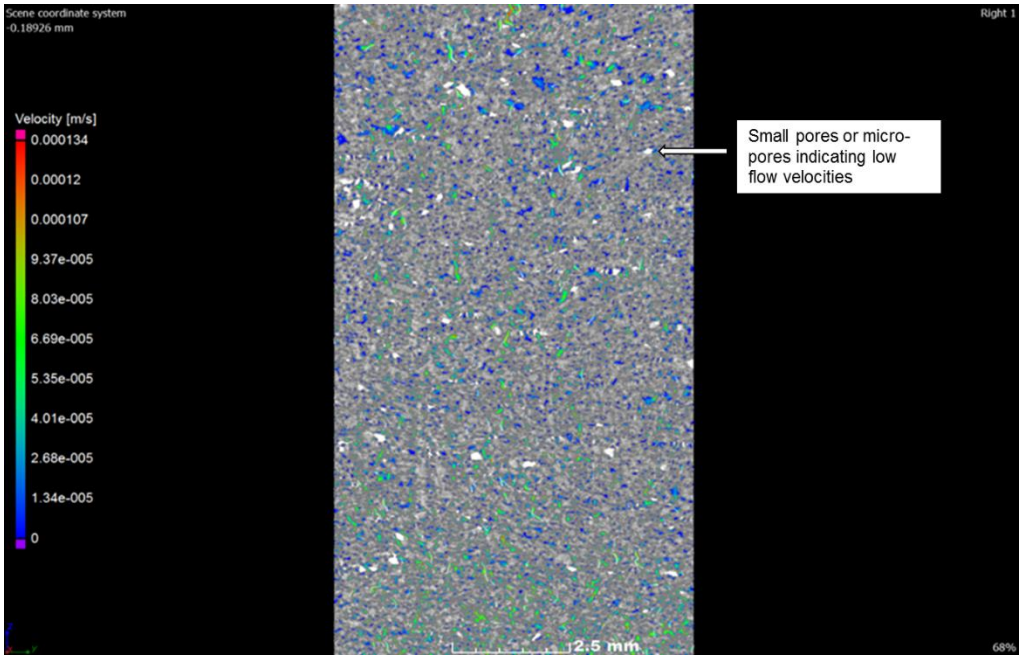

Figure 4.22. An X-ray micro-computer tomography (microCT) 2D slice image of the very fine sand with smaller pore areas, therefore showing low flow velocities as indicated by the blue areas through the pores.

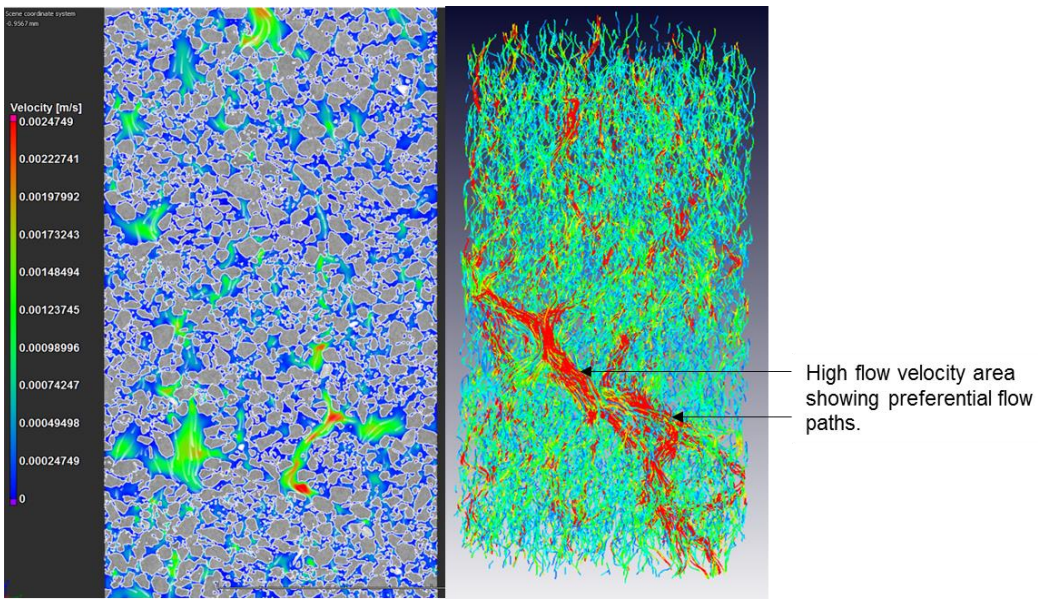

Figure 4.23. An X-ray micro-computer tomography (microCT) 2D slice image of the medium sand with larger pore areas that results in high flow velocities as indicated by the green – red areas. The microCT 3D image-based of the streamlines showing the preferential flow paths, through the larger pore areas that also causes high flow velocity.

4.1.7 Image processing and analysis limitations

4.1.7.1 The effect of resolution on image data quality

In this section, the limitations with X-ray microCT for soil samples will be discussed by looking at the effects that resolution and voltage might have on microCT image-based analysis. Figure 4.24 shows an image of the very fine sand scanned at a resolution of 15 µm. With smaller particle sizes it is difficult to see the fine soil particles within a resolution of 15 µm (Fig 4.24). Image data of the very fine sand scanned at a resolution of 5 µm are shown in Figure 4.24. The soil particles are more visible in Figure 4.25 of the soil sample scanned at a resolution of 5 µm than in Figure 4.24 due to the higher resolution. Differences between the soil particles and the pore spaces can easily be distinguished, making the segmentation process easier (Fig 4.25).

The resolution in X-ray microCT plays an important role in the acquisition of the CT images, determining the image quality but limiting the field of view (much like an optical microscope) (Du Plessis et al. 2017). A higher resolution is best used when analysing smaller objects for more detail, for example for soil with smaller particles (Mees et al. 2003). However, to scan a soil sample at a higher resolution a small soil sample is required (Mees et al. 2003). Larger soil samples will be further away from the x-ray source and therefore the resolution will be poorer which results in fewer details detected (Zappala et al. 2013). If a large soil sample of a soil that consists of mostly clay and silt (finer particles) is scanned, a lot of the details will be missed due to resolution limitations (Zappala et al. 2013). Therefore, the identification of the soil material/particles and air/void spaces will be difficult.

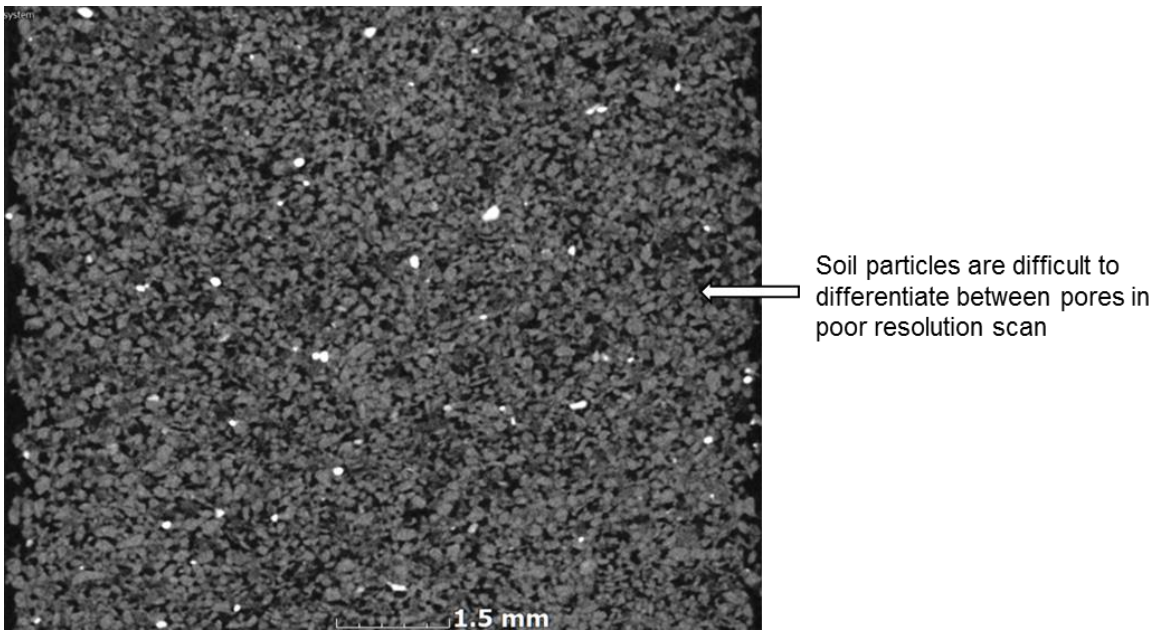

Figure 4.24. A raw X-ray micro-computer tomography (microCT) 2D slice image of the very fine sand scanned at 15 µm, showing the difficulties to distinguish between the soil particles (grey areas) and the pore spaces (darker/black areas).

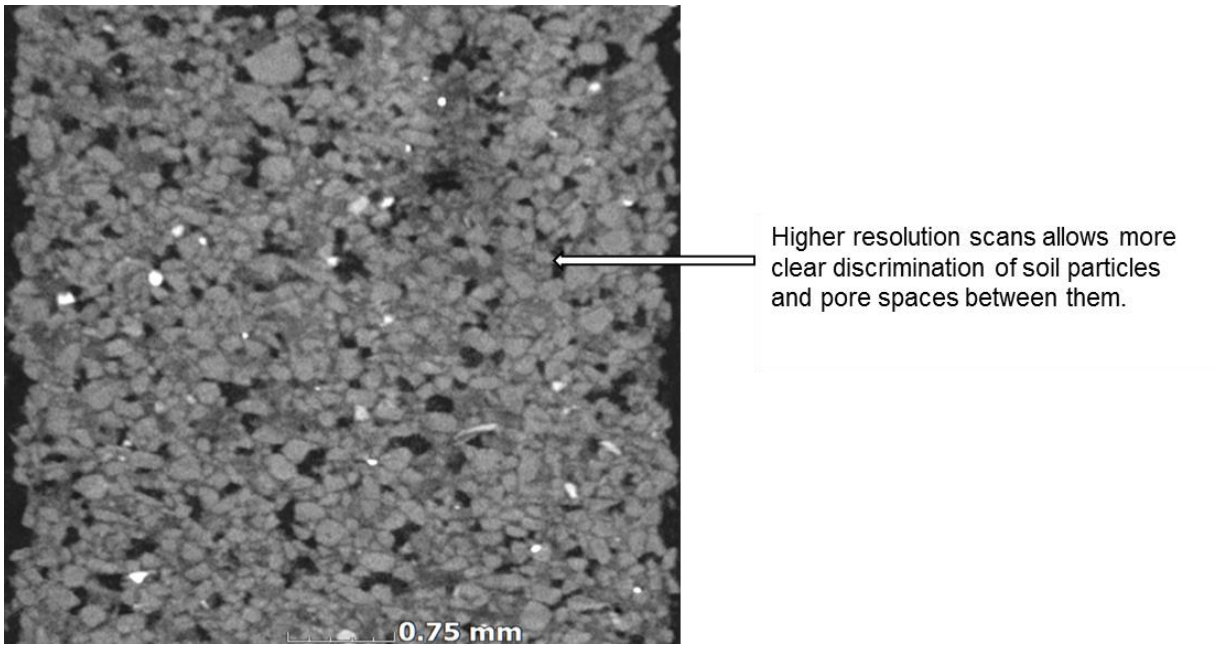

Figure 4.25. A raw X-ray micro-computer tomography (microCT) 2D slice image of the very fine sand at 5 µm, presenting how you can discriminate between soil particles (grey areas) and the pore spaces (darker/black areas).

The segmentation process separates the soil from the material to create the region of interest discussed in Section 3.7. The image data below shows the segmentation of the samples scanned at 15 (Fig 4.26) and 5 µm (Fig 4.27). Due to a lower resolution, the distinguishing between the soil particles and pore spaces are challenging (Fig 4.26). With the image processing and analysis, especially the segmentation process of the material (soil particles) can be inaccurate because the soil particles are not easily detectable as shown in Figure 4.26. The segmentation of the very fine sand that was scanned at 5 µm, shows that the segmentation process of the soil particles is unchallenging because of the higher resolution (Fig 4.27). The segmentation of soil images is

very important for the measurement of properties as well as for detecting and recognising objects in the soil (Cortina-Januchs *et al.* 2011). The segmentation of images can be difficult within soil especially when it comes to differentiating between pores and soils because of the low contrast between soil and pores (Cortina-Januchs *et al.* 2011).

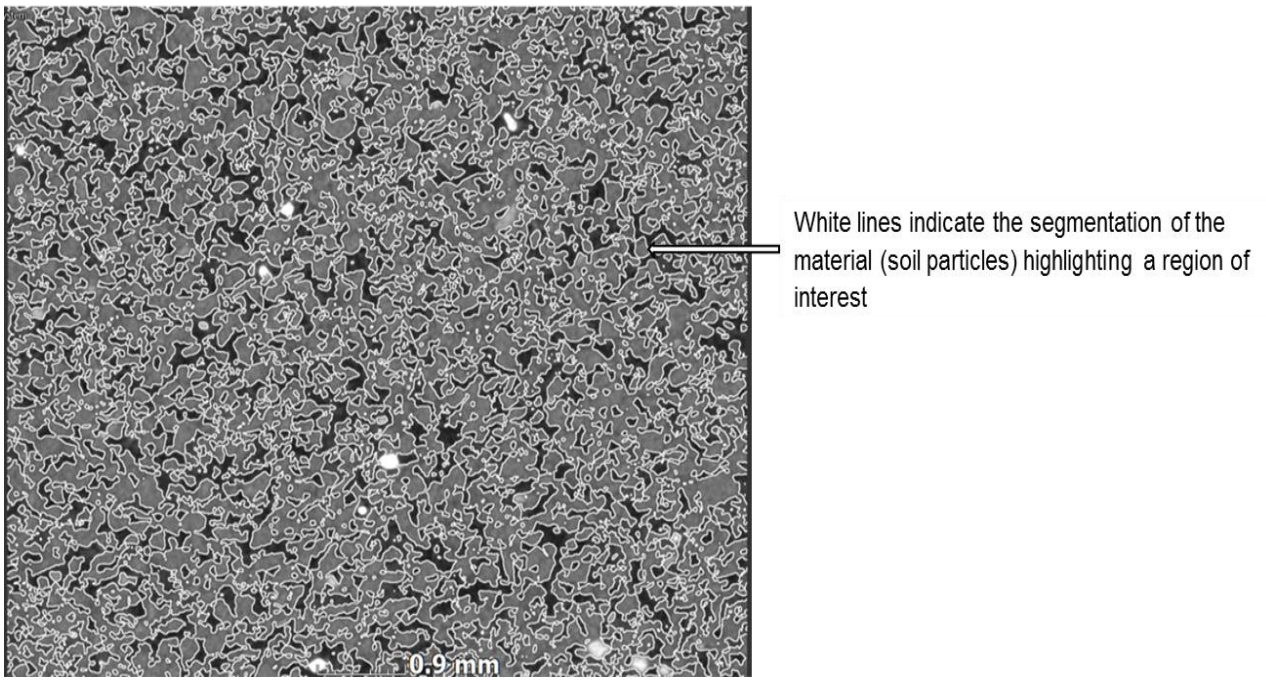

Figure 4.26. A 2D slice image of X-ray micro-computer tomography (microCT) image-based analysis of the segmentation process of material (soil particles) for the very fine sand scanned at 15 µm, to create a region of interest (ROI) for the soil particles. The white lines are an indication that the very fine sand is segmented, and the ROI is created.

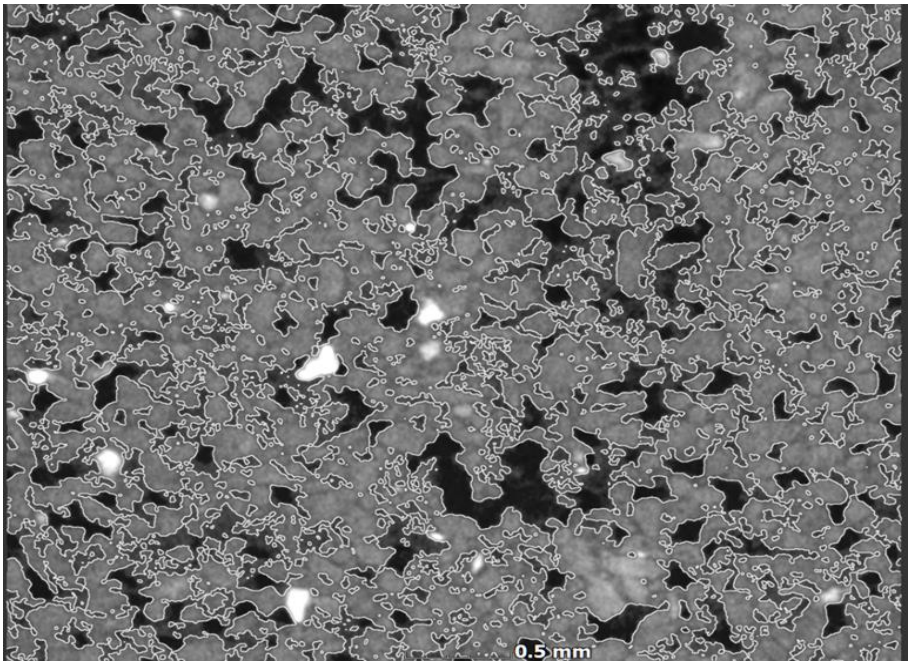

Figure 4.27. An X-ray micro-computer tomography (microCT) 2D slice image-based analysis of the segmentation process, to select the region of interest (ROI) which is the material (soil particles) of the very fine sand scanned at 5 µm (white lines are the edges of the material that is selected), displaying the difficulties of segmenting the soil particles.

4.1.7.2 The effect voltage has on image data quality

Figure 4.28 shows an example of a raw microCT image of the medium sand sample scanned at 80 kV voltage. The raw microCT image shows artefacts which are visible as star-shaped streaky artefacts in Figure 4.28, which were caused by some extremely high-density particles. High-density materials are mostly found in soil such as quartz. The artefacts might influence the results of the microCT simulation for estimating K_{sat} because the segmentation process of the material will include the artefacts as shown in Fig 4.30. Therefore, the microCT analysis might overestimate the material (soil particles) found within a sample and cause an apparent blockage in the vicinity. The medium sand was scanned at a voltage parameter of 180 kV and shows no artefacts (Fig 4.29). If the voltage is increased as shown in Figure 4.29 it minimizes the possibility of artefacts, therefore minimizing errors that might influence the analysis.

As mentioned above, both the resolution and voltage will affect the image processing and analysis of a CT scan soil sample. The term *resolution* is commonly used to denote the reconstructed voxel size (Cnudde & Boone 2013). For information on ideal scan parameters, the general guidelines in Du Plessis *et al.* (2017) can be consulted, which includes aspects on artefacts.

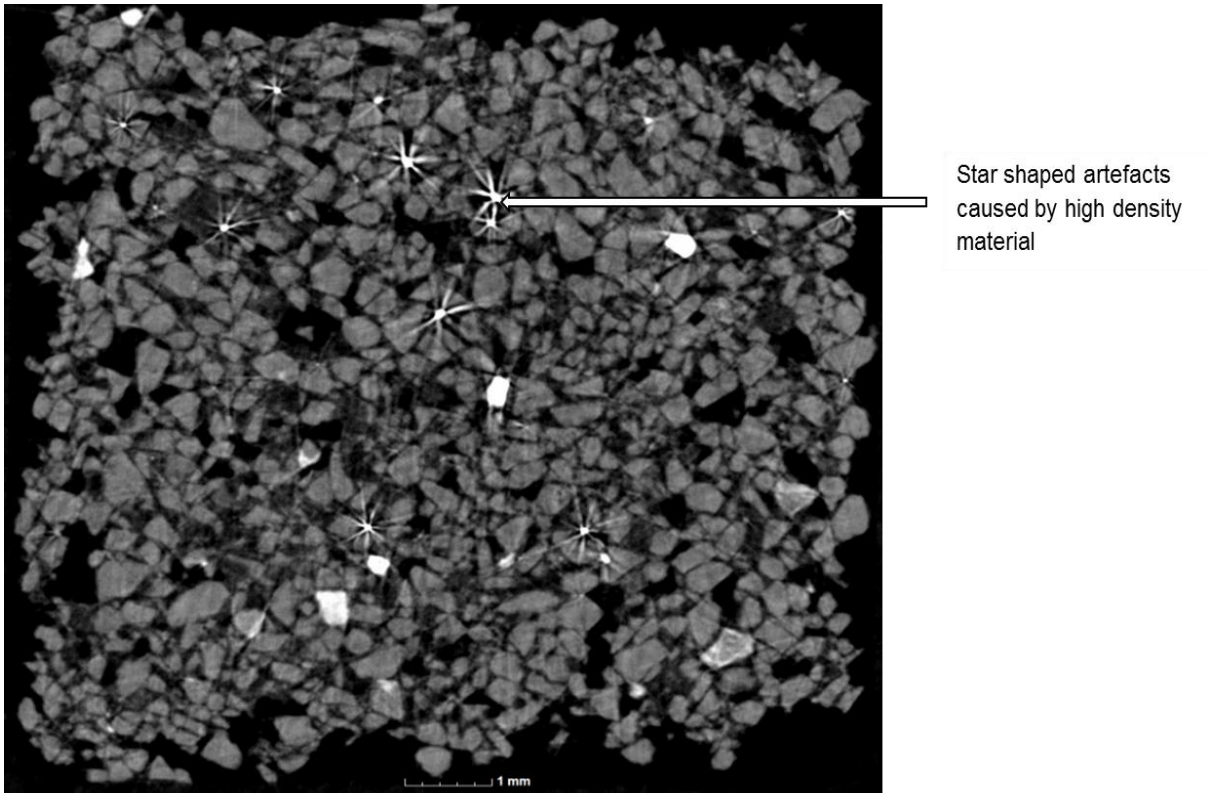

Figure 4.28. An X-ray micro-computer tomography (microCT) raw scan 2D slice image of the medium sand scanned at a voltage of 80 kV, showing how low voltage can cause star shaped artefacts on the high-density materials.

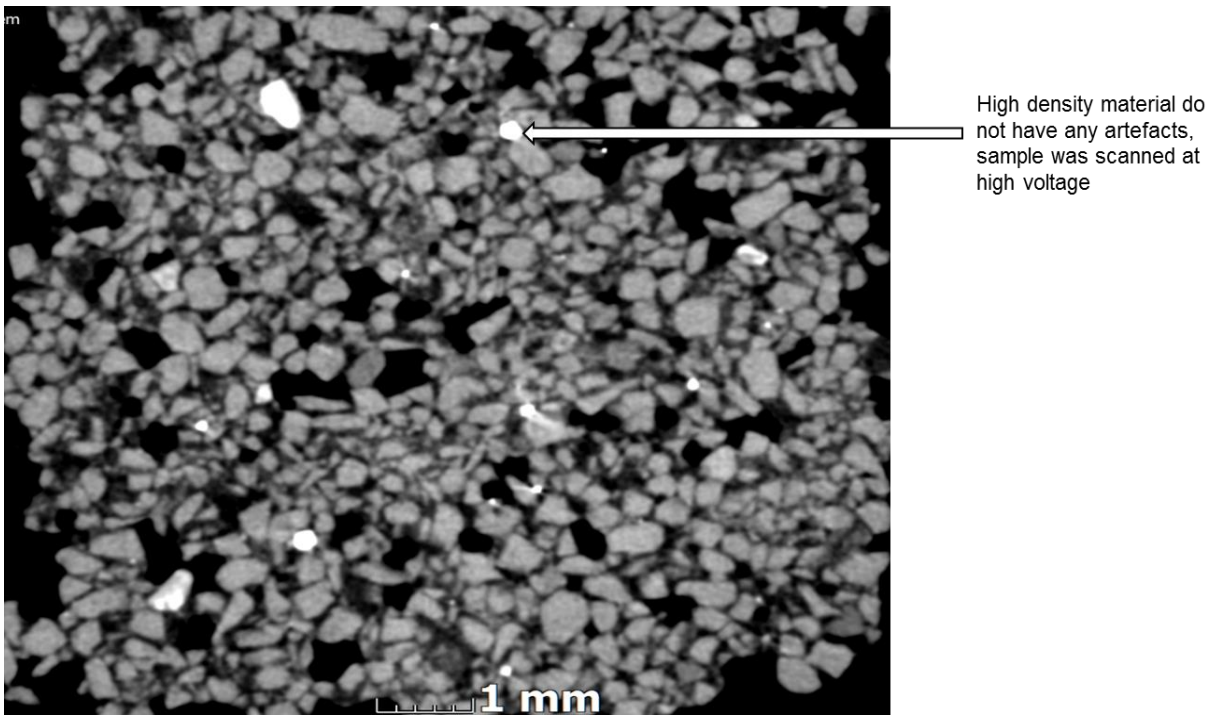

Figure 4.29. A raw X-ray micro-computer tomography (microCT) scan 2D slice image of the medium sand scanned at a voltage of 180 kV, showing how a sample with high voltage sample has no artefacts on the high-density materials.

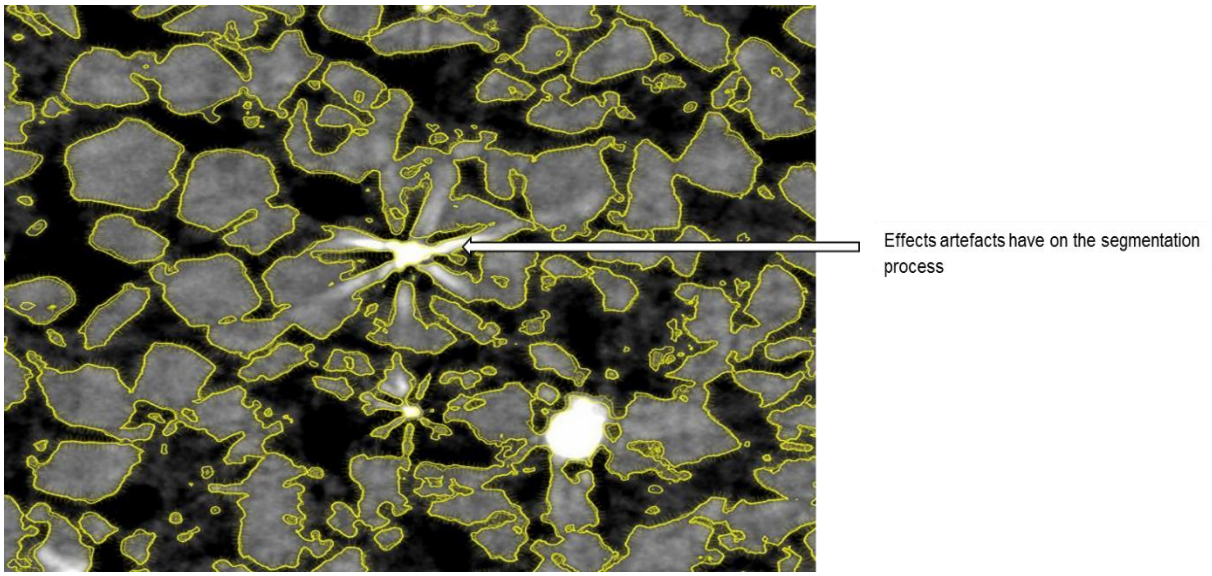

Figure 4.30. An example of an X-ray micro-computer tomography (microCT) 2D slice image-based analysis showing the surface determination (yellow lines) of the material (soil, grey areas), and displaying how the artefacts (white specs) will influence the segmentation process of selecting a region of interest (ROI) of the selected soil material.

4.1.8 Conclusion of homogeneous soil results

Results show that for the soils with larger particles such as the very coarse, coarse and medium sand, K_{sat} values analysed by microCT image-based analysis were underestimated, compared to the K_{sat} obtained from the constant hydraulic head test of both the large and small samples. The soil with smaller particle sizes such as the fine and very fine sand K_{sat} obtained from both the microCT image-based analysis (scanned at 15 µm and 5 µm) and the constant hydraulic head

test (large and small column) compared well. The very coarse sand K_{sat} values determined by the constant hydraulic head test of the small column were overestimated compared to the constant hydraulic head test of the large column. The coarse sand K_{sat} obtained from the constant hydraulic head test of the small column was underestimated compared to the constant hydraulic head test of the large column. The K_{sat} analysed by the microCT simulations of the 15 µm and 5 µm scanned samples of the different sand fractions compared well.

High variations between the number of replicates of the K_{sat} values were more predominant in the larger soil particle sizes such as the very coarse and coarse sand. The K_{sat} of the different sand fractions determined by the different methods were mostly within the same order of magnitude. The coarse sand K_{sat} values analysed by the microCT simulations were not within the same order of magnitude compared to the K_{sat} constant hydraulic head test of both the large and small column. The very coarse and fine sand K_{sat} measured by the constant hydraulic head test of the large sample were not within the same order of magnitude compared to the K_{sat} values obtained from the other methods. However, if the K_{sat} values are within the same order of magnitude for different methods, it shows confidence in the capabilities of the different methods for determining the K_{sat}. Literature states that determining the K_{sat} of the same soil type with different methods will result in different K_{sat} values (Nagy *et al.* 2013; Tracey *et al.* 2015; Elhakim 2017; Parvin *et al.* 2017).

The porosity values analysed by the microCT image-based analysis were overestimated compared to the laboratory method. There were high variations predominantly between the porosity values of the different sand fractions with larger soil particles such as the very coarse, coarse, and medium sand. The porosity values obtained from the microCT image-based analysis of the 5 µm scanned samples showed high variations between the number of replicates for the different sand fractions, compared to the porosity values analysed by the microCT image-based analysis of the 15 µm scanned sample.

The results highlight the problems of the sampling method for the microCT image-based analysis. Factors such as sampling procedures for microCT scans might have disturbed the sample due to the handling of sample and transportation of samples from the laboratory to the CT scanner facility. Thus, these factors influenced the porosity and K_{sat} values determined by the microCT technology. The plastic straw sample holder could also be one of the factors that influenced the porosity and K_{sat} values because of the fragility of the sample.

The importance of sampling a smaller sample for microCT image-based analysis and simulations were also highlighted, due to resolution limitation. Higher resolutions that provide more detail within soil samples require smaller sample sizes. From a soil scientist perspective, the sample size used for microCT scans is not representative in comparison to what takes place in the natural environment of soils. Soils are not homogeneous in nature and vary from layer to

layer. They are also variable within layers due to mechanical, biological, and chemical factors. If larger soil samples are scanned, limitations within microCT such as the resolution would be a problem. As demonstrated by the 40 µm scanned sample of the small column, larger soil samples cannot be scanned at higher or finer resolutions. MicroCT simulations and analysis could not be performed on the coarse, medium, fine, and very fine sand but only on the very coarse sand. Smaller soil samples are therefore highly recommended for performing microCT analysis and simulation.

4.2 HETEROGENEOUS SOIL RESULTS AND DISCUSSION

4.2.1 Soil texture analysis results of the heterogeneous soils

Table 4.6 shows the heterogeneous soils that were collected. The types of soil were all sandy soils but with different compositions ranging from coarser texture sandy soils such as the coarse sand and pure fine sand to finer textured sandy soils such as the sandy clay loam, sandy loam, and sandy clay. The sandy clay soil has the highest percentage of clay particles and the lowest percentage of sand particles compared to the other soils (Table 4.6). The pure fine sand has the lowest percentage of clay particles and the highest percentage of sand particles (Table 4.6).

Table 4.6. The texture analysis of the heterogeneous sandy soils (field-collected) used in this study.

Soil Texture	Clay	Silt	Sand	Coarse sand	Medium sand	Fine sand
				(%)		
Coarse sand	5.2	8.3	86.5	38.8	26.1	35.1
Pure fine sand	1.6	0.5	97.9	3.5	29.2	67.3
Sandy clay loam	26.8	14.9	58.3	9.2	14.0	76.8
Sandy loam	12.9	26.4	60.7	8.5	40.6	50.9
Sandy clay	34.7	13.0	52.3	7.8	13.5	78.7

4.2.2 Particle density, bulk density and porosity values of the heterogeneous soil

The particle density, bulk density and porosity results are presented in Table 4. 7. The pure fine sand has the highest bulk density value of the soil types and the sandy clay loam has the lowest bulk density as indicated in Table 4.7. The bulk density of soil is related to the soil compaction. Soil with a high soil bulk density will be more compacted than soil with a low bulk density (Hamblin 1985). Compaction within a soil will also influence the movement of water through soil (Hamblin 1985). Soils that are more compacted will have problems with water moving through the soil, due to the reduction of large pores and the pore connectivity of the soils (Arya 1981). This influences the K_{sat} and will result in lower K_{sat} values.

Table 4.7. The mean values of the particle density, bulk density, and the porosity of the different soil types measured with the standard methods.

Soil Texture	Average Particle density (g/cm^3)	Average Bulk density (g/cm^3)	Average Porosity (cm^3/cm^3)
Coarse sand	2.467	1.297	0.474
Pure fine sand	2.631	1.421	0.460
Sandy clay loam	2.347	1.190	0.493
Sandy loam	2.310	1.225	0.469
Sandy clay	2.355	1.295	0.450

4.2.3 Saturated hydraulic conductivity (K_{sat}) results for the constant hydraulic head test and microCT simulations

The K_{sat} values of the coarse sand, pure fine sand, sandy clay loam, sandy loam and sandy clay soils measured by the constant hydraulic head test and microCT simulation are presented in Figure 4.31. The K_{sat} values of the coarse sand, pure fine sand, sandy clay loam and sandy loam analysed by the microCT simulations shows that the K_{sat} values were underestimated compared to the K_{sat} determined by the constant hydraulic head test (Fig 4.31). However, the coarse sand K_{sat} values of the two methods were converging to the 1:1 line, indicating that the K_{sat} values determined by the two methods compared well (Fig 4.31). The K_{sat} values of the sandy clay measured by the two methods were on the 1:1 line, showing a good comparison between the K_{sat} of the two methods (Fig 4.31).

The discrepancy of the K_{sat} values can be due to the methodology used (Nagy *et al.* 2013). Other possible causes include resolution limitations within microCT also referred to in Cássaro *et al.* (2017). Elliot *et al.* (2010) reported that the underestimation of K_{sat} by CT imaging could be a result of the small pores, that are not taken into account when predicting K_{sat}. Errors within the sampling methodology for both the microCT analysis and constant hydraulic head test also influence the K_{sat} found in Vogel and Kretzschar (1996) and Arya (1981).

There were high variations between the number of replicates of the K_{sat} values for the coarse sand, pure fine sand and sandy loam measured by the constant hydraulic head test as indicated by the large error bars (Fig 4.31). In particular, there were high variations between the number of replicates of the K_{sat} for the sandy clay loam analysed by the microCT simulations as indicated by the small error bars. Variations of the K_{sat} values of the coarse sand, pure fine sand, and sandy loam can be due to soil structural changes caused by the sample preparation procedures. Errors with the measurement of soil water characteristics are caused by structural changes during soil sample preparation, handling, and treatment (Arya 1981).

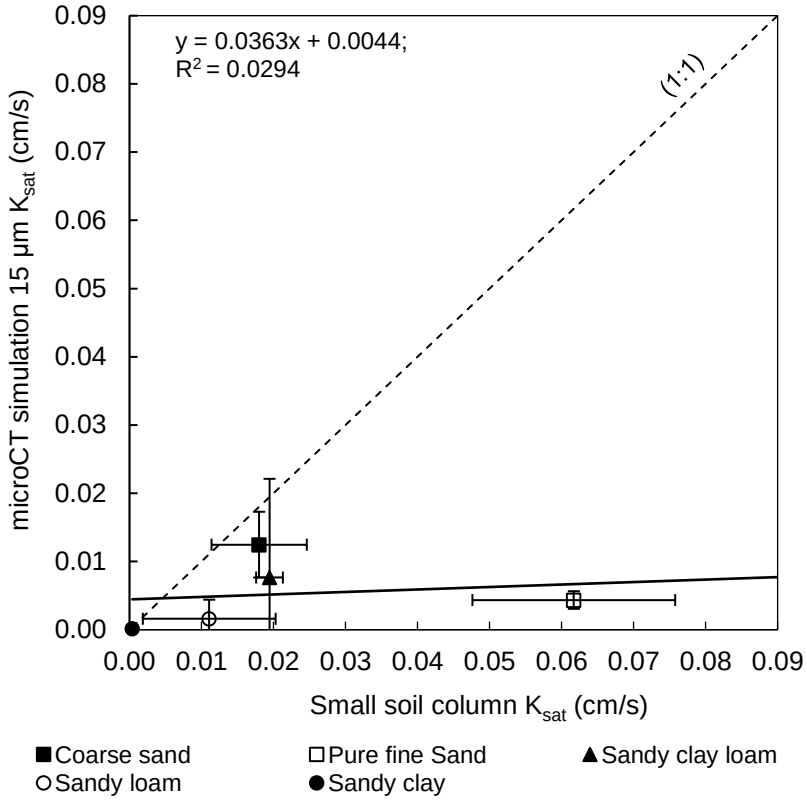

Figure 4.31. The saturated hydraulic conductivity (K_{sat}) results of the different soil types (coarse sand, pure fine sand, sandy clay loam, sandy loam and sandy clay) measured by constant hydraulic head test of the small soil column and the X-ray micro-computer tomography (microCT) simulation fit against the 1:1 line.

As observed in Figure 4.31, the pure fine sand K_{sat} values measured by the constant hydraulic head test were higher than for the coarse sand. The pure fine sand K_{sat} determined by the microCT simulations were lower than for the coarse sand. The finer-textured soils K_{sat} may be expected to be lower than for coarser textured soils. 2-D visualization of image-based analysis showed that the pure fine sand (B) has smaller particles and thus smaller pore spaces (Fig 4.32). The coarse sand (A) consists of larger particles (Fig 4.32).

MicroCT simulation performs the analysis based on the image data of the soil sample that detects smaller pore spaces within the pure fine sand. Limitations within microCT simulation of direct pore-scale modelling include that the technique does not consider the curvature interfaces that control capillary forces within the soil (Bultreys et al. 2016). The constant hydraulic head test does, however, consider the curvature interfaces that control capillary forces. The flow through soil is dominated by capillary forces (Bultreys et al. 2016). This explains why the Ksat for the pure fine sand analysed by the microCT simulation were higher and underestimated compared to the Ksat obtained from the constant hydraulic head test.

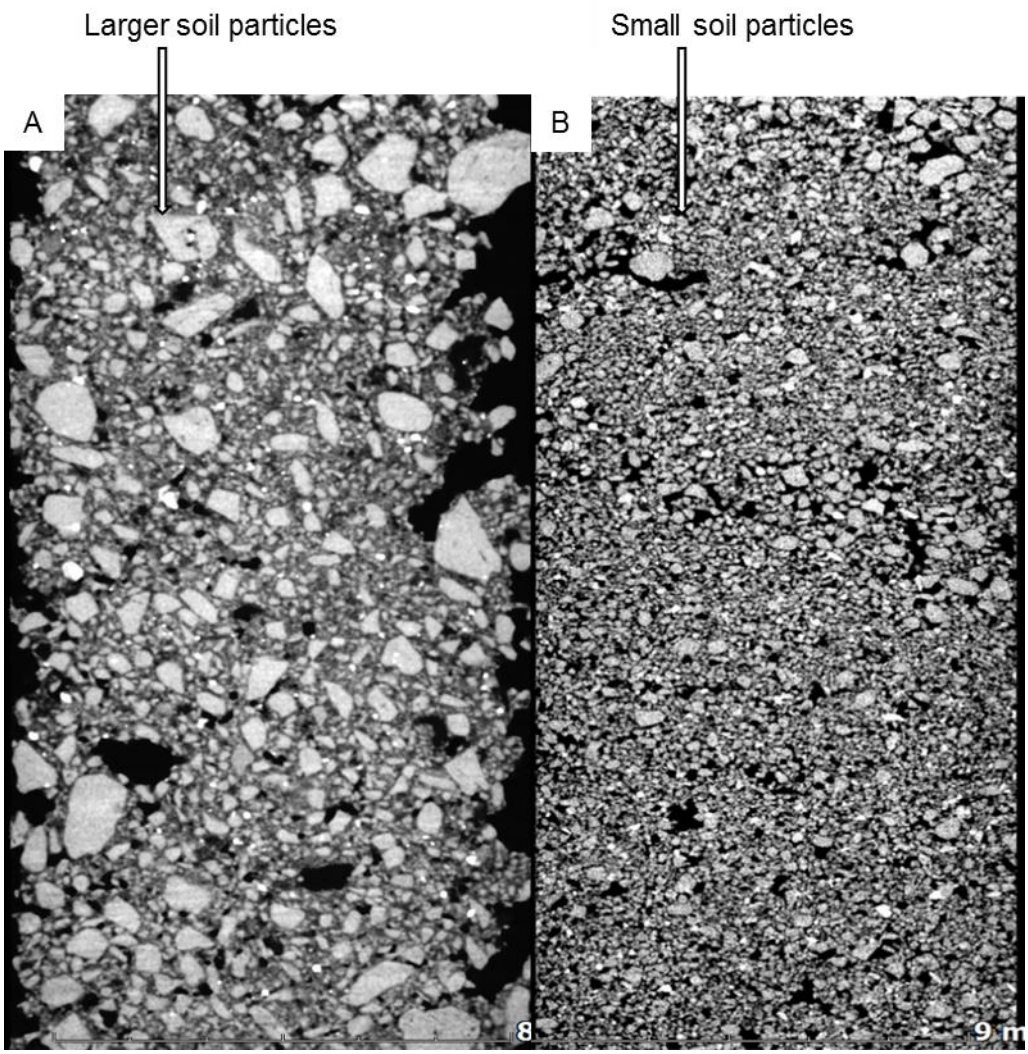

Figure 4.32. A raw X-ray micro-computer tomography (microCT) scan images data of the (A) coarse sand (larger soil particles) (left) and the (B) pure fine sand (smaller soil particles) (right) displaying how the soil particles differ in size.

This can be further explained by Table 4.7 which shows that the pure fine sand has a low slit or clay percentage, while the coarse sand has higher silt and clay percentages (Table 4.7). Clay and slit are finer textured soils and these soils have high capillary forces and a high water holding capacity (Hillel 2004). Soils with high capillary forces and a high water holding capacity have low hydraulic conductivity (Hillel 2004). Therefore, the pure fine sand consists of 97.9% pure fine sand and the coarse sand has 86.5% sand content. Thus, the coarse sand had a lower K_{sat} than the pure fine sand that was determined with the constant hydraulic head test because of the composition of the soil textural class. The composition of a soil textural class influenced the K_{sat} values (McKenzie & Jacquier 1997). MicroCT technology can depict the topological features of the soil such as the soil structure, particle size and pore size distribution but cannot accurately quantify the soil textural properties that also influence the hydraulic behaviour within the soil (Vogel & Kretzschar 1996).

4.2.4 The porosity results of the X-ray microCT analysis and laboratory bulk density method

The porosity values of the heterogeneous soil obtained from both the laboratory method and microCT analysed are presented in Table 4.8 and will not be compared on the 1:1 line. This is due to the changes caused by the bulk density after the constant hydraulic head test that was not taken into account. Therefore, the laboratory porosity values were still measured based on the bulk density the soil was initially packed within the small column. Unfortunately the soil were discarded before the change in bulk density could be calculated to measure the porosity. The soil used for the microCT porosity analyses were sampled after the constant hydraulic head test.

In Table 4.8 the porosity obtained from the microCT analysis of the different soil types shows that the soil consolidated after the constant hydraulic head test as indicated by the lower porosity values. The sandy clay loam, sandy loam and sandy clay soils however shows significantly low porosity values that were measured by microCT analysis (Table 4.8). This might be due to resolution limitations within the microCT technology as mentioned in Section 4.1.7.1.

Table 4.8. The mean porosity values of the laboratory and microCT measured porosity.

Soil Texture	Mean Laboratory Porosity (cm^3/cm^3)	Average MicroCT Porosity (cm^3/cm^3)
Coarse sand	0.474	0.437
Pure fine sand	0.460	0.429
Sandy clay loam	0.493	0.217
Sandy loam	0.469	0.201
Sandy clay	0.450	0.202

The smaller pores within the soil might have been missed by microCT image-based analysis of the porosity of the soil. In Helliwell *et al.* (2014) the smaller pores within the finer textured soils were missed and therefore the analysed porosity scanned at a coarser or lower resolution such as 15 µm will be inaccurate. If smaller parts or smaller samples were scanned at a higher or finer resolution, the smaller pores would be detected by microCT image-based analysis and that will result in a more accurate porosity value (Cássaro *et al.* 2017). Cássaro *et al.* (2017) found similar results where the remaining porosity of the clay soil was not detected because it is composed of smaller pores, which limit of detectability with the image resolution used. It is expected that larger pores which contribute to most of the bulk porosity will be measured easily and accurately by means of microCT (Helliwell *et al.* 2014).

4.2.5 MicroCT Image-based analysis small column scanned at 40 µm small column scanned before and after the constant hydraulic head test

One sample of each of the different heterogeneous soils was scanned before and after the constant hydraulic head test (small column). These samples (small column of 67.348 cm^3 or 67 348 mm^3) were scanned at a 40 µm voxel size resolution. The same samples were scanned before and after the constant hydraulic head test (small column) to visualize whether there were any errors with the packing of the soil samples or whether the constant hydraulic head test might have significantly changed the structure of the soil.

A raw 2D image data of the coarse sand sample scanned before the constant hydraulic head test (A) and a raw image data of the coarse sand sample scanned after the constant hydraulic head test (B) are shown in Figure 4.33. Cracks are visible along both edges of the sample before the constant hydraulic head test (A) (Fig 4.33). These cracks can cause preferential flow paths during the constant hydraulic head test that can influence the K_{sat} results. The samples scanned after the constant hydraulic head test shows how the cracks were filled with soil particles (Fig 4.33).

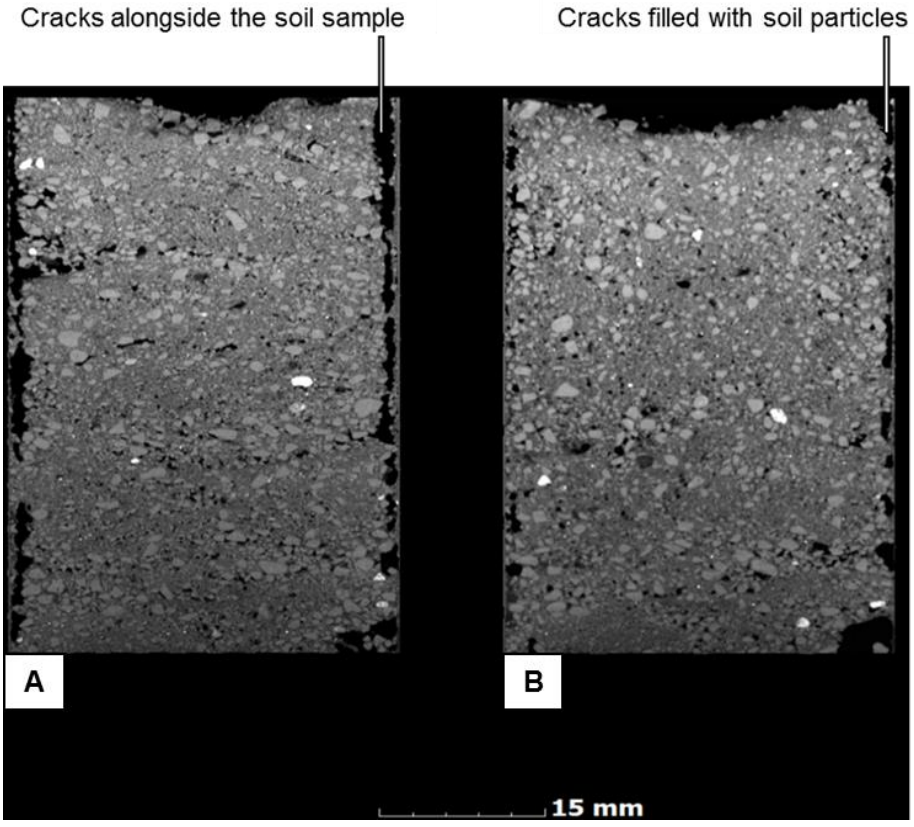

Figure 4.33. A raw 2D X-ray micro-computer tomography (microCT) slice images of the (A) “before” and (B) “after” scans of the coarse sand scanned at 40 µm, showing the cracks alongside the soil samples.

The raw 2D slice images of the pure fine sand samples scanned before the constant hydraulic head test (A) and after the constant hydraulic head test (B) are shown in Figure 4.34. As observed by the 2D image, there were layers present within the soil sample both before (A) and after (B)

the constant hydraulic head test (Fig 4.34). These layers were caused by the packing procedure of the samples for the small column as described in Section 3.2.1. There were no significant structural changes within the soil sample after the constant hydraulic head test (B) (Fig 4.34).

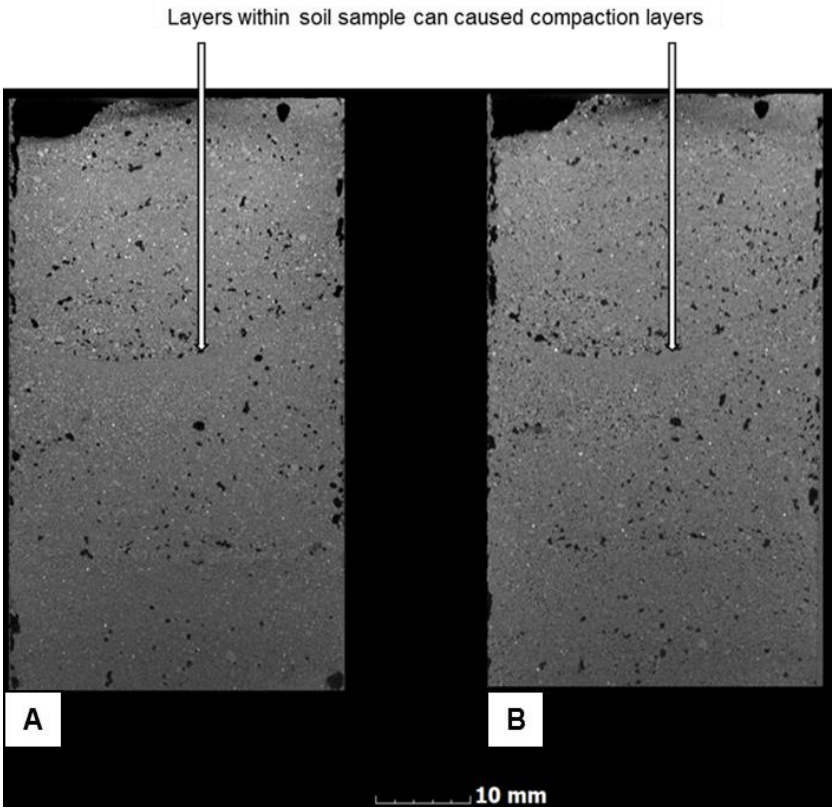

Figure 4.34. A raw 2D x-ray micro-computer tomography (microCT) slice images of the (A) **"**before" and (B) "after" scans of the pure fine sand scanned at 40 µm, showing layers within the soil.

Figure 4.35 shows the 2D slice image of the sandy clay loam scanned before the constant hydraulic head test (A) and after the constant hydraulic head test (B). Before the constant hydraulic head test (A) there were cracks alongside the walls of the column (Fig 4.35). There were no structural changes after the constant hydraulic head test (B) (Fig 4.35). Layers can be observed within the soil before (A) the constant hydraulic head test caused by the packing procedure (Fig 4.35).

The 2D slice image of the sandy loam before the constant hydraulic head test (A) and after the constant hydraulic head test (B) are shown in Figure 4.36. Cracks alongside the sides of the column were visible for the sample scanned before the constant hydraulic head test (A) (Fig 4.36). Layers caused by the packing procedure were also observed within the sample of the slice image before the constant hydraulic head test (Fig 4.36). In the slice image of the sample scanned after the constant hydraulic head test (B), the cracks alongside the column were filled with soil particles (Fig 4.36).

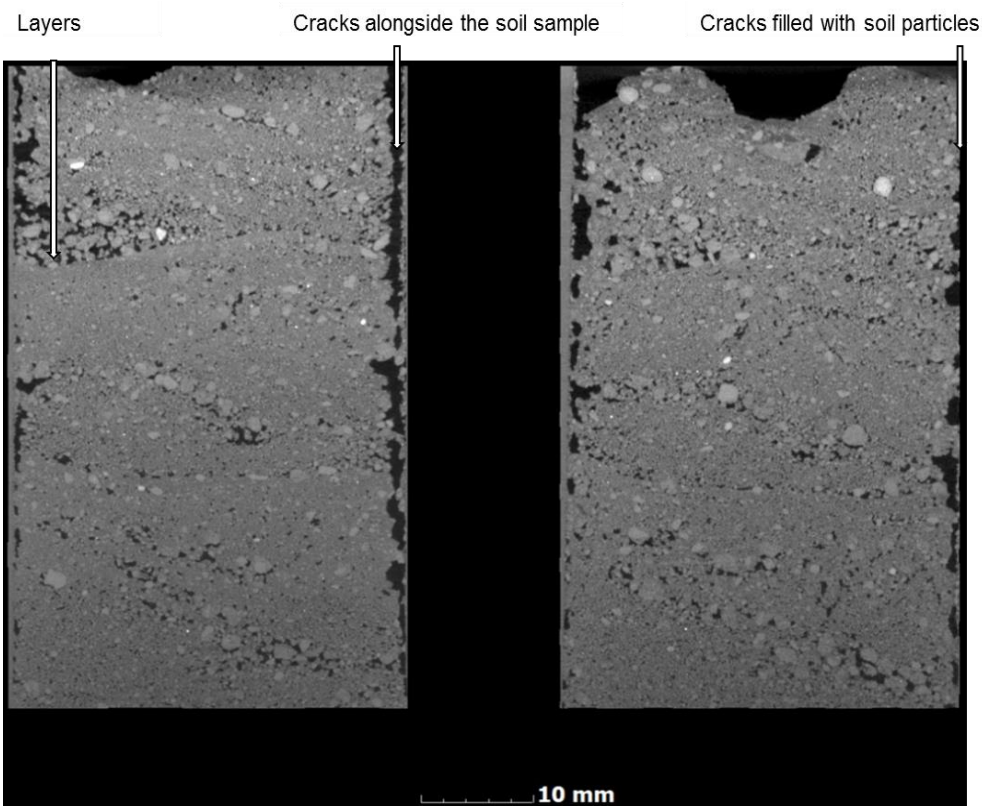

Figure 4.35. A raw 2D X-ray micro-computer tomography (microCT) slice images of the (A) **"**before" and (B) "after" scans of the sandy clay loam scanned at 40 μm, showing cracks alongside the sides of the column.

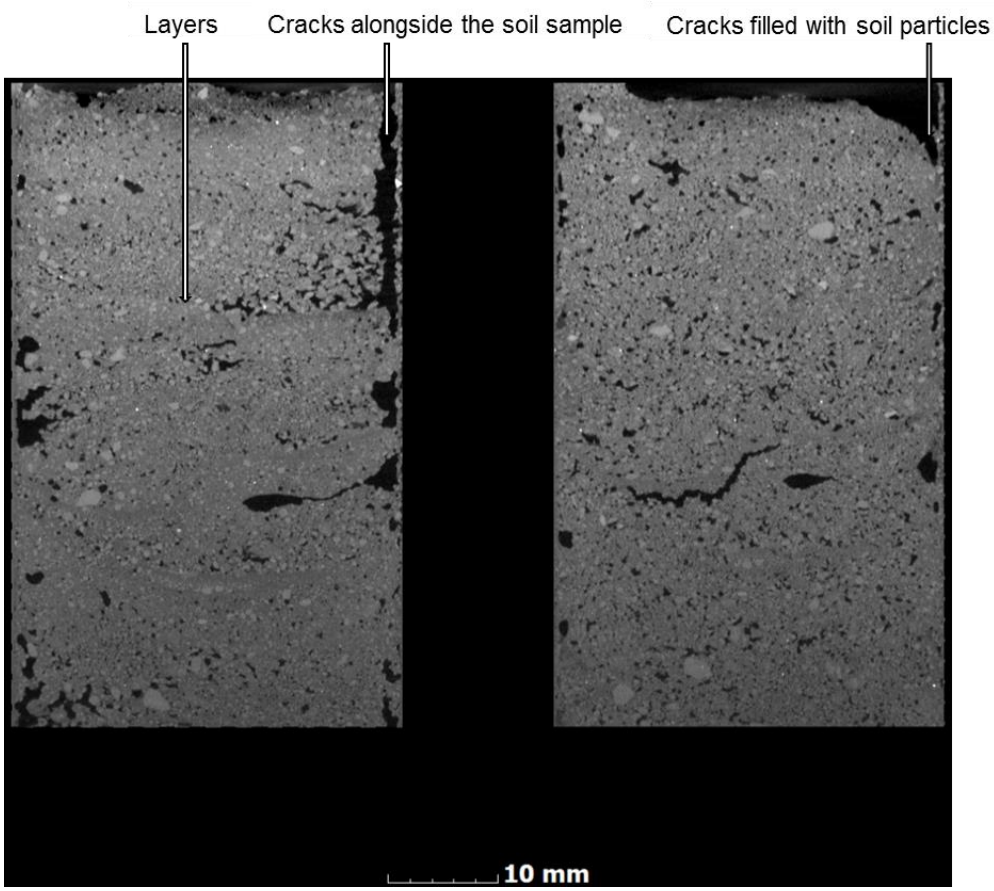

Figure 4.36. A raw 2D (X-ray micro-computer tomography) microCT slice images of the (A) **"**before" and (B) "after" scans of the sandy loam scanned at 40 μm, showing cracks alongside the sides of the column.

Figure 4.37 shows slice images of the sandy clay soil scanned before the constant hydraulic head test (A) and scanned after the constant hydraulic head test (B). In both image A and B, there were large pores visible within the sandy clay soil (Fig 4.37). These large pores were created by air that was present within the pores of the soil. This was due to the wetting of the soil before the constant hydraulic head test. Hillel (2004) stated the difficulties involved in saturating soil that can cause air entrapment. Air entrapment is caused by water entering a soil sample and encapsulating the air bubble (Hillel 2004). The air within the soil cannot escape because of the downward movement of water and the confined walls of the cylinder (column) that prohibits the air from escaping and creating air bubbles (Hillel 2004). The air bubbles block the pore passages and will affect the K_{sat} results of the constant hydraulic head test. The air bubbles within the soil were examined as an open large pore space with the microCT image-based analysis, but in reality, it was an air bubble.

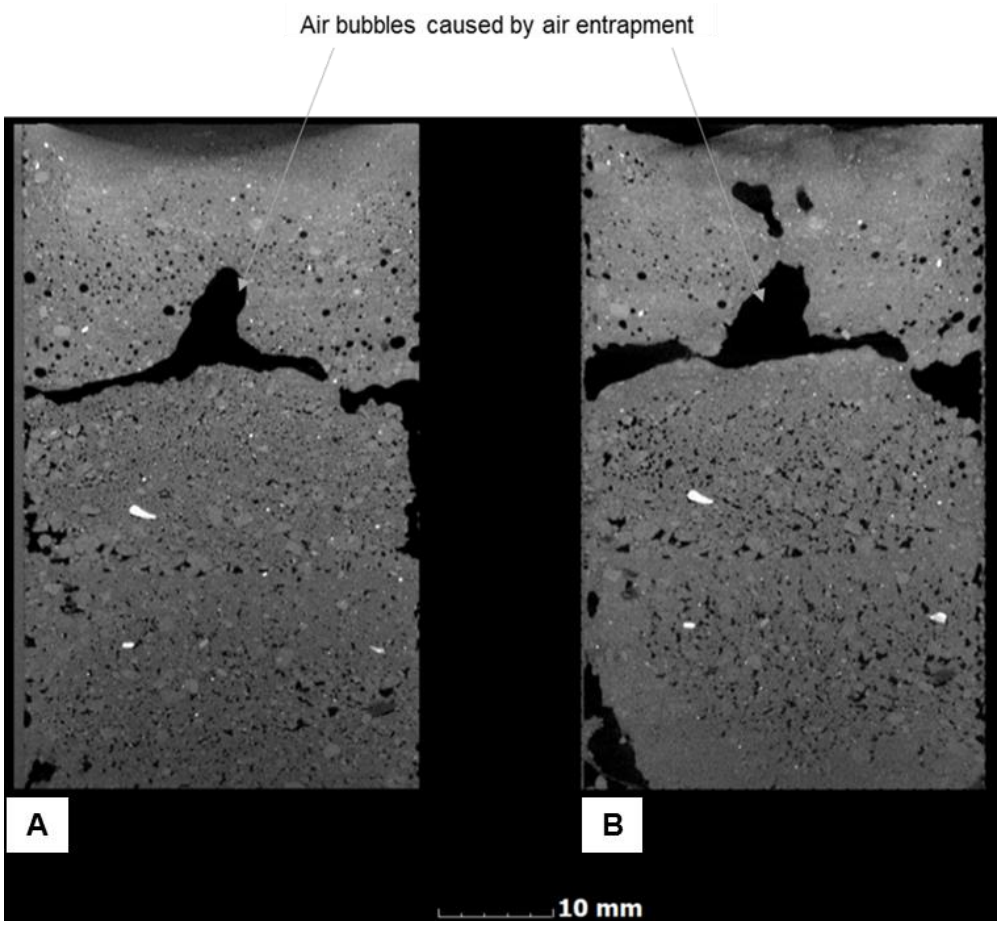

Figure 4.37. A raw 2D (X-ray micro-computer tomography) microCT slice image of the (A) “before” and (B) “after” scans of the sandy clay scanned at 40 μm, showing the air bubbles caused by entrapment.

The microCT images in this series identified a variety of factors which can affect the K_{sat} results obtained from the constant hydraulic head test such as preferential flow paths along the sides of the column, air entrapment, and layering that was formed by the packing of the soil samples as presented in Figure 4.33, Figure 4.34, Figure 4.35, Figure 4.36 and Figure 4.37. As observed in the before and after constant hydraulic head test scanned images in Figure 4.34, Figure 4.35,

and Figure 4.36, the packing procedure created layers within the soil sample also. These layers within the soil samples were created by the packing procedure, where the soil was packed in the column layer by layer. The layering of soil can cause compaction within a sample and will therefore influence the flow of water through a soil sample. McKenzie & Jacquier (1997) showed how morphological features such as the structure and compaction could influence the K_{sat} in soils. Soil compaction of a soil sample that influences the bulk densities also affected the K_{sat} values in Chakraborty *et al.* (2006). Research done by Peth *et al.* (2010) also depicted the effects that hydraulic behaviour can have on the soil structure, through microCT technology. The soil structural changes due to hydraulic behaviour were also examined by 3-D visualizations through CT scans of before and after infiltration (Mooney 2002). Mooney (2002) showed how in undisturbed soil samples, pores were well connected in the upper layers and poorly connected in the lower layers.

The cracks in these soil samples might have been caused by the packing procedure of the soil into the column (Fig 4.33, Fig 4.34, and Fig 4.35). As mentioned, the soil was packed into the column layer by layer and wetted layer by layer. This procedure might have caused shrinkage of the soil upon drying because some of the soils consisted of a high clay content that will cause shrinkage and swelling of a soil sample. Soils with high clay content can swell and shrink upon wetting and drying (Hillel 2004). Therefore, the cracks along the sides of the column might have been formed through the shrinkage of the soil after the constant hydraulic head test.

These cracks alongside the column will result in high K_{sat} values for these specific samples due to the preferential flow paths. The cracks, which were seen as larger pore spaces, alongside the soil sample, created preferential flow paths as shown in Figure 4.38 and Figure 4.39. Figure 4.38 shows a slice image of the microCT flow simulation of the coarse sand and the flow velocities. Figure 4.39 shows a 3D image of the microCT simulations of the flow simulations. The preferential flow paths showed high flow velocities (see Fig 4.38 and Fig 4.39).

Large pores or macropores have always caused preferential flow paths and in the field, it can be caused by burrowing animals such as earthworms or deteriorated roots channels (Parvin *et al.* 2017). The preferential flow paths will affect the hydraulic conductivity results, and therefore might cause an overestimation of the hydraulic conductivity of a specific soil sample (Parvin *et al.* 2017). The 2-D and 3-D visualization is a powerful technique that considerably assists in understanding how soil structure and pore connectivity influence water movement, particularly in soils where the preferential flow is prevalent (Mooney 2002).

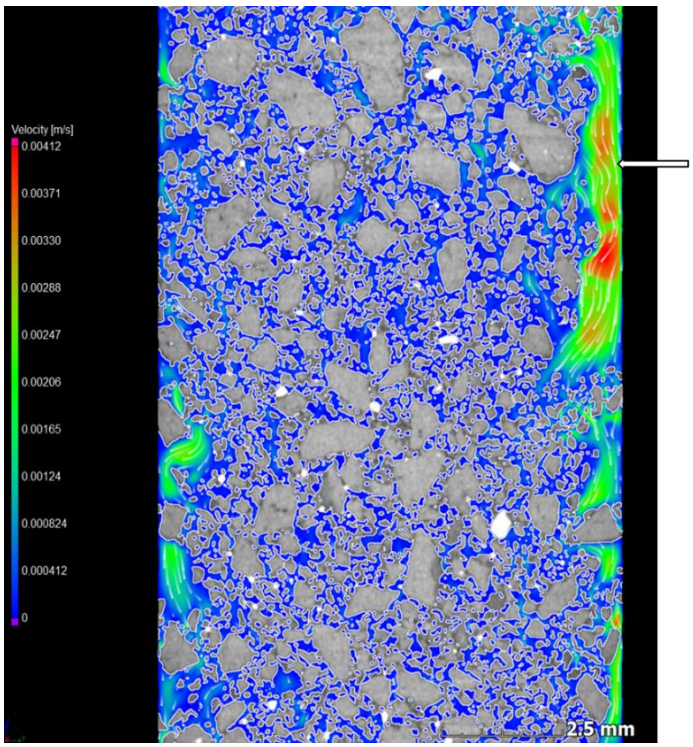

Example of the coarse sand in a 2D image, showing how cracks along the side of the soil sample can create preferential flow paths. The purple - blue areas indicates low flow velocity areas and the green-red shows high flow velocities

Figure 4.38. X-ray micro-computer tomography (microCT) scan of raw 2D slice image of the coarse sand showing the flow simulation velocities of the preferential flow paths.

3D image of the streamline velocities showing how the cracks alongside the soil sample creates preferential flow paths. The green – red lines indicates the high flow velocity areas and the purple to blue lines indicates low flow velocity areas.

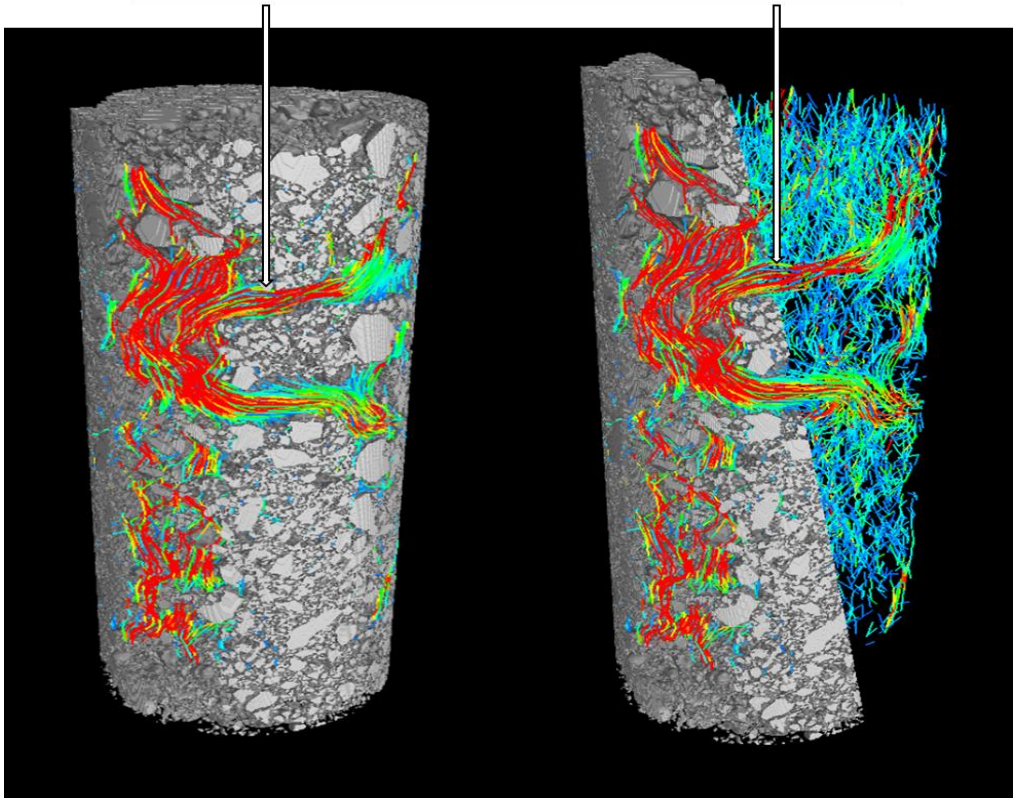

Figure 4.39. X-ray micro-computer tomography (microCT) image data of a 3D Image of the coarse sand showing the streamlines of the flow paths along the sides of the soil sample and indicating preferential slow paths.

4.2.6 Conclusion of heterogeneous soil

The K_{sat} values of all the different heterogeneous soil types analysed by the microCT simulations were underestimated compared to the K_{sat} obtained from the constant hydraulic head test of the small column. The analysis of the porosity by means of the microCT image-based analysis of the heterogeneous soils, especially for the finer textured soils, could not be quantified. The limitations of microCT technology such as resolution highly influence the application of this technology on heterogeneous soil samples. Thus, smaller pore areas were missed and the microCT image-based analysis obtained inaccurate results. The accurate quantification of pore spaces by microCT technology in heterogeneous soil with very broad pore size distributions remains challenging (Bultrey *et al.* 2016). It is important to recall that the scale and size of the sample for microCT scans can be problematic and therefore can measure inaccurate K_{sat} and porosity results of the different soil types.

Advantages of the microCT technology include its non-invasive capabilities to internally visualize the morphology of a soil sample such as the soil structure and particle or pore distribution. This was shown by the different soil types scanned at 40 µm before and after the constant hydraulic head test. The 2D imaging showed how the packing of the soil into the small column resulted in: (i) layers that could cause soil compaction; (ii) air bubbles that can impede the flow of water during the constant hydraulic head test and (iii) cracks alongside the column that can cause preferential flow paths. Therefore, the microCT technology can be useful for investigating structural changes within a soil sample due to analysis conducted in the laboratory such as the constant hydraulic head test or the examination of soil samples after sample preparations.

CHAPTER 5 : CONCLUSION AND RECOMMENDATIONS

5.1 CONCLUSION

This study aimed to investigate a simplified and effective methodology that can be used to analyse the K_{sat} with microCT simulations and whether microCT image-based analysis can provide additional insight into laboratory methods if the two applications are used in combination.

The K_{sat} of the heterogeneous and homogeneous soil analysed by the microCT simulations were underestimated compared to the K_{sat} determined by the constant hydraulic head test, particularly that of the homogeneous very coarse and coarse sand K_{sat} analysed by the microCT simulation. The medium, fine, and very fine sand K_{sat} obtained from both methods compared well though. However, most of the different homogeneous soil K_{sat} values fell within the same order of magnitude as was obtained from the different methods. This showed the capabilities of the microCT application for quantifying the K_{sat} of the homogeneous soil when within a suitable resolution range.

The heterogeneous coarse sand, pure fine sand, sandy clay loam, and sandy clay soil K_{sat} were also underestimated by the microCT simulations. The sandy clay K_{sat} analysed by microCT simulations compared well with the K_{sat} determined by the constant hydraulic head test. This shows that challenges still remain when applying the microCT simulations on heterogeneous soil as heterogeneous textured soils has a broad pore and particle size distribution. Other limitations are that the microCT simulations' direct pore-scale modelling does not consider the curvature interfaces that control capillary forces within the soil.

The porosity values of the homogeneous soil analysed by the microCT image-based analysis were overestimated compared to the laboratory measured porosity. The porosity values of the heterogeneous soil obtained from microCT image-based analysis for the coarse and pure fine sand were higher than the sandy clay loam, sandy loam and sandy clay soils. The sandy clay loam, sandy loam and sandy clay soils porosity were measured inaccurately by microCT due to resolution limitations. High variations in the porosity values between the number of replicates for the homogeneous soil that were quantified by the microCT image-based analysis were more predominant in the very coarse, coarse, and medium sand. The variation between the numbers of replicates were due to the different sample sizes. Random particle sizes cause different pore sizes that resulted in small fields of view, hence the small sample size increases the observed variability due to the physical condition of the samples themselves. In addition, the small pore spaces are missed and cause another source of potential error. These similar limitations within microCT image-based analysis with regards to the resolution were found by Tracey *et al.* (2015), Bultreys (2016) and Cássaro *et al.* (2017).

A critical factor identified was the sampling procedure for the microCT scans, which affected the results of both the porosity and K_{sat} due to the following three factors:

I. That smaller samples improve resolutions obtained therefore benefits microCT simulations and analysis;
II. A smaller sample size results in a smaller field of view, which is potentially misleading, i.e. missing of large cracks or connected pore spaces when sampling only a small section from the large or small column; and
III. The sampling method may disturb the soil structure strongly affecting the simulation as well as the porosity results.

The sampling method was not effective, especially for the plastic straw soil samples that were scanned at 5 µm, even though the small sample could be scanned at a higher or finer resolution. The fragile sample holder was difficult to mount for microCT scans. The results show that a different sampling procedure (sample holder, handling of sample and transport of sample) should be considered for the future scanning of small soil samples or more sample replicates should be scanned. Despite these limitations, this work has demonstrated a simplified method for microCT simulations and analysis in soils using specific sample sizes (3.5 cm^3 cuvette and the 0.687 cm^3 plastic straw methods). The soil samples should be scanned at higher or finer resolutions to see more detail of the soil particles. It is important to recall that the sampling procedure of the soil samples for the microCT scans was not based on prior experiments and was rather innovative.

Advantages of the microCT application include that it can observe the internal structure of the soil such as the particle size distribution and the pore geometry (pore size distribution and pore connectivity) with its non-invasive capabilities. As demonstrated by the heterogeneous soil samples scanned at 40 µm (small column 67.348 cm^3) before and after the constant hydraulic head test, the microCT images could depict structural changes or sampling errors that might occur during the sample preparation process. The microCT 2D slice images showed how the packing of the soil into the small column resulted in:

I. Layers within the soil sample that could cause soil compaction, and therefore impede the flow of water through the soil;
II. Air bubbles can also slow down the flow of water during the constant hydraulic head test; and
III. Cracks alongside the column that can cause preferential flow paths and increase the K_{sat} values.

As mentioned above, sample preparations can cause structural changes that influence the measurement of soil hydraulic properties. Therefore, this technique can be used in combination with the constant hydraulic head test or any other laboratory methods during the sample preparation processes of soil samples to detect inaccurate packing of soil samples. Other benefits

of this technique within soil science include to investigate soil compaction, to observe root distribution within undisturbed soil samples, and to examine soil structure and pore geometry of soil samples.

As discussed above, the sample holder and sampling procedure greatly affected the results. The simplicity of the sampling method and procedures made it cost-effective. It is important to scan smaller sample sizes to quantify soil hydraulic properties with microCT technology, even though the sampling of smaller sample sizes can be an issue. The microCT simulations and analysis provided satisfactory results for the homogeneous soil but were not effective on heterogeneous soil. MicroCT scans were useful for identifying problems within the samples such as air bubbles and cracks. The application can be useful for various other analyses because both qualitative and quantitative analysis can be performed from one scanned soil sample. It must however be kept in mind that the microCT scan field of view is meniscal compared to soil in its natural structural state and that factors than may influence K_{sat} and porosity, such as cracks or compaction layers, might be missed by using microCT scan simulations and result in total unrealistic estimations of K_{sat} and porosity of the soil in its natural state.

5.2 RECOMMENDATIONS

The work presented here aimed to demonstrate how microCT simulations can be used, and what the limiting factors are to be considered in future work when more accurate results are required. Better sampling preparation procedures of soils for both laboratory constant hydraulic head test and microCT simulations and image-based analysis should be considered. For microCT it is recommended to sample undisturbed soil samples hence avoiding the packing of the soil into the columns. The plastic sample holder for smaller samples was fragile to handle and therefore a more supportive in structure sample holder is recommended.

By the results presented on how the constant hydraulic head test had an effect on the soil sample after the test was performed it is recommended to scan the samples before performing microCT analysis. To directly compare the K_{sat} values of the constant hydraulic head test and microCT simulations it is best to downsize the setup of the constant hydraulic head test. This will allow the same soil sample size to undergo microCT analysis and the constant hydraulic head test. For better image quality and to improve microCT data analysis it is best to scan soil samples at a higher resolution and voltage.

CHAPTER 6 : REFERENCES

Arya, L.M. and Paris, J.F., 1981. A physicoempirical model to predict the soil moisture characteristic from particle-size distribution and bulk density data 1. *Soil Science Society of America Journal*, *45*(6), pp.1023-1030.

Blake, G. R., & Hartge, K. H. (1986). Bulk Density. In A. Klute (Ed.), *Methods of Soil Analysis. Part 1 - Physical and Mineralogical Methods,* pp. 367–371. Madison: American Society of Agronomy, Inc.

Bultreys, T., Boone, M.A., Boone, M.N., De Schryver, T., Masschaele, B., Van Hoorebeke, L. and Cnudde, V., 2015. Fast laboratory-based micro-computed tomography for pore-scale research: illustrative experiments and perspectives on the future. *Advances in Water Resources*, *95*, pp.341-351.

Bultreys, T., De Boever, W. and Cnudde, V., 2016. Imaging and image-based fluid transport modeling at the pore scale in geological materials: A practical introduction to the current state-of-the-art. *Earth-Science Reviews*, *155*, pp.93-128.

Cai, Y., Liu, D., Mathews, J.P., Pan, Z., Elsworth, D., Yao, Y., Li, J. and Guo, X., 2014. Permeability evolution in fractured coal—combining triaxial confinement with X-ray computed tomography, acoustic emission and ultrasonic techniques. *International Journal of Coal Geology*, *122*, pp.91-104.

Cantatore, A. and Müller, P., 2011. Introduction to computed tomography. Technical University of Denmark Mechanical Engineering. 77 p.

Cássaro, M., Augusto, F., Posadas Durand, A.N., Gimenez, D., Vaz, P. and Manoel, C., 2017. Pore-size distributions of soils derived using a geometrical approach and multiple resolution microCT images. *Soil Science Society of America Journal*, *81*(3), pp.468-476.

Chakraborty, D., Chakraborty, A., Santra, P., Tomar, R.K., Garg, R.N., Sahoo, R.N., Choudhury, S.G., Bhavanarayana, M. and Kalra, N., 2006. Prediction of hydraulic conductivity of soils from particle-size distribution. *Current Science*, pp.1526-1531.

Chapuis, R.P., 2004. Predicting the saturated hydraulic conductivity of sand and gravel using effective diameter and void ratio. *Canadian Geotechnical Journal*, *41*(5), pp.787-795.

Clausnitzer, V. and Hopmans, J.W., 1999. Determination of phase-volume fractions from tomographic measurements in two-phase systems. *Advances in Water Resources*, *22*(6), pp.577-584.

Cnudde, V. and Boone, M.N., 2013. High-resolution X-ray computed tomography in geosciences: A review of the current technology and applications. *Earth-Science Reviews*, *123*, pp.1-17.

Cortina-Januchs, M.G., Quintanilla-Dominguez, J., Vega-Corona, A., Tarquis, A.M. and Andina, D., 2011. Detection of pore space in CT soil images using artificial neural networks. *Biogeosciences*, *8*(2), p.279.

Crestana, S., Cesareo, R. and Mascarenhas, S., 1986. Using a computed tomography miniscanner in soil science. *Soil Science*, *142*(1), p.56.

Danielson, R.E. and Sutherland, P.L., 1986. Porosity. In A, Klute (Ed). *Methods of Soil Analysis: Part 1 Physical and Mineralogical Methods,* (pp.443-461). Madison: American Society of Agronomy, Inc.

Du Plessis, A., Broeckhoven, C., Guelpa, A. and Le Roux, S.G., 2017. Laboratory x-ray micro-computed tomography: a user guideline for biological samples. *GigaScience*, *6*(6), p.gix027.

Du Plessis, A., Yadroitsava, I., Yadroitsev, I., le Roux, S.G. and Blaine, D.C., 2018. Numerical comparison of lattice unit cell designs for medical implants by additive manufacturing. *Virtual and Physical Prototyping*, *13*(4), pp.266-281.

du Plessis, A., le Roux, S.G. and Guelpa, A., 2016. The CT Scanner Facility at Stellenboschics University: an open access X-ray computed tomography laboratory. *Nuclear Instruments and Methods in Physics Research Section B: Beam Interactions with Materials and Atoms*, *384*, pp.42-49.

du Plessis, A., Tshibalanganda, M. and le Roux, S.G., 2020. Not all scans are equal: X-ray tomography image quality evaluation. *Materials Today Communications*, *22*, p.100792.

Elhakim, A.F., 2016. Estimation of soil permeability. *Alexandria Engineering Journal*, *55*(3), pp.2631-2638.

Elliot, T.R., Reynolds, W.D. and Heck, R.J., 2010. Use of existing pore models and X-ray computed tomography to predict saturated soil hydraulic conductivity. *Geoderma*, *156*(3-4), pp.133-142.

Farber, L., Tardos, G. and Michaels, J.N., 2003. Use of X-ray tomography to study the porosity and morphology of granules. *Powder Technology*, *132*(1), pp.57-63.

Fatehnia, M., Tawfiq, K. and Ye, M., 2016. Estimation of saturated hydraulic conductivity from double-ring infiltrometer measurements. *European Journal of Soil Science*, *67*(2), pp.135-147.

Fernandez-Illescas, C.P., Porporato, A., Laio, F. and Rodriguez-Iturbe, I., 2001. The ecohydrological role of soil texture in a water-limited ecosystem. *Water Resources Research*, *37*(12), pp.2863-2872.

Fourie, W., Said, R., Young, P. and Barnes, D.L., 2007, March. The simulation of pore scale fluid flow with real world geometries obtained from X-ray computed tomography. *In Proceedings of the Boston COMSOL conference*.

Gee, G.W. and Bauder, J.W., 1986. Particle-size analysis. In A. Klute (Ed.). *Methods of soil analysis: Part 1 Physical and mineralogical methods*, (pp. 399–404). Madison: American Society of Agronomy, Inc.

Hamblin, A.P., 1986. The influence of soil structure on water movement, crop root growth, and water uptake. *Advances in Agronomy*, *38*, pp. 95-158). Academic Press.

Helliwell, J.R., Miller, A.J., Whalley, W.R., Mooney, S.J. and Sturrock, C.J., 2014. Quantifying the impact of microbes on soil structural development and behaviour in wet soils. Soil Biology and Biochemistry, *74*, pp.138-147.

Hillel, D., 2004. Introduction to Environmental Soil Physics. New York: Elsevier Academic Press.

Judge, A., 2013. Measurement of the hydraulic conductivity of gravels using a laboratory permeameter and silty sands using field testing with observation wells. (Doctoral dissertation, University of Massachusetts Amherst), 109 p.

Klute, A. and Dirksen, C., 1986. Hydraulic conductivity and diffusivity: Laboratory methods In A. Klute (ed). *Methods of Soil Analysis: Part 1 Physical and Mineralogical Methods*, (2nd ed., pp. 635–662). Madison: American Society of Agronomy, Inc.

Kovacs, G., (1972). Seepage Hydraulics. Budapest, Hungary: Elsevier Scientific Publishing Company

Le Roux, S.G., Du Plessis, A. and Rozendaal, A., 2015. The quantitative analysis of tungsten ore using X-ray microCT: Case study. *Computers & Geosciences*, *85*, pp.75-80.

McKenzie, N. and Jacquier, D., 1997. Improving the field estimation of saturated hydraulic conductivity in soil survey. *Soil Research*, *35*(4), pp.803-827.

Mees, F., Swennen, R., Van Geet, M. and Jacobs, P., 2003. Applications of X-ray computed tomography in the geosciences. *Geological Society, London, Special Publications*, *215*(1), pp.1-6.

Mooney, S.J., 2002. Three-dimensional visualization and quantification of soil macroporosity and water flow patterns using computed tomography. *Soil Use and Management*, *18*(2), pp.142-151.

Nagy, L., Tabácks, A., Huszák, T. and Varda, G., 2013. Comparison of permeability testing methods. In *Proceedings of the 18th International Conference on Soil Mechanics and Geotechnical Engineering, Paris* (pp. 399-402).

Nemes, A. and Rawls, W.J., 2004. Soil texture and particle-size distribution as input to estimate soil hydraulic properties. *Developments in Soil Science*, *30*, pp.47-70.

Nolen-Hoeksema, R., 2014. Defining and determining permeability. *Oilfield Review*, 26(3). 2 p.

Onur, E.M., 2014. *Predicting the permeability of sandy soils from grain size distributions* (Masters Dissertation, Kent State University). 137 p.

Parvin, N., Beckers, E., Plougonven, E., Léonard, A. and Degré, A., 2017. Dynamic of soil drying close to saturation: What can we learn from a comparison between X-ray computed microtomography and the evaporation method? *Geoderma*, *302*, pp.66-75.

Peth, S., Nellesen, J., Fisher, G., Beckman, F. and Horn, R., 2010. Dynamics of soil pore space structure investigated by X-ray microtomography. In *19th World Congress of Soil Science, Soil Solution for a Changing World* (pp. 1-6).

Pires, L.F., Borges, J.A., Bacchi, O.O. and Reichardt, K., 2010. Twenty-five years of computed tomography in soil physics: A literature review of the Brazilian contribution. *Soil and Tillage Research*, *110*(2), pp.197-210.

Raeini, A.Q., Blunt, M.J. and Bijeljic, B., 2014. Direct simulations of two-phase flow on micro-CT images of porous media and upscaling of pore-scale forces. *Advances in Water Resources*, *74*, pp.116-126.

Rethati, L. and Kézdi, Á., 1990. Handbook of Soil Mechanics: Application of soil mechanics practices. Budapest, Hungary: Elsevier.

Rogasik, H., Onasch, I., Brunotte, J., Jegou, D. and Wendroth, O., 2003. Assessment of soil structure using X-ray computed tomography. *Geological Society, London, Special Publications*, *215*(1), pp.151-165.

Sandoval, G.F., Galobardes, I., Teixeira, R.S. and Toralles, B.M., 2017. Comparison between the falling head and the constant head permeability tests to assess the permeability coefficient of sustainable Pervious Concretes. *Case Studies in Construction Materials, 7*, pp. 317-328.

Scheidegger, A.E., 1957. Physics of flow through porous media. Canada: University of Toronto Press. p. 233.

Taina, I.A., Heck, R.J. and Elliot, T.R., 2008. Application of X-ray computed tomography to soil science: A literature review. *Canadian Journal of Soil Science*, *88*(1), pp.1-19.

Tracy, S.R., Daly, K.R., Sturrock, C.J., Crout, N.M., Mooney, S.J. and Roose, T., 2015. Three-dimensional quantification of soil hydraulic properties using X-ray Computed Tomography and image-based modeling. *Water Resources Research, 51*(2), pp.1006-1022.

Tu, J., Yeoh, G.H. and Liu, C., 2018. *Computational fluid dynamics: a practical approach*. Cambridge: Butterworth-Heinemann.

Van Geet, M., Lagrou, D. and Swennen, R., 2003. Porosity measurements of sedimentary rocks by means of microfocus X-ray computed tomography (μCT). *Geological Society, London, Special Publications*, *215*(1), pp.51-60.

Van Leer, B. and Powell, K.G., 2010. Introduction to computational fluid dynamics. *Encyclopedia of Aerospace Engineering*. pp.1-15.

Vogel, H.J. and Kretzschmar, A., 1996. Topological characterization of pore space in soil—sample preparation and digital image-processing. *Geoderma, 73*(1-2), pp.23-38.

Wagner, A.J., 2008. A practical introduction to the lattice Boltzmann method. *Adt. notes for Statistical Mechanics*, *463*, 663 p.

Wildenschild, D., Vaz, C.M.P., Rivers, M.L., Rikard, D. and Christensen, B.S.B., 2002. Using X-ray computed tomography in hydrology: systems, resolutions, and limitations. *Journal of Hydrology*, *267*(3-4), pp.285-297.

Zappala, S., Helliwell, J.R., Tracy, S.R., Mairhofer, S., Sturrock, C.J., Pridmore, T., Bennett, M. and Mooney, S.J., 2013. Effects of X-ray dose on rhizosphere studies using X-ray computed tomography. *PloS ONE*, *8*(6). 6 p.